2012

How Does Hydropeaking Alter the Hydrology of a River Reach? A Combined Water Budget, Modeling, and Field Observation Study. Deerfield River, Massachusetts

Brian C. Yellen
University of Massachusetts Amherst

HOW DOES HYDROPEAKING ALTER THE HYDROLOGY OF A RIVER REACH? A COMBINED WATER BUDGET, MODELING AND FIELD OBSERVATION STUDY. DEERFIELD RIVER, MASSACHUSETTS

A Thesis Presented

by

BRIAN CARL YELLEN

Submitted to the Graduate School of the
University of Massachusetts Amherst in partial fulfillment
of the requirements for the degree of

MASTER OF SCIENCE

February 2012

Geosciences

HOW DOES HYDROPEAKING ALTER THE HYDROLOGY OF A RIVER REACH? A COMBINED WATER BUDGET, MODELING AND FIELD OBSERVATION STUDY. DEERFIELD RIVER, MASSACHUSETTS

A Thesis Presented

by

BRIAN CARL YELLEN

Approved as to style and content by:

_____
David F. Boutt, Chair

_____
Stephen B. Mabee, Member

_____
Jonathan D. Woodruff, Member

_____
R. Mark Leckie, Department Head
Department of Geosciences

ACKNOWLEDGEMENTS

I thank my advisor, David Boutt, for his continual support and guidance throughout this project. He is perennially receptive to new ideas and different perspectives and ready to discuss them as a peer in pursuit of new knowledge. I thank my wife, Marcelia Muehlke, for accompanying me on trips to the field site to maintenance a piece of equipment or just to float down the river on a hot afternoon. Her unofficial and impropmtu minor in geology is well deserved. I am grateful to my fellow graduate students, especially Liam Bevan, for lively discussion about our work and other stuff too. Thanks to my committee for their thoughtful comments and insights.

Steve Sauter of Ashfield, MA provided invaluable weather data. The Banks family of Charlemont, MA offered access to their property and dug well.

ABSTRACT

HOW DOES HYDROPEAKING ALTER THE HYDROLOGY OF A RIVER REACH? A COMBINED WATER BUDGET, MODELING AND FIELD OBSERVATION STUDY. DEERFIELD RIVER, MASSACHUSETTS

FEBRUARY 2012

BRIAN C. YELLEN, Sc.B., BROWN

M.S., UNIVERSITY OF MASSACHUSETTS AMHERST

Directed by: Professor David F. Boutt

Hydroelectric releases on the Deerfield River in northwestern Massachusetts affect surface water-groundwater interactions there by daily reversing the head gradient between river and groundwater. Artificially elevated stage drives river water into the riparian aquifer. Water budget analysis indicates that roughly 10% of this bank-stored water is permanently lost from the river system in a 19.5 km reach, likely as a result of transpiration by bank vegetation.

Field observations as well as two-dimensional modeling results show that water losses are not uniform throughout the study reach. Riparian aquifer transmissivity in river sub-reaches largely determines the magnitude of surface water-groundwater exchange as well as net water loss from the river. These newly documented dam-induced losses from river systems inform decisions by river managers and hydroelectric operators of additional tradeoffs of oscillatory dam-release river management.

TABLE OF CONTENTS

LIST OF TABLES

LIST OF FIGURES

CHAPTER 1

INTRODUCTION

Purpose

For decades, ecologists have documented and publicized the impacts of hydroelectric facilities on fish and other biota. Recently, hydrologists have recognized the potential for dam operations to alter surface water-groundwater (SWGW) interactions (Arntzen et al., 2006; Boutt and Fleming, 2009; Sawyer et al., 2009). Most notably, hydropeaking -dam releases during periods of peak electricity demand- raises river stage abruptly. When the river reverts to low flow, stage falls rapidly. These unnatural fluctuations continually reverse the vertical head gradient (VHG) between the river and underlying bed materials. Head gradient reversal causes the river to change from gaining to losing or vice versa. Whereas most river reaches consistently gain or lose water within a given season, dam-controlled rivers switch from gaining to losing on the time scale of energy demand cycles, which are typically daily. Recognition of this reversal in VHG and associated flow reversal during stage manipulations raises several questions for hydrologists.

This study seeks to shed light on how hydropeaking modifies SWGW interactions not only at an individual location, but at the reach scale. Specifically, can the amount of SWGW exchange be quantified? Furthermore, to what extent do changing hydrogeologic parameters of the adjacent riparian aquifer affect the magnitude of exchange? Initial insights gleaned from comparing upstream and downstream discharge made it apparent that hydropeaking may impact the overall water budget of the downstream river reach. This paper sheds light on the value and limitations of studying SWGW interactions at different spatial scales – from point observations to entire reach integration. A variety of approaches yield a coherent and

consistent story of hydropeaking leading to increased losses, especially at areas of greater riparian aquifer transmissivity.

Previous Work

Several underlying processes must be understood before we can definitively answer questions regarding effects of hydropeaking on biota and underlying aquifers. Macroinvertebrate species assemblage and abundance provide the most robust, quick measure of stream health (Karr, 1991). Several ecologists have documented changes in species assemblage and abundance of macroinvertebrates as a result of dam hydropeaking (Cole, 2007; Cereghino et al., 2002). Alterations to the natural stream temperature regime as well as bed scour have been put forward to explain the effects of hydropeaking on macroinvertebrates. Hydrologic variables, such as reversal of VHG and associated pumping of river water into the bank are difficult to measure, and therefore have been disregarded. However, the marked influence of SWGW interactions on physical parameters within the stream environment mandate a deeper understanding of the hydrology of hydropeaking rivers.

The hyporheic zone in dam-controlled rivers: functions and fluxes

The science community has often viewed ground water and surface water as separate and distinct systems (Kalbus et al., 2006; Brunke, 1997). Drastically different governing mechanisms for these two systems have made this distinction seem reasonable. Surface water is characterized by transience and turbulence. River discharge and chemical constituents can change on hourly to daily scales. Conversely, groundwater within aquifers typically displays gentle gradients, slow flow velocities and relative stability.

Scientific disciplines with arbitrarily defined topical boundaries have reinforced the notion that surface water and ground water are separate entities. Workers in the growing field

of surface water-ground water interactions have begun to characterize mixing between surface streams and underlying aquifers, thereby bridging two formally distinct fields. Their work has shed light on the importance of this intermediate mixing zone. The region where surface water and ground water mix, termed the hyporheic zone (HZ), serves physical, chemical and ecological functions within rivers. The crucial and varied services provided by the HZ demand that we better understand the processes therein.

What are the ecological and hydrologic functions of the hyporheic zone?

Hydrologists and ecologists alike have credited the HZ with several important roles within river systems. From an ecological perspective, the HZ's primary importance stems from its role as host to various invertebrates and biofilms that collectively provide a trophic link between allochthonous organic detritus and larger heterotrophs (Clapcott, 2010). Hydrologists have credited the HZ with flood attenuation and assisting in baseflow maintenance during dry periods. Geobiochemists have noted the role that the HZ plays in filtering nutrients and dissolved metals from water as it passes through hyporheic biofilms and redox gradients below streams (Hancock, 2002).

Defining the extent and transient nature of the hyporheic zone

In simplest terms, the HZ is the portion of the substrate below and adjacent to rivers where surface water and ground water mix. Brunke (1997) was hesitant to apply a finite definition to the HZ due to its inherently transient characteristics, which serve to define it. The HZ displays aspects of both surface water and ground water systems in changing proportions over time and space. A rigid definition of this transience would negate functional understanding. It can safely be said that the HZ is typified by steep chemical and temperature

gradients. It functions as the site of surface water-ground water exchange for mass movement of water, dissolved constituents, heat and nutrients.

Workers from different disciplines who study processes within the HZ define its extent differently. Ecologists define the HZ as an ecotone characterized by a unique species assemblage collectively referred to as the hyporheos (Boulton et al., 1998). Hydrologists have defined the hyporheic zone based on the distance that river water penetrates into the subsurface before returning to the river channel (Sawyer et al., 2009).

Determinants of flow magnitude and direction: sediment, geomorphology and colmation

The extent of the HZ and the flux magnitudes between surface water and ground water depend on two main factors: the hydraulic conductivity of bank media and the head gradient between river water and ground water (Freeze and Cherry, 1979). In the case of dam-controlled rivers, the head gradient is often a function of anthropogenic stage fluctuations. Abrupt increases and decreases in stage can cause a head gradient reversal and reverse the flow direction into or out of the bank. In more natural river settings, hyporheic flow direction is generally controlled by geomorphology. Using flume simulation, Vaux (1968) found that downwelling of river water generally occurred where the longitudinal river profile formed a concave shape and the river became shallower. These transitions from deeper to shallow water generally occur where pools drain into riffles. Downwelled water tends to upwell at the bottom of the riffle.

Hydraulic conductivity is largely a function of the properties of the bank media. Connant (2004) found a direct correlation between areas of ground water discharge and grainsize of bank and aquifer media. In a river bottom comprised of clay, silt and sand, most of the ground water discharge occurred in the sandy portion of the river bottom. Furthermore,

hydraulic conductivity and dam-induced head gradients have been observed to vary inversely (Arntzen et al., 2006). This makes intuitive sense since areas of limited permeability will tend to maintain larger head gradients between surface water and ground water since water cannot advect as quickly though low K media.

How do rapid stage fluctuations affect the hyporheic zone?

Several studies have documented enhanced hyporheic pumping due to dam-induced rapid changes in stage (Arntzen et al., 2006, Saywer et al., 2009, Boutt and Fleming, 2009). These frequent flow reversals due to reversals in the head gradient impact the hydrology and thereby the ecology of river systems.

Faunal assemblages and trophic interactions are highly dependent on processes within the HZ (Brunke and Gosner, 1997). Howard et al (2006) modeled the changes in HZ characteristics in response to rapid stage fluctuations. They noted that rapidly changing conditions as a result of hydraulic gradient reversals pose a threat to the hyporheos, which relies on generally stable daily conditions. Hanrahan (2008) noted limited effects on the temperature and hydraulic gradients in salmon spawning sites in the Snake River due to dam releases. However, it is noted that the data collection period for this study was characterized by atypically stable discharge. Furthermore, the limited extent of the flood plain aquifer within the sample reach led the author to caution generalizing these results beyond rivers with similar geomorphic settings.

Geist and Dauble (1998) noted that hyporheic upwelling is a major requirement of salmonid spawning sites. The temperature and chemical stability of the upwelling water proves essential to incubating eggs. Dam-controlled stage fluctuations can alter this stability by

changing the vertical head gradient on an hourly as opposed to seasonal time scale with potentially adverse effects on salmonid spawning success.

Davy-Bowker (2006) contrasted areas of hyporheic downwelling and upwelling by sampling benthic macroinvertebrates in pool-riffle sequences of a stream reach in Dorset, England. Both biodiversity and abundance of individuals were significantly greater at the tops of riffles where the localized head gradient caused water to downwell carrying dissolved oxygen and nutrients. To date, no one has studied the impact of dam-induced hyporheic pumping on the hyporheos. Evaluating whether dam-induced hyporheic pumping increases or reduces macroinvertebrate and microbial biomass abundance remains a major unknown in dam-controlled rivers.

Recent studies have highlighted the effects of dam control and associated hyporheic pumping on contaminant transport within surface water bodies. Fritz and Arntzen (2007) noted a dilution of Uranium as a result of hyporheic water influx. The concentration of Uranium in the Columbia River due to contaminated ground water discharge was mitigated during low flow dam releases by an influx of bank storage. Boutt and Fleming (2009) modeled the fate of a conservative solute in a dam-controlled river and found that more mass is introduced from the river into the underlying aquifer under rapidly fluctuating conditions even when net hyporheic water flux is zero.

How have workers measured hyporheic exchange in the past?

Advection through the HZ affects resident biota as well as the hydrology of the river and associated aquifer system. Because advection in the subsurface occurs through an infinite number of flow paths at rates that are too slow to measure directly, it is usually necessary to use indirect methods of measurement that make use of HZ-associated processes. These methods

range from the relatively straight-forward use of relative head differences between surface water and ground water to more abstract methods that trace heat anomalies through the subsurface. Each method of measuring SWGW interactions comes with inherent benefits and drawbacks.

Extensive attempts to directly measure SWGW fluxes have yielded only limited success at characterizing processes at sufficiently large scale so as to be useful. Seepage meters seal off a section of the river bottom, usually by embedding an inverted bucket in the stream bottom. A plastic bag attached to the only opening in the enclosure collects water that seeps from the substrate. The direction of hyporheic flux can vary on the reach scale and magnitude of flux can vary by orders of magnitude on even smaller scales. Due to this heterogeneity, direct measurements of seepage are generally far too spatially limited to capture processes in an entire reach.

A water balance approach has been used to determine the magnitude of groundwater discharge or recharge at the reach scale in rivers. Similar approaches have been use to approximate bank storage during flood waves. However, no study has evaluated dam-induced hyporheic fluxes using differential upstream/downstream discharge observations.

Several workers have measured head differences between surface water and underlying substrate to evaluate the direction and magnitude of hyporheic flux (Hanrahan 2008, Sawyer et al 2009, Arntzen et al 2006). In order to measure head, piezometers may be installed in the river bed as well as adjacent to the river. When installed directly in the river bottom, the difference in head between the river and that at some depth in the substrate provides the vertical hydraulic gradient. When piezometers are installed in the bank, the difference in elevation between the river stage and the water table allows for calculation of horizontal hydraulic gradient adjacent to the river. The hydraulic gradient indicates which way and how

hard flow is driven. With knowledge of hydraulic conductivity of the riverbed media, the head gradient allows for calculation of the magnitude of hyporheic flow.

In addition to measuring water directly, several methods have been developed to measure hyporheic flows that make use of tracers. By evaluating the ratio of a tracer introduced from one system into another it is often possible to determine the flux of the medium – water in this case – that transports the tracer. Reuhl et al (2006) used sodium bromide to evaluate to what extent a losing river in California recharged a local aquifer. Unrecovered tracer was accounted for as groundwater recharge. However, hyporheic paths that reintroduced the tracer back into the stream also had to be considered.

Using heat as a tracer for ground water flow has received extensive attention in recent years (Anderson, 2005). Temperature anomalies along stream bottoms have long been recognized as areas of ground water discharge. However, capturing the heterogeneity of a riverbed can be difficult and thus can limit the usefulness of information. Hatch (2006) developed a method to evaluate changes in temperature gradients over time at different depths in the HZ to calculate flux. This method is very powerful in that it allows for long term monitoring of hyporheic processes with minimal cost and labor. However, the Hatch method is limited to a point measurement and does not take into account spatial heterogeneities at the reach scale.

Conant (2004) used a combination of sparse piezometers and dense temperature measurements to better capture riffle-scale heterogeneities. This method provided accurate measurements of SWGW interactions across the river. However, the need for hundreds of temperature readings precluded collecting time series data. Thus, this method provided only a snapshot of SWGW interaction.

Summary

The HZ serves important ecological and hydrological functions within streams. The HZ is home to essential biota within stream ecosystems and provides suitable conditions for fish egg incubation. Flux into the bank and riverbed provide bank storage during flood peaks, mitigating deleterious effects of peak flows. Yet, despite the importance of processes within the HZ, its transient characteristics and heterogeneity make it difficult to study and therefore, poorly understood. Of special concern are the effects of dam control on the HZ.

Several methods exist to measure hyporheic flux. Each method has distinct advantages and disadvantages. Optimizing data collection demands consideration of the drawbacks and strengths of different HZ measurement methods. Moving forward, hydrologists are tasked with better understanding advection of water through the hyporheic zone under transient conditions such as flood waves. Better understanding of flow mechanisms will allow for better stream management to meet ecological and societal needs.

Site Description

The Deerfield River watershed spans 1722 km^2 across portions of southern Vermont and northwestern Massachusetts before entering the Connecticut River in Greenfield, MA (figure 1.1). The study reach of concern in this paper stretches 19.5 km from the Fife Brook Dam in Rowe, MA to USGS gaging station 01168500 in Charlemont, MA. In the span of the study reach, the river's watershed area increases 40.4% from 666 km^2 at upstream end of the reach to 935 km^2 downstream. In this reach, four major tributaries (watershed area > 30 km^2) enter the DFR, accounting for roughly 80% of the increase in watershed area. Small catchments make up the remaining 20% of areal increase.

The largely forested watershed (>96%) experiences typical Northeastern United States climate throughout most of its area, except in the extreme upper watershed where higher elevation (>800 m) is responsible for alpine to high-alpine conditions. Average precipitation within the watershed ranges from 110-130 cm depending on elevation, though most of the study reach likely falls at the low end of this range and may exceed it at highest elevations.

A steep gradient and humid climate makes the DFR ideal for hydroelectric power generation. The Harriman and Somerset reservoirs in the Vermont part of the watershed provide most of the storage for downstream run-of-river (without significant impoundment storage capacity) generating facilities. These large upstream reservoirs are drawn down in late winter (appendix figure A.1), providing storage for flood control during the spring freshet and power generation as the stored spring floods are parsed out during summer peaks in energy demand (Moriarty, Personal Communication, 2010). Storage of the spring flood suppresses the annual hydrograph, largely preventing Q events greater than 400 m^3/s within the study reach.

During the summer, the hydrograph within the reach is dominated by the signature of Fife Brook dam and Bear Mountain pump storage facility. The small impoundment ($5*10^6$ m^3 estimated by author), which mostly provides water for pump storage generation, also allows for hydropeaking – releasing more water to meet energy need at times of peak demand (figure 1.2). During the summer of 2010, dam releases ranged from 3 to 37 h with a median duration of 7 h.

Within the 19.5 km study reach, the river drops from 223 mASL to 158 mASL through the Berkshire Hills physiographic province (Friesz, 1996), characterized by narrow river valleys surrounded by steep bedrock hill slopes. Low gradient valley bottoms generally contain 0-20m stratified drift and or alluvium. In lower portions of the mainstem DFR, glacial scour over-deepened bedrock valleys, which subsequently filled with stratified drift providing storage for significant riparian aquifers. The majority (70%) of riparian groundwater recharge derives from

the metamorphic crystalline bedrock uplands via runoff, fracture flow and shallow subsurface flow (Friesz 1996). Other recharge occurs via direct precipitation inputs to water bodies and the valley bottoms, which are composed mostly of stratified drift emplaced during the last glacial maximum.

Previous work in the area (Mabee et al., 2007) detailed the extent and nature of the valley fill aquifer spanning the lower 14 km of the study reach. Strata there are typical of glacial morphosequence valleys (Koteff, 1974); fining upwards glaciofluvial deposits throughout the site with glaciolacustrine varved fines overlying the most downstream parts of the reach in Charlemont (figure 1.3). As remnant lobes of the retreating Laurentide Ice Sheet melted, the glacial terminus in the valley moved progressively upstream, depositing several coarse ice-contact deltas, most of which have been reworked by the modern river. This reworking of coarse delta sediments mantled the modern valley in very high conductivity (30-100 m/d) modern alluvium. Several alluvial terraces record distinct paleo-base levels. As glacial lakes drained and the valley matured, the mainstem of the river has incised through this surface alluvium in most locations and its bed directly overlies glaciofluvial sediments. At pinch points, where resistant bedrock outcrops, clay-rich residue on extracted in-stream piezometers indicated that the river runs directly over till in these areas. At the most down-stream sections of the reach, the river may flow directly over glaciolacustrine material. For a more details description of the valley's deglaciation history, see Fleming (2009).

Depth to bedrock in two distinct basins within Charlemont approached 50m, but is much less in most places. Upstream sections of the river flow over much thinner sediment packages and in some places directly over bedrock. Seismic surveying in the broadest upstream basin (site 2) revealed a depth to bedrock of only 10m at the survey location (figure 1.4). More information will be provided on the valley cross sections in chapter four.

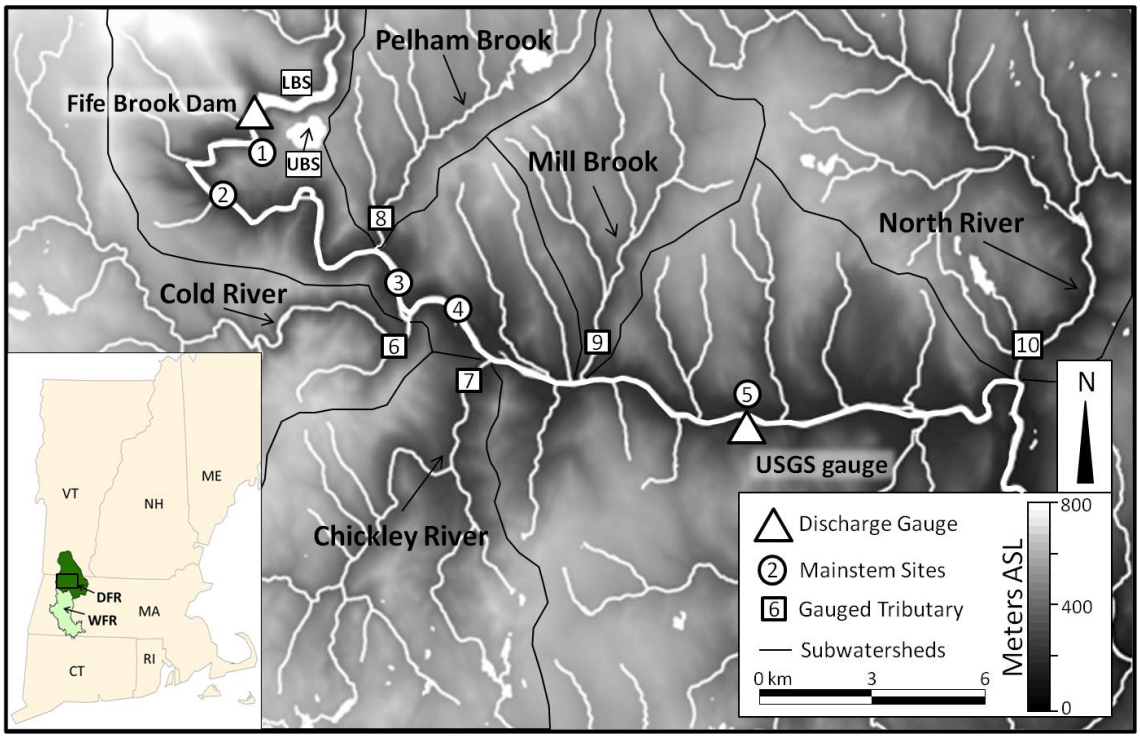

Figure 1.1 – Site map of the study area. The entire DFR watershed is shown at bottom left spanning parts of Vermont and Massachusetts. The Westfield River watershed (WFR) is just south of DFR. In the shaded elevation map, the mainstem of the DFR runs eastward with the study reach defined by the two discharge sites (triangles). The Lower Bear Swamp (LBS) impoundment and Upper Bear Swamp (UBS) pump-storage reservoir appear in the northwest corner of the blown up area. Four large tributaries within the study reach, as well as North River are labeled.

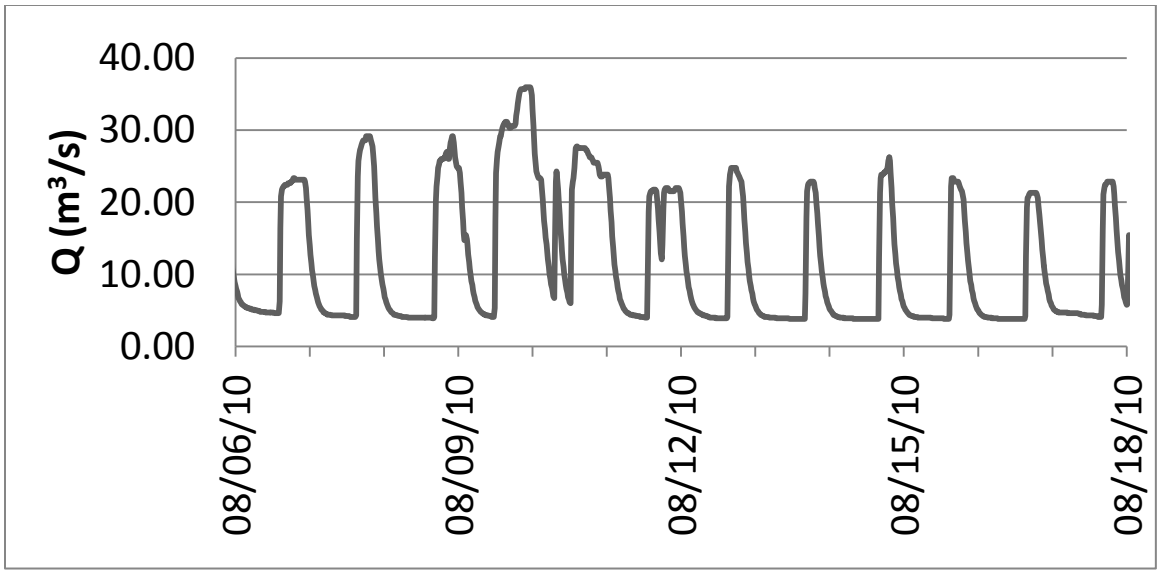

Figure 1.2 - Example of DFR Q taken from the USGS gage in Charlemont, MA capturing a range of typical summer flows. A precipitation event occurred on 8/9.

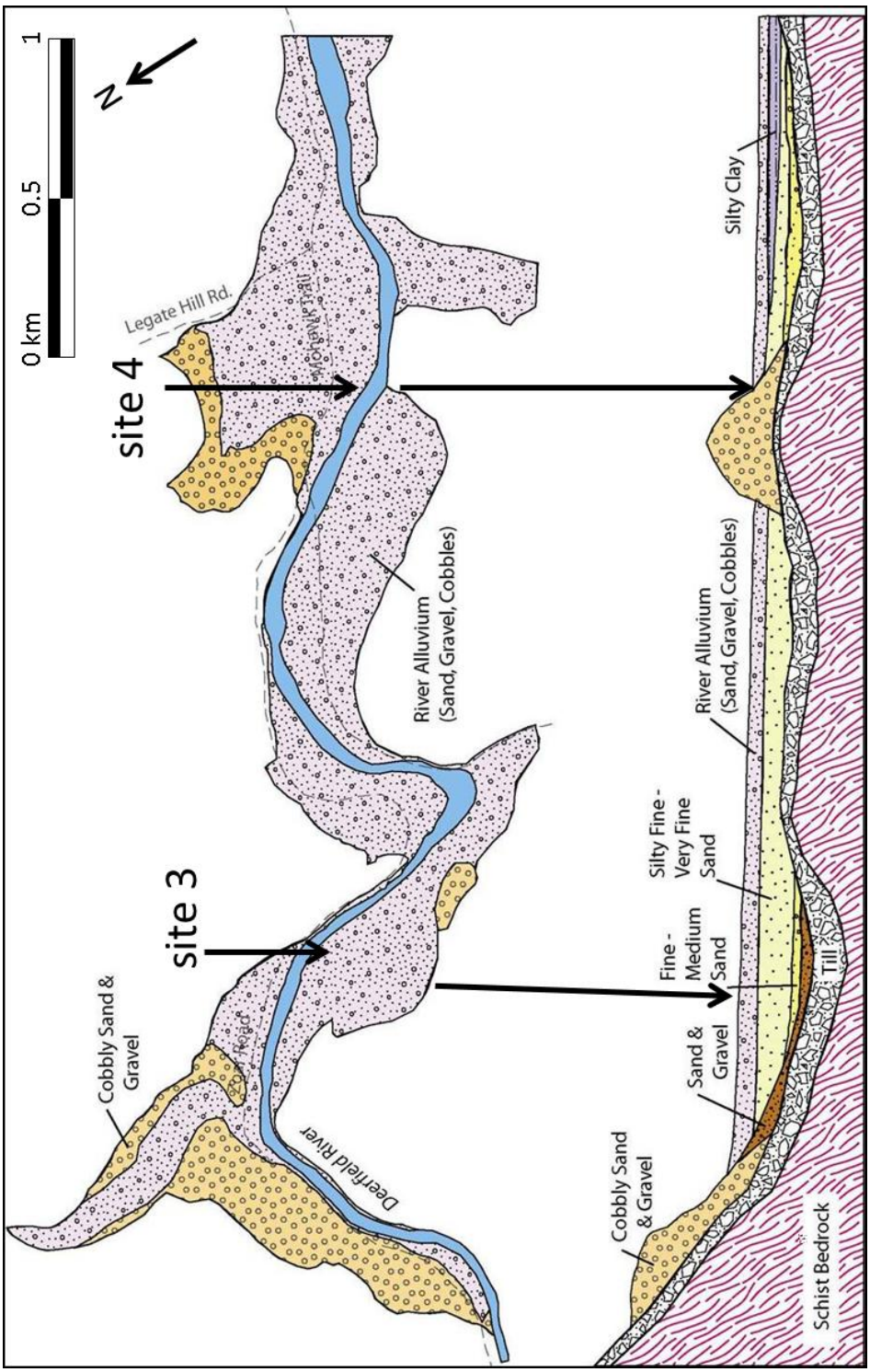

Figure 1.3 – map view (left) and cross section view (right) of surficial geology of the lower two thirds of the study reach showing the glaciofluvial and glaciolacustrine deposits that fill the over-deepened bedrock valley (modified from Mabee et al., 2007). The location of sites 3 and 4 are indicated by black arrows on both the map and cross section views.

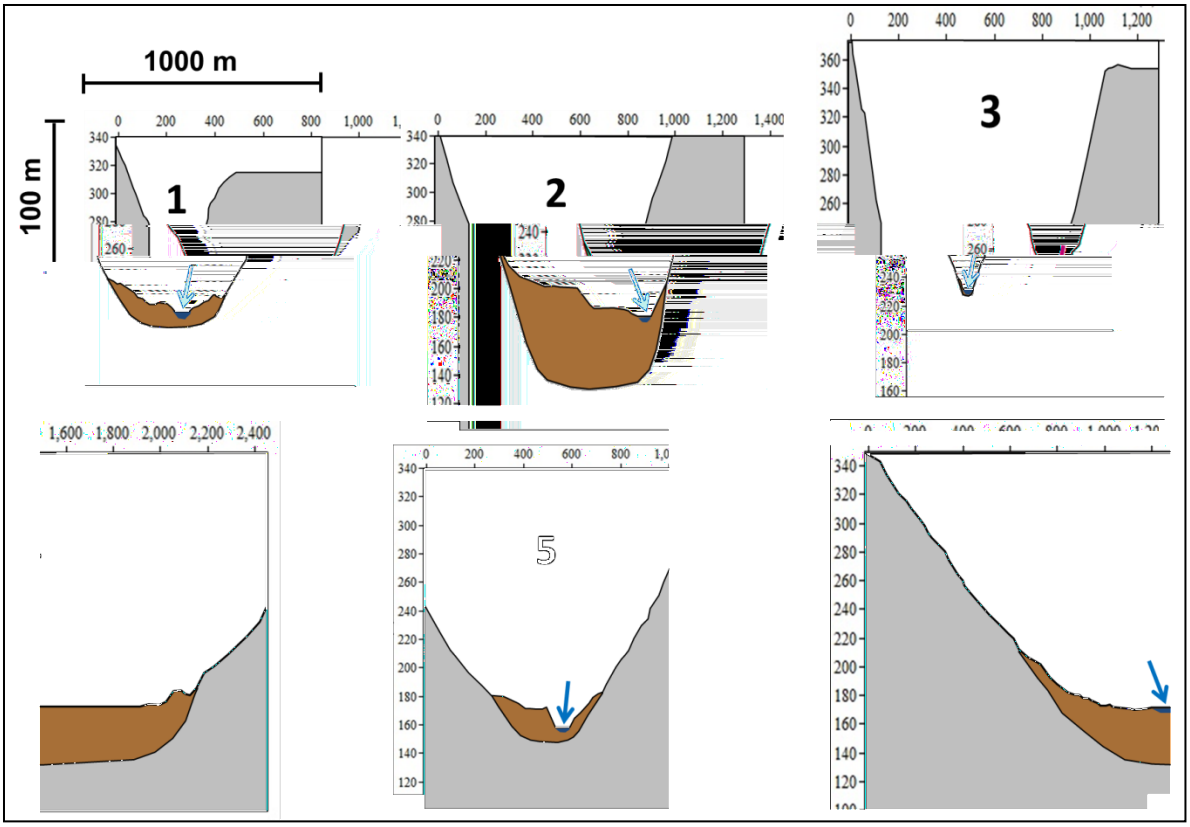

Figure 1.4 – Vertically exaggerated valley cross sections showing the extent of valley fill (brown) overlying bedrock (grey) at the five main-stem study sites. The river location is shown in blue and denoted by an arrow. The scales are consistent for all images and are 6.3 times vertically exaggerated.

CHAPTER 2

WATER BUDGET APPROACH

Introduction

A water budget is a simple tool that accounts for inputs to and outputs from a system. Any difference between inputs and outputs represents a change in the total water mass –or storage – of the system. In most watersheds, where surface water bodies account for a small percentage of total watershed area, changes in storage are largest within the voluminous subsurface where water moves at slower rates than at the surface. A typical water budget for a specific watershed might account for net precipitation inputs (P) and outputs by streams (Q) and evapotranspiration (ET). When P > [Q + ET] water has been stored in the system as either soil moisture or a head increase within the saturated zone.

Over longer durations, changes in storage go to zero and all P can be accounted for by Q, ET and in some cases, groundwater flow out of the basin. A water budget approach is so valuable because it provides an estimate of changes in water mass in the subsurface without direct measurements of soil moisture or changes in head which can be highly spatially and temporally heterogeneous making accurate field sampling nearly impossible at large scales.

In this study, a water budget is used to evaluate how stream water interacts with the underlying valley aquifer as it flows down a 19.5km reach of the DFR. Comparisons of Q at the upstream and downstream ends of the reach revealed that downstream Q during the summer is consistently smaller than that upstream. In temperate New England where most streams are gaining, this finding was unexpected, especially given that four significant tributaries enter the DFR within the study reach, increasing the watershed area by 40% between gaging stations.

A water budget was constructed for the system to estimate losses from the river to the groundwater (GW) system by accounting for measurable fluxes into and out of the system. We

focus on rain-free periods because this study is not concerned with water yield or the fate of P inputs, but rather the water already in the river. Focusing on periods dominated by base flow contributions minimizes error associated with tributary rating curves. We also wanted a time when regional hydraulic gradients towards the stream were minimized (or absent we found upon closer look). The water budget equation used is shown below.

$$GW = output - input \quad [2.1]$$

$$GW = (Q_{dn} + E) - (Q_{up} + Q_{trib}) \quad [2.2]$$

where Q_{up} is discharge 100m downstream of the Fife Brook dam, Q_{trib} is the combined discharge of the four largest tributaries in the reach, Q_{dn} is discharge at the downstream end of the reach and E is direct evaporation from the surface of the DFR (Figure 2.1 –). GW, the difference between inputs and outputs, represents changes in storage of the groundwater system. The two terms on the right side of equation 2.2 are reversed from general convention in order that negative GW values indicate times when the river was losing water to the groundwater system. A negative mass balance at daily time-scales was constant and detected during two different field seasons. The negative GW term is often referred to herein simply as "loss" from the river system. A detailed description of water budget component estimation is given below for each of the terms in equation 2.2.

Inputs

This project accounted for two main inputs to the 20km study reach: 1) water released from the Fife Brook Dam at the upper end of the reach; 2) water entering the reach from four main tributaries. Because only precipitation-free time periods were chosen for water budget

analysis, accounting for direct precipitation inputs was not necessary. Groundwater inputs were not directly approximated as they would represent the residual of the water balance.

Upstream Discharge - Q_{up}

Upstream discharge data for the 2010 summer field season were obtained from the utility sector. Discharge was measured directly below the Fife Brook dam, just downstream of the confluence of Fife Brook tributary with the main stem of the Deerfield River. Discharge values are reported every 15 minutes. Frequent calibration of the discharge-stage relationship at this location has shown measurement error consistently below and often far below 5%. Values from this data set have been used for calculations, but are not disclosed herein.

Prior to securing 2010 dam release data, a publicly available 2005 discharge record from the same site as above was used to perform preliminary water budget calculations. This required creating a rating curve that related observed tributary flows from 2010 to a USGS gauge on a local, unregulated basin. This process will be described below. Gaps in the 2005 data were removed and only continuous records were analyzed.

Tributary Data - Q_{trib}

Beginning in May of 2010, discharge gauging stations were established on the three largest tributaries that enter the Deerfield River in the study reach: Cold River, Chickley River and Pelham Brook (see table 1). Mill Brook was not directly measured due to limited equipment. Historical data (Hansen et al., 1973) were used to relate Mill river discharge to that of Pelham Brook. A total of six simultaneous discharge values for the two drainages showed that Mill Brook discharge was on average 0.736 of Pelham Brook discharge (figure 2.2). The Pelham Brook discharge record was multiplied by this factor to simulate a Mill Brook discharge record. While this is not a particularly sophisticated technique for reconstructing discharge, it is suitable in this case given that these two streams account for less than 0.5% of the total system

flux during summer baseflow conditions. These two small (~31km^2) drainages are immediately adjacent and should therefore receive similar rainfall. Similar topography and land-use assure that discharge records resemble one another.

The three directly gauged tributaries plus Mill Brook accounted for 79.7% of the increase in watershed area between the upstream and downstream DFR gauge sites. Small, low order streams make up the remaining unaccounted drainage area. Because it would be impractical to measure every small stream, this measurement error was accepted. Were one to correct for the unaccounted area by scaling total discharge up by roughly 20%, total tributary discharge would be greater and increase the "inputs" term of the water budget equation. Increasing the input side of equation 2.1 would make the GW term more negative and make the magnitude of calculated losses from the system greater.

Three discharge-stage data points establish rating curves for each gauged tributary (figure 2.3). While this is a relatively small number of measurements, because only precipitation-free periods during typically low discharge summer months were used, a less-robust stage-discharge relationship was acceptable. Furthermore, the small relative contribution to the system further minimizes the error associated with modestly fit rating curves.

Each gauging station consisted of two stage datums: 1) a graduated stake; 2) a large (> 1m diameter), immovable rock which could be used for stage measurement. The rock was chosen for corroboration since all the gauging sites were accessible to the public and the graduated stakes were susceptible to tampering. Comparison with the fixed boulder data indicated that none of the stakes were compromised during the time when rating curves were established.

Absolute pressure transducers (Solinst Levelogger Model 3001; resolution = 3mm) in the three gauged tributaries recorded ongoing stage measurements every 15 minutes throughout the summer research season. Each pressure transducer was fastened to a rock and then submerged to a depth of ~30cm and placed in a crevasse below a large boulder. This method assured that instruments would not be tampered with or stolen. A subaerial pressure transducer of the same specifications as above recorded atmospheric pressure changes at Mohawk State Forest (site 3). The Pelham Brook pressure transducer was removed on June 25, 2010 when it was needed elsewhere in the study. It was determined that a long enough record had been established to allow for correlation with Cold River (figure 2.4).

All tributary stage records were first cleaned by subtracting the value of atmospheric pressure obtained from the subaerial pressure transducer. Barometric pressure values were checked against a nearby Ashfield, MA meteorological record and matched well. An observed stage value recording the river's stage on the graduated stake was used to reference the pressure transducer record. The difference between unreferenced measured value and observed value was removed by adding a constant to the entire stage record. Last, a unique discharge-stage relationship was used to calculate discharge from stage records. All tributary Q records were then summed to arrive at a Q_{trib} time series.

For analyses during the 2005 field season, it was necessary to interpolate a Q_{trib} record since no direct observational data from the four gauged tributaries were available. A long-term USGS discharge record from a nearby unregulated basin with very similar land use and geomorphic characteristics (North River - Colrain, MA) was compared to the Q_{trib} record for 2010. A quadratic relationship was used to relate Q_{trib} to the long-term North River record and simulate a 2005 record for Q_{trib}. The simulated Q_{trib} record erred by an average of 23% from the observed record (figure 2.5). While this error is large, its significance is minimized by the small

Q_{trib} contribution of total Q. Q_{trib} made up less than 10% of daily Q_{dn} volume. Therefore, a 23% error in this small component represents less than 3% error in terms of the total system for 2005 analyses.

Outputs

Downstream Discharge - Q_{dn}

Instantaneous Q measurements taken at 15 minute intervals were downloaded from a USGS gauge (site 01168500) in Charlemont, MA, 19.5km downstream from the Q_{up} site. The USGS periodically checks accuracy of stage gauges and rating curves. Reported error during the summer of 2005 period of analyses was 3.8% and that for the 2010 analyses was 0.7%.

Evaporation - E

Steve Sauter of Ashfield, MA provided 10 minute tabulated weather data from his home weather station located at a distance of 11km from the USGS gauge in Charlemont (Q_{dn}) and 20km from the Fife Brook Dam (Q_{up}). Temperature, relative humidity, incoming radiation and wind speed records were compared to simultaneous data from a weather station in Greenfield, MA (20-30 km from river reach) to validate the reliability of these data. Trends in all records matched well at hourly and monthly timescales.

Because this study primarily concerns water in the river and not that within the entire watershed, only direct evaporation from the river surface was considered. Several empirical and physically based methods have been developed to estimate evaporation based on various weather parameters. The Penman (1948) method of estimating evaporation based on net energy balance and aerodynamic parameters has become the standard for engineering applications (Dingman, 1994). Due to a lack of all data parameters required for the Penman method, a simplified version of the equation (Valiantzas, 2006) was employed. This simplified method required time series of temperature, relative humidity, incoming solar radiation at the

earth's surface and upper atmosphere and wind speed. Evaporation is calculated as the difference between an incoming energy term and outgoing energy term plus another term that represents aerodynamic resistance.

The Valiantzas (2006) method was followed exactly except for the R_a term describing solar radiation incident at the surface of the atmosphere. This parameter was estimated using the established relationship

$$0.75R_a \approx R_s \quad [2.3]$$

where R_s is incident radiation at earth's surface on a cloud-free day. Cloudless days were selected by visually inspecting the solar radiation records and choosing a day with minimal deviation from a predicted bell-shaped record. Any deviation from the predicted curve was corrected with a linear function between neighboring sections of the curve. Maximum R_a for July 5 using this method was 0.078 MJ/m^2/min, 5% below the extraterrestrial solar constant. The small discrepancy can be explained by the slightly oblique summer sun angle in this location 20º north of the Tropic of Cancer and indicates that equation 2.3 closely estimated R_a.

Analysis

Rain free periods of a week or more were identified during the summers of 2005 and 2010 for which we had reliable data to account for water budget inputs (see table 2.2). Because flood wave propagation takes a finite amount of time, simultaneous discharge records show a lag in the downstream response to a given dam release (figure 2.6). Asynchronous responses to dam releases necessitated modification of Equation 2.2 to calculate net gains or losses from the groundwater system over daily to weekly analysis periods. Each component of the water budget was lagged behind Q_{up}. Q_{dn} was lagged by 4.5h, which corresponded to the average time it took a 25m^3/s pulse to travel the reach. E and Q_{trib} were each lagged 2h to provide average values of the duration of a given flood wave to travel the entire study reach. When integrating

over multiple-day analytical periods, these time lags should be irrelevant. When analyzing individual flood events, they may affect calculations.

In order to ascertain to what extent different variables drive the system, individual dam-release events were delineated (figure 2.6). Each event's beginning and end was denoted by a departure and subsequent return to minimum baseflow releases from Fife Brook Dam. Values were calculated for each water budget component for given release events and summed to evaluate the extent of loss for individual dam periods. In this way, data points could be parsed from the various time series described in equation 2.2. By creating several individual data points, the results of the water balance equation could be compared to potential drivers.

Results

The DFR study reach consistently loses water to the adjacent aquifer over 24h periods during summer months. Several week-long summations of the GW term in equation 2.1 during different summer months across two different years all show water losses from the river system to the groundwater system (table 2.2). Given the combination of New England's temperate climate and the reach's expansive till-mantled upland watershed draining towards the valley fill aquifer (figure 2.1)**,** one would expect the water table to slope towards the river and drive water there. Computation of the water budget during April or May indicates that this is the case in the spring (figure 2.7). However, persistent losses from the river system during dry summer periods suggest that some mechanism, in concert with abrupt stage changes, drives water permanently away from the river.

A time series of the GW term of equation 2.1 shows a clear negative trend in the magnitude of temporary gaining periods throughout summer of 2010 (figure 2.9). Short gaining periods occur at the beginning of the low stage phase of the near sinusoidal discharge series. As discussed earlier, the drop in stage causes a local temporary head gradient reversal back

towards the river. Sharp excursions from the steady decrease in the GW term are explained by hydrograph spikes in the Q_{trib} record (figure 2.8). Lack of tributary stage-discharge data points at high stage values makes the magnitudes of these displayed hydrograph spikes uncertain. If water entering from tributaries was more accurately measured at high stage, these excursions of the GW time series would likely be much smaller.

Two possible mechanisms may explain permanent losses from the river: A) stage increases drive water into long-term groundwater storage; B) transpiration by riparian vegetation removes water from the aquifer allowing for repeated losses. Correlation between the amount of loss for individual flood events and several independent variables was tested. The variables tested were: (1) the magnitude of the stage change for an individual event; (2) the duration of the elevated stage event; (3) evaporative flux from the river as a proxy for potential evapotranspiration by riparian vegetation.

It was hypothesized that a higher hydraulic gradient away from the river caused by a larger dam release would drive more water into the riparian aquifer and therefore correlate well with reach-scale loss. However, the August 2005 analysis period showed no correlation between the changes in discharge from before to during a dam release and the amount of loss for that release (figure 2.10). The duration of high discharge events varied a great deal from as short as 7h to as long as 24h. A longer period of time during which high stage caused a hydraulic gradient away from the river would drive more water out of the river. Two events extending well into the following calendar day were considered outliers and discarded. Duration of dam release versus reach-scale loss was plotted for the remaining eight events for this rain-free period (figure 2.11). A tight cluster of data points around 7.5h with no visible trend indicated that flood duration did not adequately explain the variation in the amount of loss for a given event.

Last, ET from riparian vegetation was invoked to explain persistent losses throughout the summer. Because vegetative transpiration data were not available, direct evaporation from the DFR study reach surface was used as a proxy for ET forcing. Generally shallow water tables in the riparian zone, bolstered by daily bank storage events make it likely that riparian vegetation exists in an energy, rather than moisture-limited growing regime. Therefore, evaporation from an open water surface calculated using an available energy method such as Penman (1948) provides sufficient approximation of AET from riparian forests. Although evaporation rate did not correlate well with total reach-scale loss, total estimated volumetric evaporation from the study reach displayed a strong relationship (R^2=0.65) with reach loss (figure 2.12).

Total volumetric evaporation calculated as the product of linear evaporation rate, area of the study reach and duration of the flood proved to be a better causal variable for two reasons: (1) total evaporation factored in the effects of evaporative forcing as well as the duration of the event – a longer event would permit more evaporation to occur – and (2) removal of water from the riparian aquifer was necessary to explain persistent and increasing losses throughout the summer. Thus, total evaporation was really an incorporator of both natural evaporative variables and human-controlled flood duration.

A faulty downstream gauge could provide an alternate explanation for why inputs to the river reach exceed outputs. If either the upstream gauge overestimated discharge or the downstream gauge underestimated discharge, the GW term in equation 2.1 would be driven towards the negative side. However, separate pieces of evidence indicate that faulty rating curves or gauges cannot explain the perceived losses. The upstream gauge underwent a complete overhaul in 2008 (Brett Towler, personal communication, April 27, 2011). Several tests against the amount of electricity produced as well as direct flow observations confirmed

the gauge and rating curve's accuracy. Prior to 2008, it was noted that the rating curve underestimated the amount of water being released upstream. More water was released than that which was reported. Therefore, 2005 analyses could be driven more negative were the new rating curve applied. The consulting firm responsible for the rating curve calibration would not release information to adjust old discharge data.

Underestimation of Q_{dn} at the downstream gauge is unlikely given accuracy data reported by the USGS and results of equation 2.1 during periods of recharge. USGS reported anywhere from 3.8% overestimation to 0.7% underestimation during the analysis periods (table 2.2). Neither correction when applied to equation 2.2 changed results of the analysis significantly. Because the error may not apply at all stage conditions due to the irregularity and changing nature of the river bottom, error was not applied to final analyses reported in table 2.2. Further evidence that the gauges were accurate was found when the first week of May 2005 was analyzed. During this spring recharge period prior to leaf-out, Q_{dn} exceeded [Q_{up} + Q_{trib}] by 19.8%, indicating that the river is indeed gaining during the spring.

Discussion

This water budget approach to understanding the effects of hydropeaking on SWGW interactions suggests that the DFR study reach loses water as a result of hydroelectric management practices, perhaps in concert with the effects of riparian vegetation. Comparison with the adjacent and geomorphologically similar, but minimally regulated Westfield River watershed (figure 2.13) shows the impact on summer flows in the DFR. Although at respective gage sites the DFR watershed area is 62% than that of the Westfield, its July and August discharge exceeds the Westfield's by 67%.

Juxtaposition of a relatively smaller watershed and larger discharge shows the extent to which the DFR's summer stage is elevated, thereby affecting the gradient across the SWGW

exchange zone. Whereas in-depth accounting of the DFR study reach shows inputs consistently exceeding outputs, Westfield River Q increased by an average of 72% in a 28 km reach between the confluence of its three main tributaries and the downstream gage during July and August 2010 (figure 2.13A). Although this increase was due in part to tributaries entering the Westfield, the watershed area only increases by 61%, smaller than the increase in Q. Moreover, the same analysis on the DFR study reach shows that over the course of the summer, Q_{dn} exactly equals Q_{up}, despite the watershed area increasing by 40% down the 19.5km study reach. The effect of upstream storage can be seen in the runoff generation for each river (figure 2.13B). When normalized for area, runoff from the DFR watershed nearly doubles that of the Westfield.

Previous temperate climate studies have documented the effects of riparian vegetation ET on both low-order streams (Gribovszki et a.,l 2008) and large alluvial plain systems (Krause et al., 2007). The significant role of ET suggested by this study on a large, hydropeaking river's in-stream flows, however is undocumented. Comparison with the Westfield River suggests that hydropeaking may be responsible for the losses from the river and correlation with evaporative forcing. One can imagine how hydropeaking and/or simply elevated summer Q could cause a normally gaining river to lose water. High stage events raise the water table adjacent to the river (figure 2.14). This in turn drives the capillary fringe higher allowing more vegetation to access water that would have been part of the river's Q.

At 40m distance from the bank, aquifer head has been observed to oscillate by as much as 10cm in response to dam releases. Over the course of each oscillation, media above the capillary fringe absorb water due to matric suction. Suction is sustained all summer by the cumulative effect of ET, which generally maintains an upward gradient towards the root zone, except during temporary rain-induced reversals when gravity drainage may occur. Due to capillary forces, most of the absorbed water will not drain when the high stage event ends.

Therefore, via hydropeaking, water availability in the riparian zone adjacent to these artificially high stage events can shift ET from a moisture-limited towards an energy-limited phenomenon. Each day's ET serves to maintain or intensify this gradient sucking water away from the river. ET from preceding days may play a role in the amount of loss for a given flood event due to its role removing water from the oscillating capillary fringe zone. Adjusting for the role of antecedent conditions in the correlation analysis might allow for an even better correlation between evaporative forcing and reach scale loss.

A time series of the GW term of equation 2.2 (figure 2.9) shows the cumulative effect of ET over the course of the summer. As the riparian aquifer is drawn progressively down by the seasonal effect of ET, the magnitude of brief, low-stage gaining periods decreases. By the end of summer, the river loses water almost continuously, even during low-stage events. Two factors cause a hydraulic gradient away from the river and make it nearly impossible for the river to gain even after dam release events. First, the cumulative effect of vegetative transpiration progressively removes water from the vadose zone, thereby increasing matric suction and removing water from the saturated zone and depressing the water table. Second, and unique to dam-controlled rivers, storage and suppression of the spring hydrograph in upstream reservoirs artificially subdues expected increases in head during the spring. Analysis of 2000-2008 reservoir storage volume time series indicates an average capture of 7.7e10 m^3, which if unaltered would equate to an average spring discharge increase of 12.23 m^3/s. Krause et al (2007) showed that in large order streams, surface water-groundwater dynamics play a larger role in changes in riparian aquifer head than direct precipitation inputs. Whereas most valleys experience a significant freshet during which high river stage induces bank storage and raises the riparian water table, the DFR begins summer already at a deficit because the freshet is dampened.

If hydropeaking indeed can induce a typically gaining river reach to lose water permanently, dam operators face a whole new set of considerations when drafting dam-release procedures. From an ecological standpoint, these results may be heartening. Short-term bank-storage from previous releases may bolster minimum flows via the contribution of groundwater, at least early in the summer. While increasing the total volume of low flows, this riparian zone water will further act as a thermal improvement due to its relatively lower temperature. However, during late summer, broader seasonal drawdown of the riparian aquifer would negate this benefit due to reversal of the hydraulic gradient away from the river at nearly all times in the flood cycle.

In deregulated energy markets, optimization techniques tend to favor larger releases on days with greater demand and therefore higher energy prices (Shawwash and Siu, 2000). However, in light of the finding that up to 10% of this water may disappear from the system for every 20 km it travels, in some contexts it might be prudent to release less water than current practices call for. Of course, these changes to optimization methods will depend on downstream geomorphologic conditions, regional flood threat, head-drop at various facilities and other factors. Indeed, constrained river systems with bedrock channels will likely see little loss if the interpretation about riparian vegetation above holds true. Nevertheless, hydro operators in most watersheds face an unforeseen tradeoff to making large releases on hot days with high evaporative demand.

Conclusion

Water budget analysis shows incontrovertibly that the DFR study reach loses water, whereas an unregulated analogue (Westfield River) does not. Cross correlations with reach losses suggest that the duration of high stage events and the amount of evaporative forcing may explain in part the cause of the loss. However, limited field data from the riparian aquifer makes

it hard to draw confident conclusions. In a controlled environment where variables can be changed one at a time, stronger causal links could be made between reach losses and hydropeaking as it operates in concert with different natural variables. The next chapter will discuss two-dimensional modeling efforts to simulate the river-aquifer system and identify the causes of reach-scale losses.

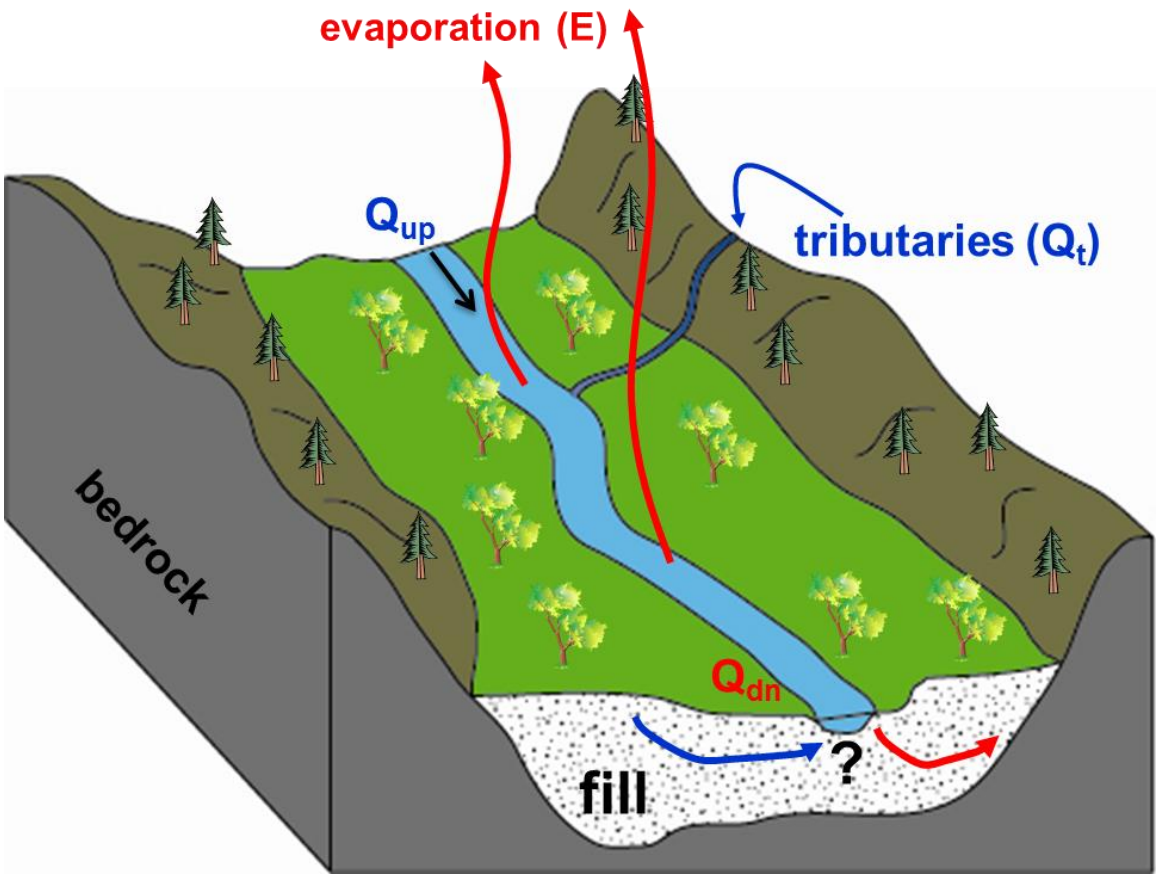

Figure 2.1 – A schematic of the water budget equation [2.2] showing inputs and outputs. Arrows in the riparian aquifer show the GW term and indicate the uncertainty with its direction depending on time.

	Chickley River	Cold River	Pelham Brook	Mill Brook	Other areas
Watershed Area (km^2)	70.0	83.0	30.9	30.7	54.6
% of total area	26.3	30.7	11.4	11.3	20.2
Avg baseflow (m^3/s)	0.18	0.21	0.09	0.08	NA

Table 2.1 - Attributes of DFR study reach tributary watersheds. Total area refers to the catchment of the Deerfield River between the upstream and downstream gauge sites.

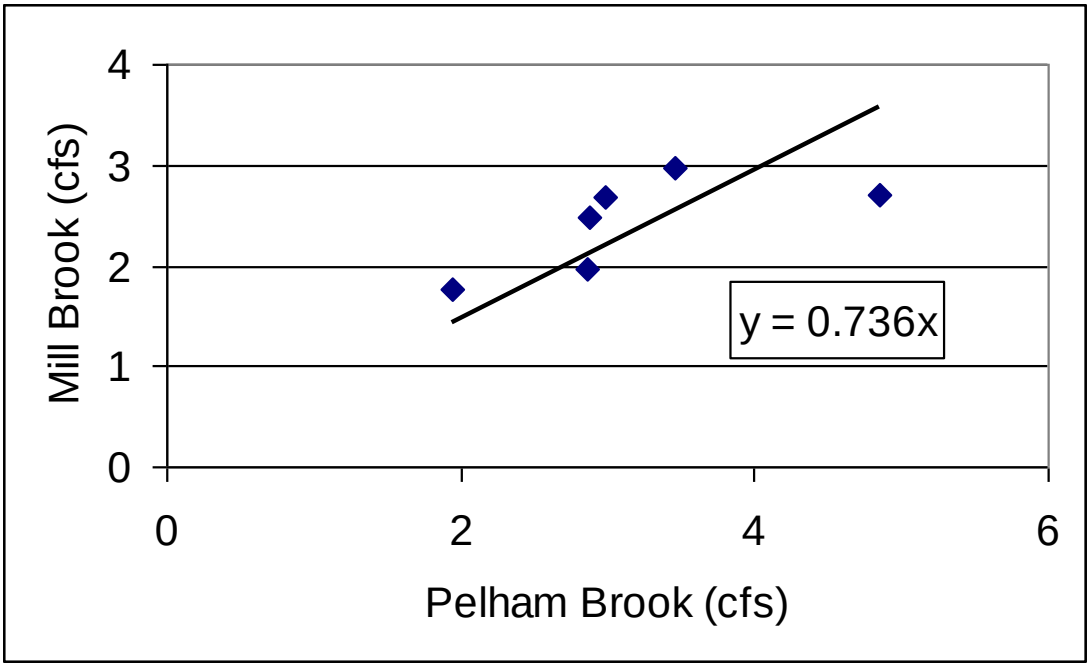

Figure 2.2 – Relationship relating Pelham Brook discharge to that of Mill Brook.

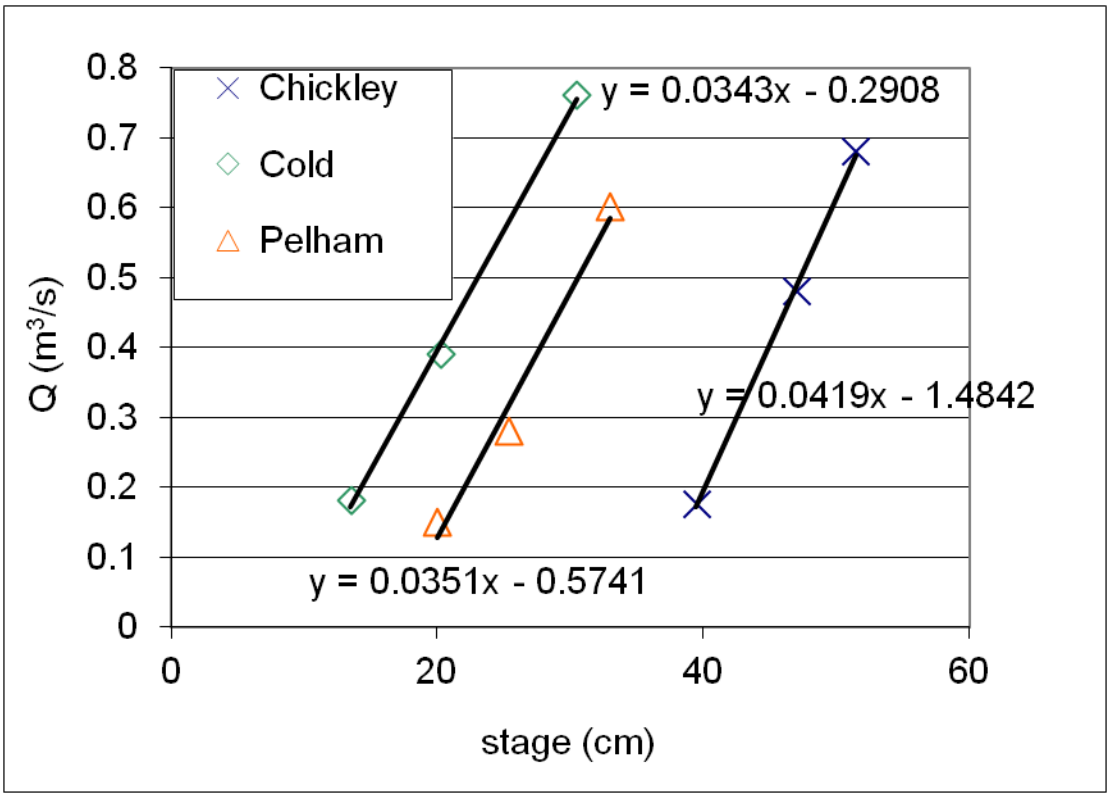

Figure 2.3 – Rating curves for the three main gaged tributaries in the DFR study reach. Equations relating stage to discharge are shown for each stream.

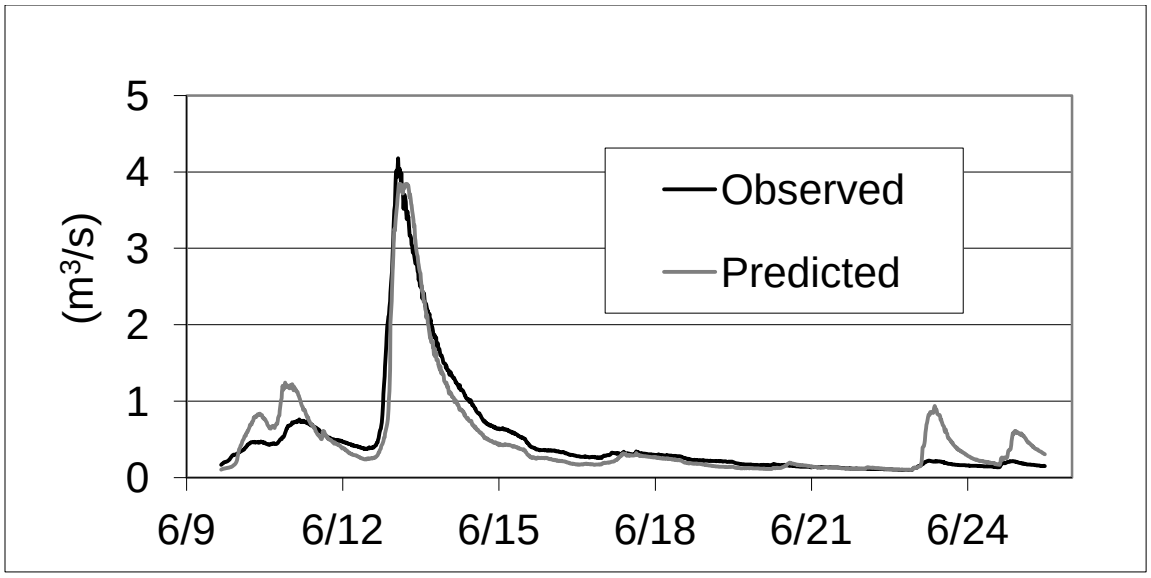

Figure 2.4 – Pelham Brook discharge prediction compared to observed data during the instrumented period prior to moving pressure transducer to another location.

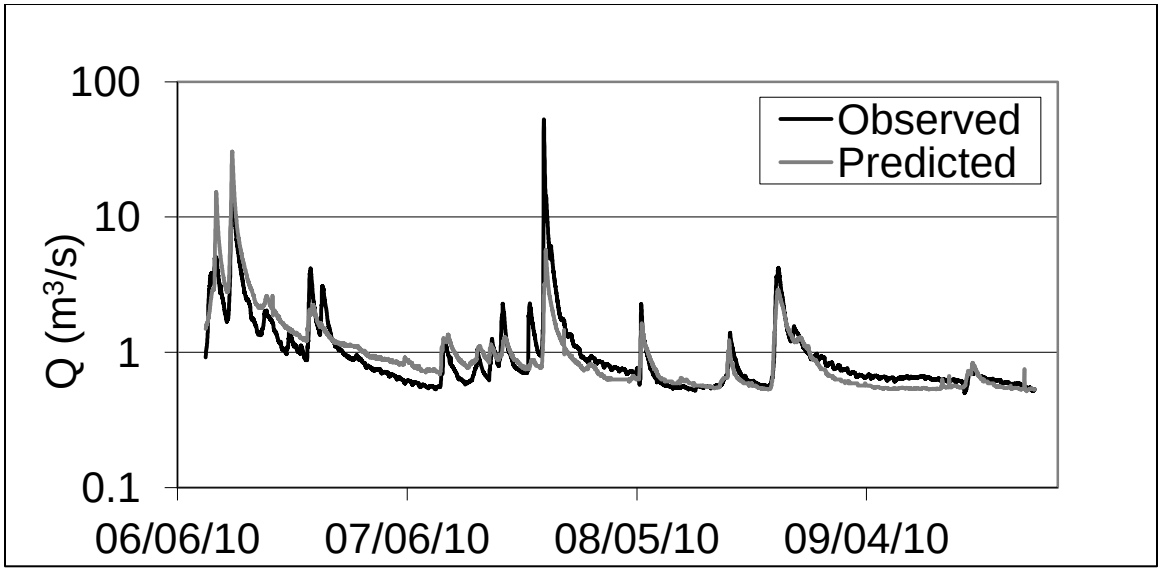

Figure 2.5 – Observed tributary Q compared to predicted flows based on a relationship with the North River Gauge.

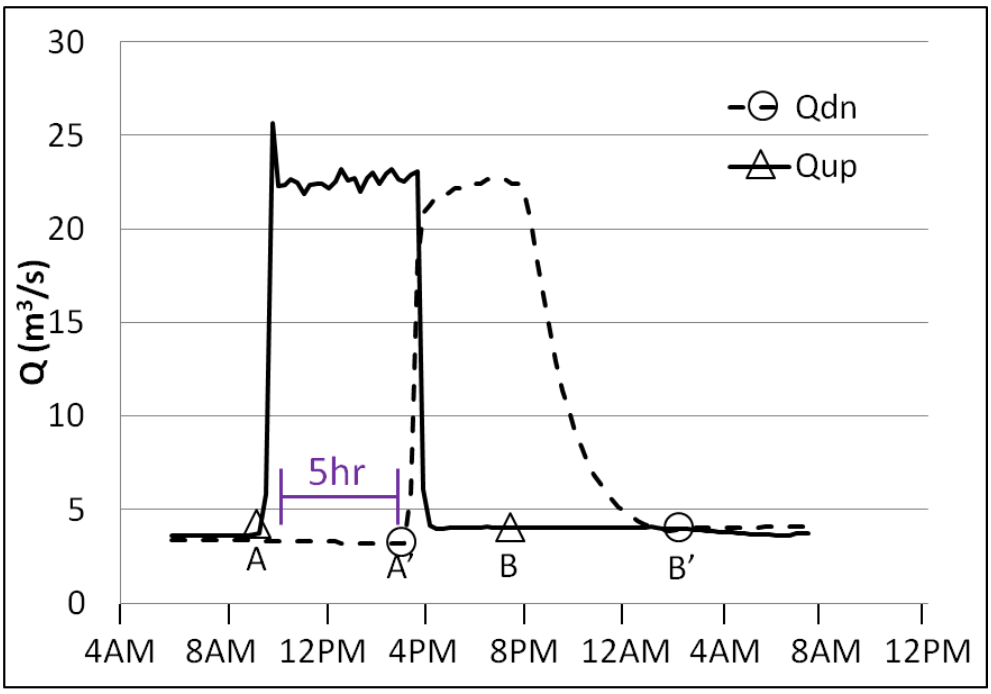

Figure 2.6 – Delineation of one flood event. Discharge records show downstream response to a dam release on 12 August, 2005. Note that a given flood event takes place upstream roughly 5hr before it appears at the downstream gage location (a lower than average discharge prolongs the lag here by 0.5h). For calculations done on individual flood events, the duration from A to B (Q_{up}) or from A' to B' (Q_{dn}) was defined by the return to baseflow at the downstream gauge.

	GW (m3/s)	Qdn (m3/s)	Qup (m3/s)	Qtrib (m3/s)	Avg E (m3/s)	Avg E (mm/d)
July 1-9, 2010	-0.99	13.27	13.75	0.64	0.117	12.92
Aug 8-16, 2010	-1.33	12.10	12.94	0.57	0.075	8.27
Sep 4-12, 2010	-0.93	6.39	6.75	0.65	0.085	9.44
Jul 22-30, 2005	-1.95	8.51	8.62	1.94	0.094	10.39
Aug 5-13, 2005	-1.52	8.38	8.85	1.13	0.083	9.20

Table 2.2 – Water budget values for five 9-day dry periods during 2005 and 2010. Evaporation rates are shown in both volume and length per time.

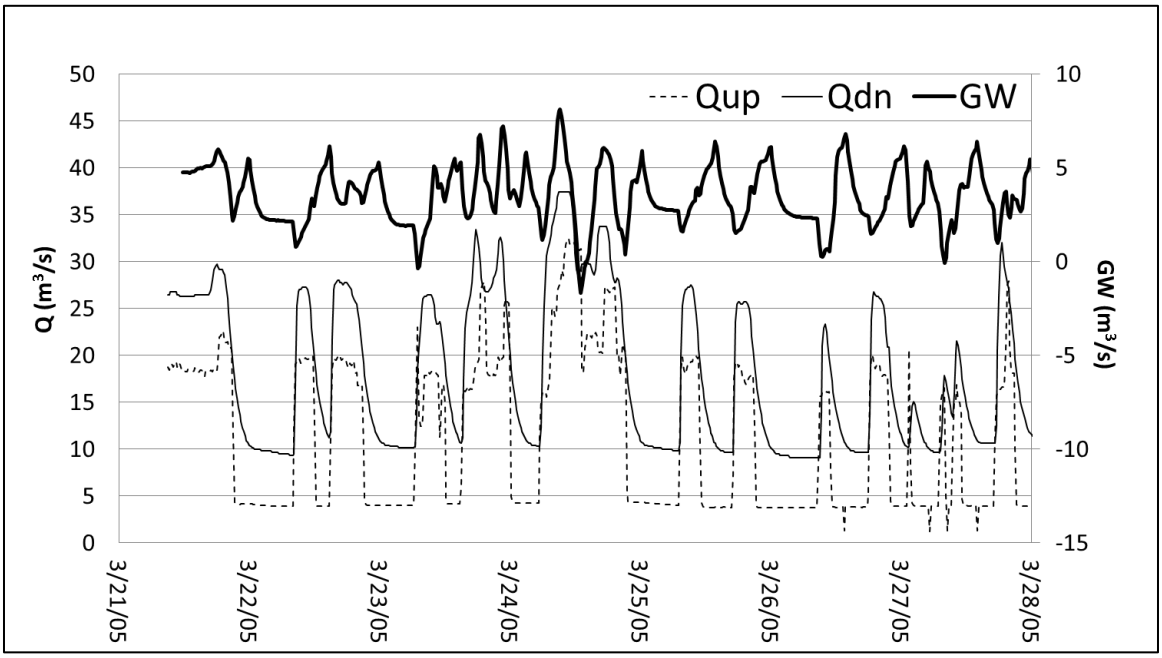

Figure 2.7 – Spring water budget analysis clearly shows a gaining river system evidenced by Q_{DN} consistently exceeding Q_{UP}. Q_{DN} has been lagged 4.5hr. The GW curve is the difference between system output (Q_{DN}) and the sum of Q_{UP} and Q_{trib} as reconstructed from the USGS North River gage (site 10). PET was not calculated during this time period and is therefore not included. PET would likely be very small due to limited thermal energy in March.

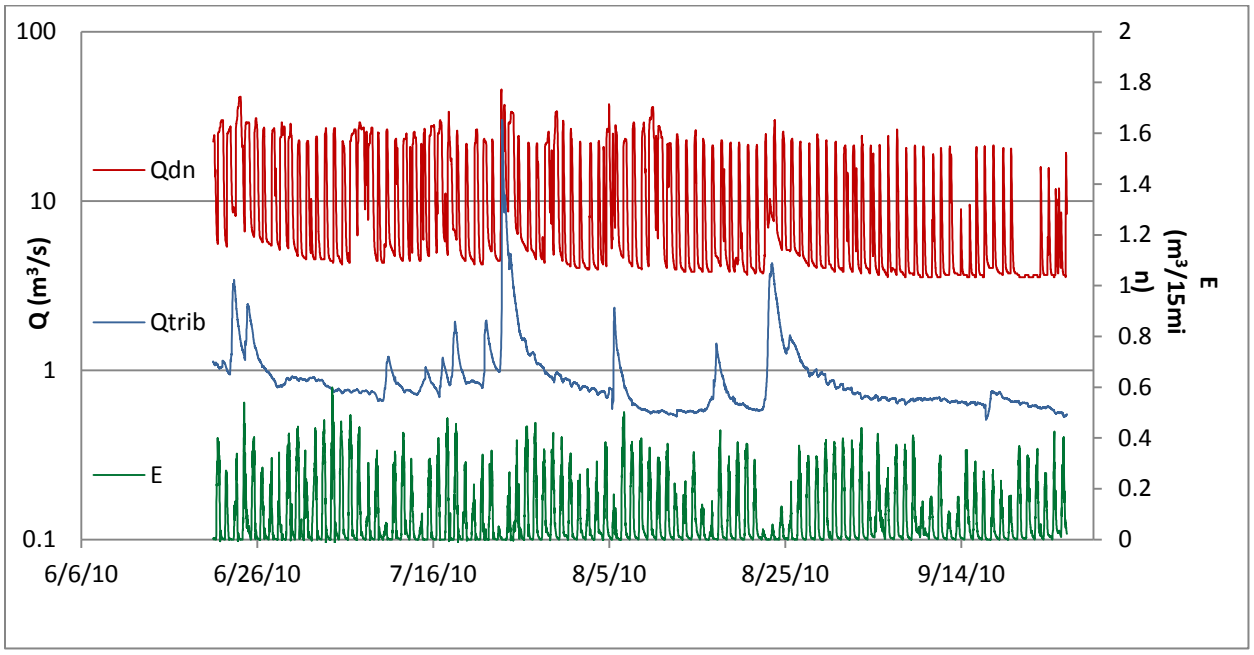

Figure2.8 – Components of the water budget during summer 2010.

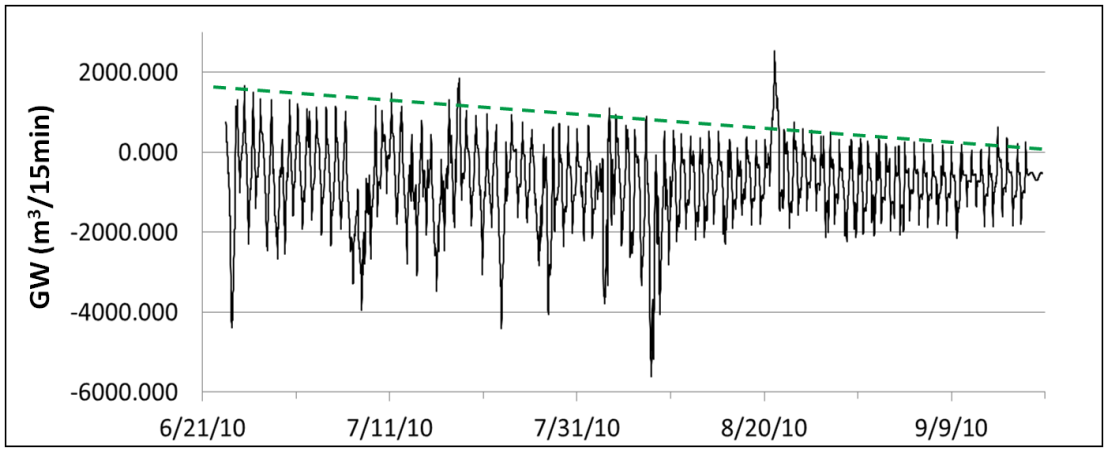

Figure 2.9 – A twelve hour moving average of time series of GW term from equation 2.1 shows a decline in the magnitude of temporary positive excursions. Dashed green line highlights this trend.

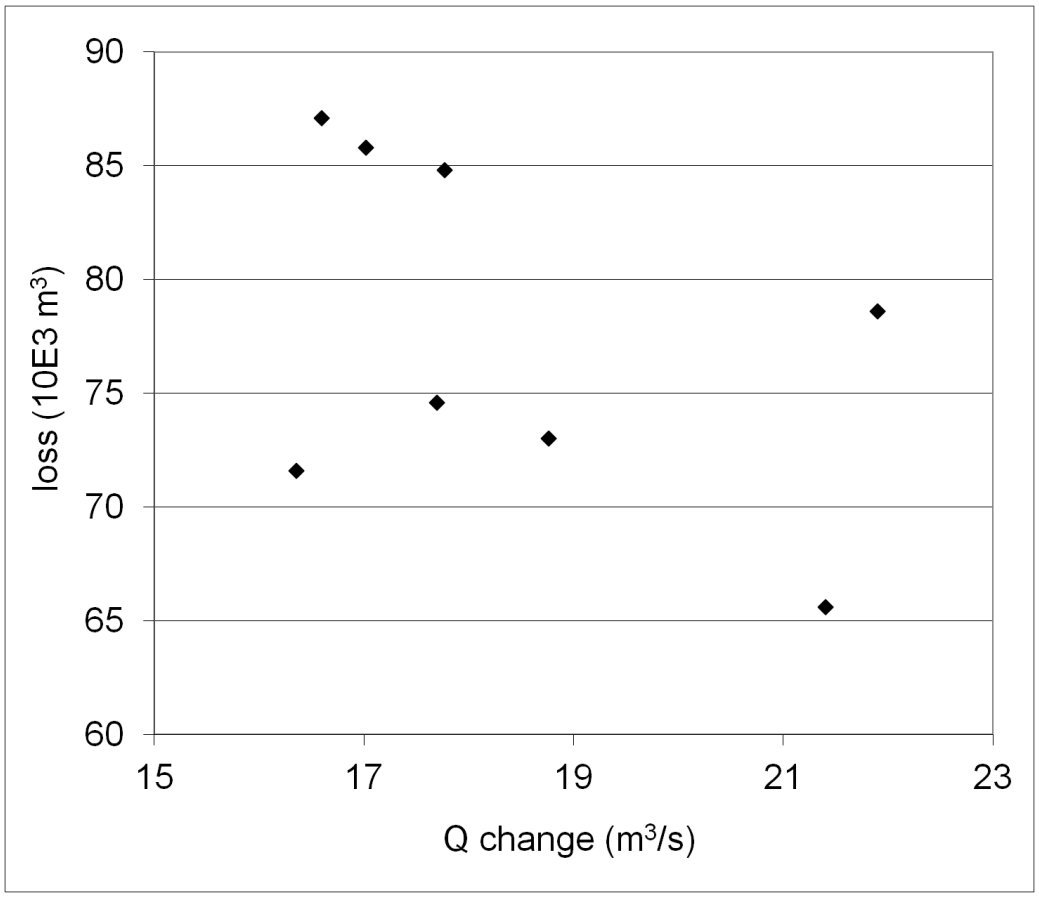

Figure 2.10 – No relationship was observed between the magnitude of change in discharge and the amount of loss.

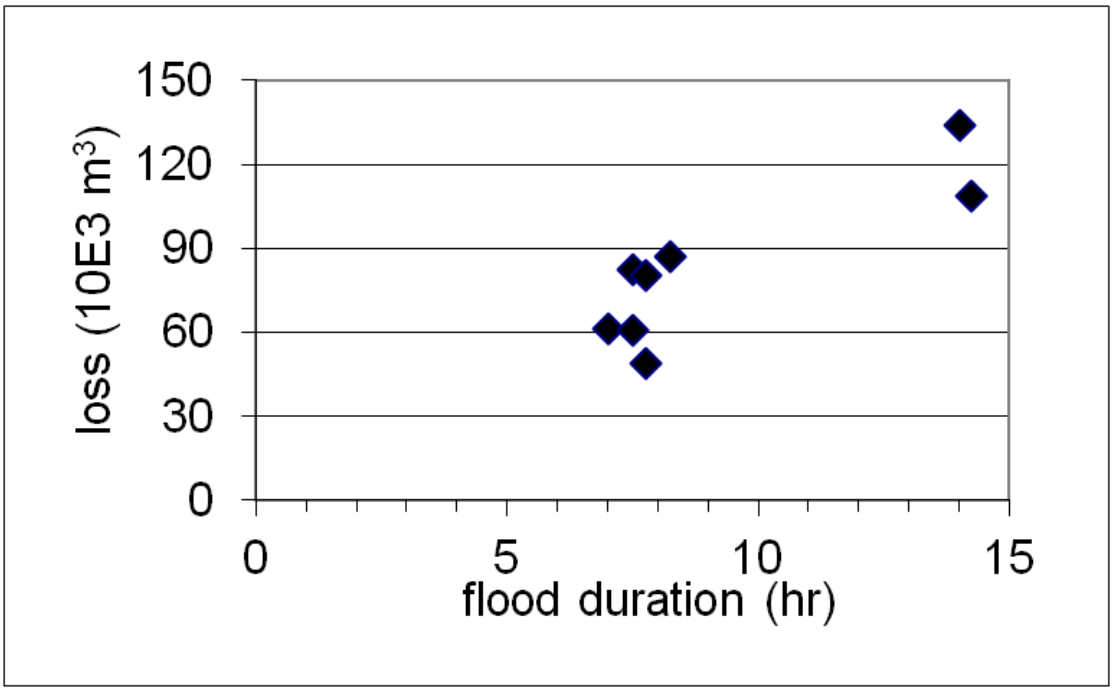

Figure 2.11 – A weak relationship between flood duration and reach-scale loss.

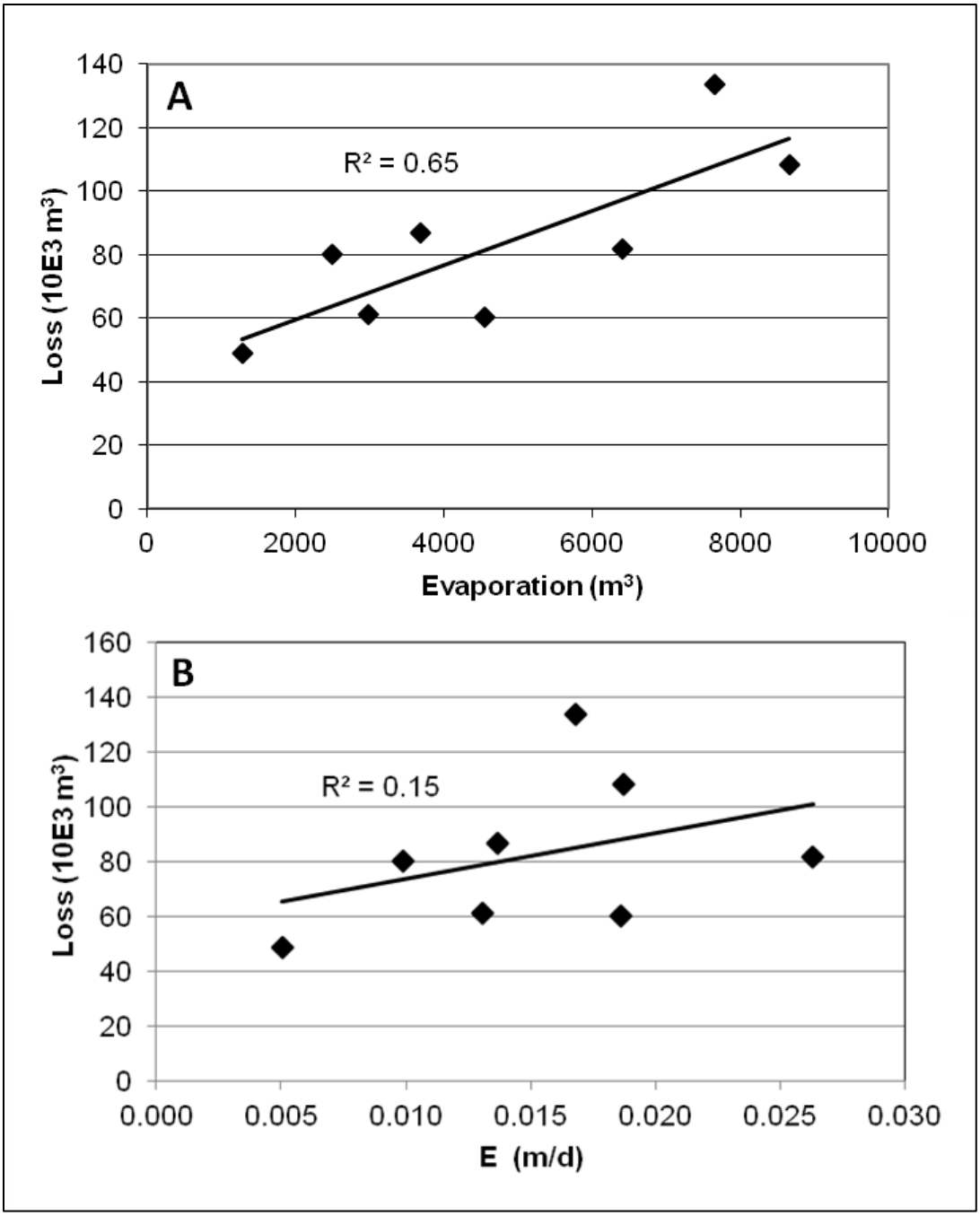

Figure 2.12 – (A) Note the robust relationship between volumetric evaporation from the river's surface for individual flood events plotted against total loss for each event. When loss is plotted against evaporation rate (B), the relationship remains positive, but the fit is much less significant.

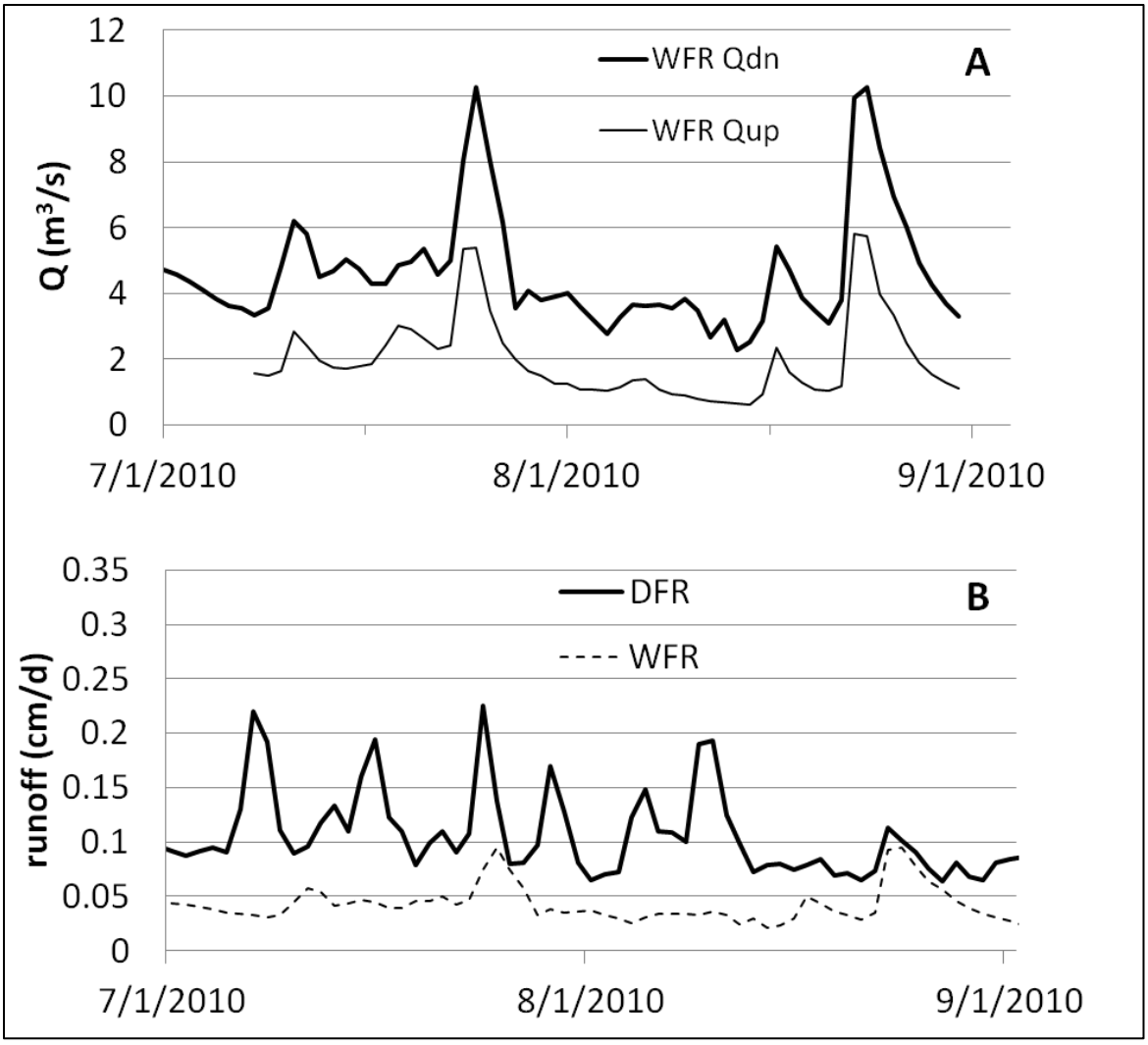

Figure 2.13 – (A) Upstream and downstream daily average discharge for the Westfield River not accounting for tributary inputs within the interim river reach. Note that discharge increases at all times. (B) Average daily runoff from Deerfield (DFR) and Westfield (WFR) Rivers. The DFR record always exceeds the WFR record.

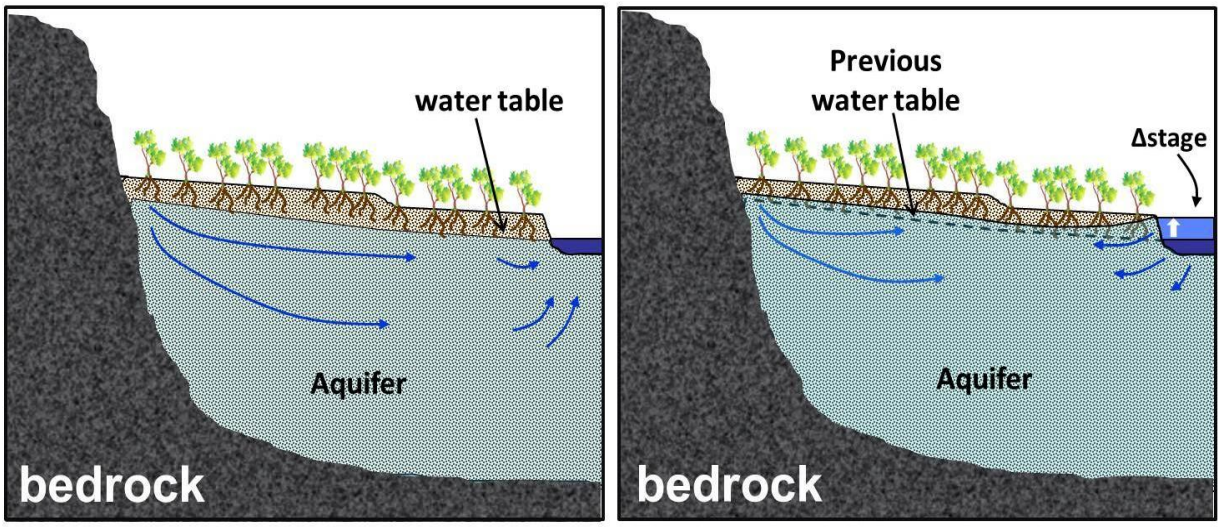

Figure 2.14 – Concept illustrating the differences between a natural riparian aquifer system (A) and one altered by hydropeaking (B). At right, a dam-induced stage increase causes the river to lose water. The dashed line enables comparison with the water table in a gaining system, typical of valley fill systems in temperate climates.

CHAPTER 3

RIPARIAN AQUIFER CROSS-SECTION MODELING

Introduction

In order to better understand field observations (detailed in the following chapter) and controls on SWGW interactions in the study reach, a series of two dimensional models of the DFR valley aquifer system was developed. The goals of the modeling experiments were to: 1) evaluate the potential to remove water from the river reach in volumes on the order of those calculated via water budget analyses; 2) test the sensitivity of the system to different internal physical characteristics and external forcing mechanisms.

Conceptual Framework

Water budget analysis of the study reach indicated that the river loses water to the groundwater system throughout the summer months when reservoir storage maintains abnormally high discharge and vegetation removes water from the coupled riparian aquifer and soil moisture. Loss to the riparian aquifer explained why inputs to the river exceeded outputs. Furthermore, three separate means of field observation supported this deductive conclusion from water budget type accounting. Monitoring wells adjacent to the river showed progressively lower head further from the river, indicating a hydraulic gradient away from the river. In-stream piezometers at five locations showed that in wider parts of the valley fill, the head in the river was often higher than that in the subsurface. Last, temperature probes in the streambed showed a close coupling between river and subsurface temperature, suggesting downward advection wherever that phenomenon was observed.

The two-dimensional (2D) physically-based model that was built provided a testing space where variables in the river-aquifer coupled system could be changed independently.

Factors that were believed to determine the extent of loss at a given point in the river were tested. Differing potential losses along the reach were explored by changing hydrogeological conditions in the models.

COMSOL multiphysics software was used to create a finite element mesh within a specified flow domain and to solve governing equations for saturated and unsaturated flow. At nodes within the mesh where pressure head < zero, this model used Richard's Equation, dependent on the hydraulic head at each node:

$$(C/\rho g + SeS/\rho g)\, dp/dt + \nabla \cdot (-K_s/(p_f g) k_r \nabla(p + \rho_f g D)) = Q_s$$

where:
ρ is the density of water
g is acceleration due to gravity
p_f is fluid pressure
S is storage
K_s is the saturated hydraulic conductivity
t is time
D is elevation above some datum in meters
Q_S is the change in storage
k_r is the permeability of unsaturated nodes
Se is a term that relates head to permeability when head < 0
C is a term that determines the pressure head of the node as a function of its water content

As k_r approaches 1, this reduces to Darcy's Law for saturated flow. Thus, when pressure head > zero, Darcy's law for saturated flow determined the change in storage of the system (see appendix 2 for full description of governing equations). Richard's equation was necessary to model changes in river stage that propagate into the bank media, continually saturating and partially draining the top of the riparian aquifer.

Each 2D model run was treated as a 1m thick cross section of a homogenous river-aquifer system. Model output quantities could then be converted to volumes and multiplied by the entire river reach to compare to loss values from the water budget analysis in part 1 of this study. Of course, the riparian aquifer does not have a fixed width down the reach. Model

calculations, therefore, can only be used to better understand natural processes, if not the precise geometry of the DFR valley.

Boundary Conditions

The boundaries of these models were set up to simulate the geometry of a typical New England post-glacial valley (figure 3.1). No flow boundaries along the left and bottom of the model simulate an over-deepened bedrock valley, subsequently filled with unconsolidated sediments. A bedrock seep provided most of the water flux in the system. The length of this seepage boundary varied depending on the geometry of the model, but its total flux was kept constant at $0.2 m^2/d$. This daily flux corresponds to a recharge rate of 0.5 mm/d falling on an average bedrock valley slope extending 400m from the valley floor to the ridge top.

One half of a hypothetical symmetrical valley was modeled. The right boundary, therefore, was no-flow due to the symmetry divide where groundwater flowpaths approach vertical. The slope of the land surface (top boundary) for various width aquifers was determined by a fixed elevation of 104m at the valley margin and 101m at the stream bank near the middle of the domain. Because only dry periods were considered in the water budget analyses, a bare minimum recharge value of 0.5 mm/d was applied to achieve realistic antecedent soil moisture conditions at the land surface. Without any recharge at all, surface conditions in model space were completely dry and caused instabilities during solving.

The bottom of the river, where SWGW exchange occurs, was modeled as a fixed head 20m long; equal to half the average width of the river within the study reach. A conductance value of 130 m^2/d based on observations in Friesz (1996) mediated flux across the river boundary. River bottom elevation was 99m above the arbitrary datum. River head oscillated in most transient model analyses between high (100.3m) and low stage (99.8m) for 0.5 d

increments (figure 3.2). In addition, control tests were performed in which river head did not vary during the duration of model time and stage was fixed at 100.05m, the average between high and low stage. During one steady state run, river stage equaled 99.8m at all times to simulate hypothetical summer conditions on an unregulated river where most of the annual discharge occurs during the spring instead of being stored and slowly released throughout the summer. One limitation of this BC was that it had a fixed length. In reality, the distance from bank to center of stream varies as a function of stage, with greatest distance at high stage and smallest distance at low stage. The possible effect of this limitation is discussed below.

Subdomains

The riparian aquifer was divided into two subdomains: (1) rooting zone and (2) valley fill (figure 3.1). The physical properties of these two zones were identical in all model runs. However, in order to simulate the effects of vegetation, water was removed from the rooting zone according to a transpiration function:

$$AET = E(\theta) * PET(t) \quad [3.1]$$

where actual evapotranspiration (AET) is the product of E, a ratio of actual to potential evapotranspiration as a function of the water content (θ) at each node and PET, the potential evapotranspiration at a given time (t) (figure 3.3). The function E(θ) is based on the transpiration reduction function reported by Metselaar and de Jong van Lier (2007) for medium to high density rooted sand and loam. They found that root water uptake equals PET at most medium to high water soil water content values, and decreases precipitously when $0.1 > \theta$.

PET(t) is a time series of evaporative demand spanning 9 rain-free days in July, 2010 taken from the water budget chapter of this study. When used to estimate plant water uptake, calculated Penman evaporation values are typically multiplied by a coefficient. Because no

published data were available for canopy forest, an average of 1 was taken from reported values for fruit orchards during mid-growing season (Allen et al., 1998). This is a conservative value considering that mature forests likely have a much higher leaf area index than orchards and more developed root zones.

In each model variation, the rooting zone subdomain stretches the length of the model's top surface and extends to a depth of 1m. In a global study of various biomes, Jackson et al (1996) found maximum temperate forest rooting depths in far excess of 1m, though the majority (60%) of roots was in the top 0.4m of soil. Despite the sparseness of roots below 0.4m, Lai and Katul (1999) found that deep roots compensate for shallow ones during times of water stress. Therefore, rather than add a depth dependent root transpiration function to $E(\theta)$, water removal from the root zone depended only on water content of the soil. If deep roots (>1m) in temperate mixed forest do indeed draw significant moisture from soil, this model may underestimate riparian ET and losses from the river system.

Procedure

Four model geometries were specified to capture a range of aquifer dimensions roughly based upon field conditions at the instrumented sites along the DFR study reach (figure 3.1). Aquifer width ranged from 100m to 1000m, with a constant horizontal to vertical ratio of 10:1, similar to field site dimensions.

Transient model runs, where river head and evaporative forcing changed continually, required initial conditions to start each run. An unrealistic initial condition could make subsequent transient model runs useless. For instance, a steep hydraulic gradient towards the river would cause the river to gain at all times, regardless of system forcing. To achieve realistic conditions, all model geometries were run in steady state at high (100m/d) and low (10m/d)

hydraulic conductivity (K) values to serve as an initial condition for subsequent transient models. Values for K were taken from Friesz (1996), representing two observed media in the Deerfield River valley. The river boundary for these steady state models was fixed at the average head value (h = 100.05m) for the time dependent river function that would be applied during the transient model run. ET from the rooting zone used the product of the E(θ) function and the average value of PET(t) from equation 3.1. Figure 3.5 shows the shape of the water table for the 500m wide model. Changing the river's head value from 100.05m to 99.8m causes the river to change from losing to gaining. The model geometry and conditions therefore make SWGW interactions very sensitive to changes in river stage.

Figure 3.6 shows initial condition head distribution and relative groundwater seepage velocities for the 500m wide model runs at K=10m/d. Note that head is highest at the riverbank (h=100.05m) and valley margin (h=101.4m). The root zone, especially distally from the river, shows up as an area of low head caused by negative pressure head values. The river is losing under steady state due to artificially elevated stage, which is theoretically maintained by partial storage of the spring freshet.

Models were run for 9 simulation days, during which time the integral of the vertical velocity across the river boundary was recorded. This integral gave a flux in units of m^2/d which were then multiplied by a conceptual thickness of 1m to convert each value to volume/time. Values from each time step were multiplied by the length of that time step, yielding the volume of water that passed up or down through the river bottom boundary for 1m of river reach in one half of a symmetrical valley. Multiplying this volume by two (to capture both halves of the modeled valley system) and then by the length of the study reach ($1.95E^4$ m), gave the total volume of water that entered and left the river during the 9 day model run. These calculations are summarized:

$$\text{Flux: } q = \int u \; dt \qquad \text{Volume: } \; loss = 2 \sum q * 1.95E4 \tag{3.2}$$

In addition to loss from the system, total hyporheic exchange was calculated by adding up the absolute values of the volumetric fluxes for the 9d model run.

$$hyporheic\ exchange = 2 \sum |q| * 1.95E4 \tag{3.3}$$

This value sheds light on how the flow regime in the hyporheic zone changed as a result of various model tests.

As mentioned earlier, although the length of the river boundary was fixed in model runs, the actual distance from bank to center of stream decreases at low stage due to the convex up shape of river channels. The area available for SWGW exchange, therefore, is smallest at low stage. Low stage corresponds with times when the river temporarily gains due to locally reversed hydraulic gradients back towards the river. Thus, by integrating over a boundary that is larger than field conditions, this method may overestimate returns to the river, thereby underestimating total reach loss.

Model Calibration

This modeling exercise was intended to help us understand a reach scale loss of water from the DFR. Because the area of interest spanned some 20 km down the valley encompassing various hydrogeological conditions, subdomain properties and boundary conditions were generalized. There is no single value for K or seepage for the entire reach, nor was it possible to estimate these parameters at the hundreds of locations that would have been necessary to accurately depict the system. Instead, initial Van Genuchten parameters and seepage values were chosen based on best estimates. These values were then adjusted until two conditions were met: (1) under oscillating river conditions, total reach loss approached values similar to

those observed; (2) at constant low stage, such as would prevail during July without reservoir storage, the river gained water at moderate to wide valley widths.

During summer, when ET and interception are at their maximum, valley fill aquifers in the Northeast gain most of their inputs from hill slope seepage at the valley margins. To arrive at a seepage value, the same recharge value of 0.0005 m/d was applied to the hill slope area of the valley. A map survey of 40 measurements on both sides of the river found an average distance from the valley bottom to the ridge top of roughly 400m excluding tributary valleys. Applying 0.0005 m/d recharge to a 400m hill slope yields 0.2 m^3/d per linear meter of valley wall. The seepage boundary at the left side of each model was therefore fixed at a value such that:

$$0.2 = l * s \qquad [3.4]$$

where *l* is the length of the boundary arc, which varied depending on the aquifer width, and *s* is the value of seepage in m/d.

Van Genuchten (1980) developed a closed-form equation to relate head (h) to K in unsaturated soils. Ideally, one uses a series of lab procedures to best fit three parameters, α, n and l. However, because this model would serve to simulate a large area with heterogeneous media, average values had to be chosen based on the shape of the soil water retention curve (figure 3.4). The default value of 0.5 was chosen for l due to model instabilities at other values. The α parameter, which determines at what suction θ begins to decrease and that at which no more water can be removed, was adjusted to match values reported by Van Genuchten (1980) for sandy media. Last, a value of 3 was selected as optimal for n because it achieved a steep curve spanning less than two orders of magnitude in head within its steeply sloped interval, similar to those reported by Charbennau et al (1999) for coarse media. However, due to model

instability, this value had to be decreased to 2, allowing the soil to exert greater suction than is likely in field conditions assuming that the grain size distribution of the upper layers of the riparian aquifer is mostly sand and coarser.

All model runs are summarized at the end of this chapter in table 3.2.

Results and Discussion

Varying Aquifer Width

Model geometries with identical boundary conditions, length to width ratios and internal properties were created at four different valley widths to test the sensitivity of SWGW flux magnitude on varying aquifer transmissivity (T). Each model was tested at both high (100 m/d) and low (10 m/d) K values because T is dependent on both thickness and hydraulic conductivity of the medium. An oscillating river function as well as a constant high head (h=100.05m) river function were used to drive the transience and to isolate the effect of hydropeaking versus simply maintaining artificially high head via use of upstream storage. As shown in figure 3.5, river stage of 100.05m caused the river to lose water at steady state, so both transient model runs were expected to lose some water.

Figure 3.7 shows a clear positive correlation between aquifer width and the amount of reach-scale loss at both high and low K. This correlation is present for both oscillating and constant elevated (stage = 100.05) river stage conditions. It is notable that the oscillating high K model runs approached field observations of reach-scale loss, which ranged from roughly 1-2 m3/s. Low K (10 m/d) model runs yielded losses roughly half those of the higher K (100 m/d) runs. For every order of magnitude increase in K, reaches that lose water as a result of hydropeaking/and or artificially high summer stage only experience a doubling of the loss.

Therefore, dam operators only need a rough estimate of K in order to predict the amount of loss to expect from hydropeaking.

It is unclear whether hydropeaking or simply elevated stage conditions are more directly related to reach losses. Valleys comprised of mostly high K media would experience generally greater losses under an oscillating or hydropeaking regime; roughly 0.2 m3/s per 20 km river reach more loss than constant high stage. At low K, however, there was minimal difference in loss between oscillating and constant river functions.

Figure 3.8 shows the difference in ET between the oscillating and fixed-stage model. Indeed there was greater ET in the oscillating model, which can only be explained by higher water content in the root zone. Thus, despite continually higher ET, the oscillating river function drove enough water into the root zone to perpetuate higher water content throughout model time (figure 3.9).

It was expected that an oscillating function would drive more water out of the river due to the known differences between wetting and drying curves for unsaturated soils (Hillel, 1998). The matric suction of unsaturated soils causes them to take on water more easily than they release it. Therefore, each high-stage phase of the flood cycle (stage=100.3m) would be expected to introduce more mass to the vadose zone than a constant stage. It is possible that the constant stage models were able to remove water via this same wetting and drying phenomenon. The diurnal effect of ET could have provided the force for wetting and drying by moving water upwards during the day and allowing water to drain back down via gravity at night (figure 3.10).

River Stage Change

Using water budget analysis earlier in this study, no strong correlation appeared for a given dam release between the magnitude of the stage change and the amount of loss from the river reach. Natural systems, however, are affected by many variables changing simultaneously and often having opposite effects from one another. The effect of a larger stage change was tested here in model space while keeping all other variables constant. The amplitude of the river function (figure 3.2) was doubled, keeping the average river head the same at 100.05m, and each model width was run at high K. It was expected that a greater stage change would drive more water into the riparian aquifer, elevate the water table to a greater degree and make more water available for vegetation, thereby augmenting reach losses.

While the total hyporheic exchange (figure 3.11) was much greater when the magnitude of river stage change increased, the amount of loss from the system only increased during wider aquifer simulations (figure 3.12). Below a crossover point at a width of roughly 275m, narrower valley fill geometries actually experienced less loss when the river stage variation increased. Smaller losses in narrower models may have been due to steeper hydraulic gradients towards the river during low stage. Because low stage during the double amplitude runs was a full 0.5m below average stage, versus only 0.25 for prior simulations, water would have been driven into the river at a higher rate.

As expected, increased stage changes at the river boundary dramatically increased total hyporheic exchange at almost all aquifer widths. However, the relationship between aquifer width and total hyporheic exchange was reversed at model geometries exceeding 200m in width. This was because return flows to the river, quantified as positive y-velocity integrals, in smaller width models drove up the total exchange. In wider models with greater cross sectional

area and more riparian vegetation, return fluxes were smaller and thus resulted in less return flow, thereby lowering total hyporheic exchange.

Given the finding that greater stage changes can cause greater permanent losses from the river system, hydroelectric operators face several unaccounted tradeoffs when using a hydropeaking generation method. Larger changes between high and low stage translate into river ecological tradeoffs, at least in broader valley aquifer geomorphological settings. In these settings, it was shown that losses from the river system increase when abrupt stage changes are greater in magnitude. This means less water in the channel to support fauna, especially as one travels further downstream. Furthermore, operators with several facilities on the same river system face economic tradeoffs when abruptly changing the stage of river reaches, indirectly reducing their total generation units due to a loss of water from their system.

Varying Evapotranspiration

When investigating causal factors for reach-scale loss on the DFR, variable evaporative forcing showed the best correlation with loss for a given individual flood. In model space, the July 2010 ET time series was multiplied by different fractions of 1 to evaluate the power of ET to control the magnitude of reach loss. Steady state conditions were established at each ET fraction and used to run transient models using the procedure detailed above.

Figure 3.13 shows an unmistakable direct relationship between the amount of ET and reach scale loss. At small fractions of actual ET, reach scale losses actually decrease to zero and can cause the river to gain. This nearly linear positive relationship between ET and reach loss confirms findings from the water budget analysis. On the hottest summer days when both evaporative and electrical demand are greatest, hydroelectrical operators releasing larger volumes for longer durations maximize the potential for this phenomenon to drive water out of

the river system. These days are also the most stressful for river fauna dependent on cooler conditions, especially considering that tributaries that typically offer thermal refuge tend to be at minimum discharge during these conditions. In consideration of the ecological harm and economic tradeoff, making the largest releases on the hottest days may not be the best procedure for dam operators and watershed managers.

Conclusion

Model results described above give us several insights into how abrupt stage fluctuations affect SWGW interactions in different geologic settings and under varying external forcing. Most importantly, it was shown that a calibrated steady state model, when driven forward in time with parameters taken from field observations, such as the magnitude of stage changes and evaporative forcing, can remove similar amounts of water as calculated via water budget means. Secondly, in wider valley-fill settings (>275m), abrupt stage changes rather than simply elevated stage may cause a river to lose more water. The loss of river water due to hydropeaking and upstream storage of the freshet is likely caused by ET by bank vegetation. River loss likely scales with the strength of evaporative forcing. Lastly, increasing the change in discharge from low to high during the hydropeaking cycle increases both the loss from the river and total exchange of water through the HZ. Thus, negative economic impacts to dam operators with several in-series facilities, as well as possible deleterious effects to HZ biota are increased with more extreme hydropeaking.

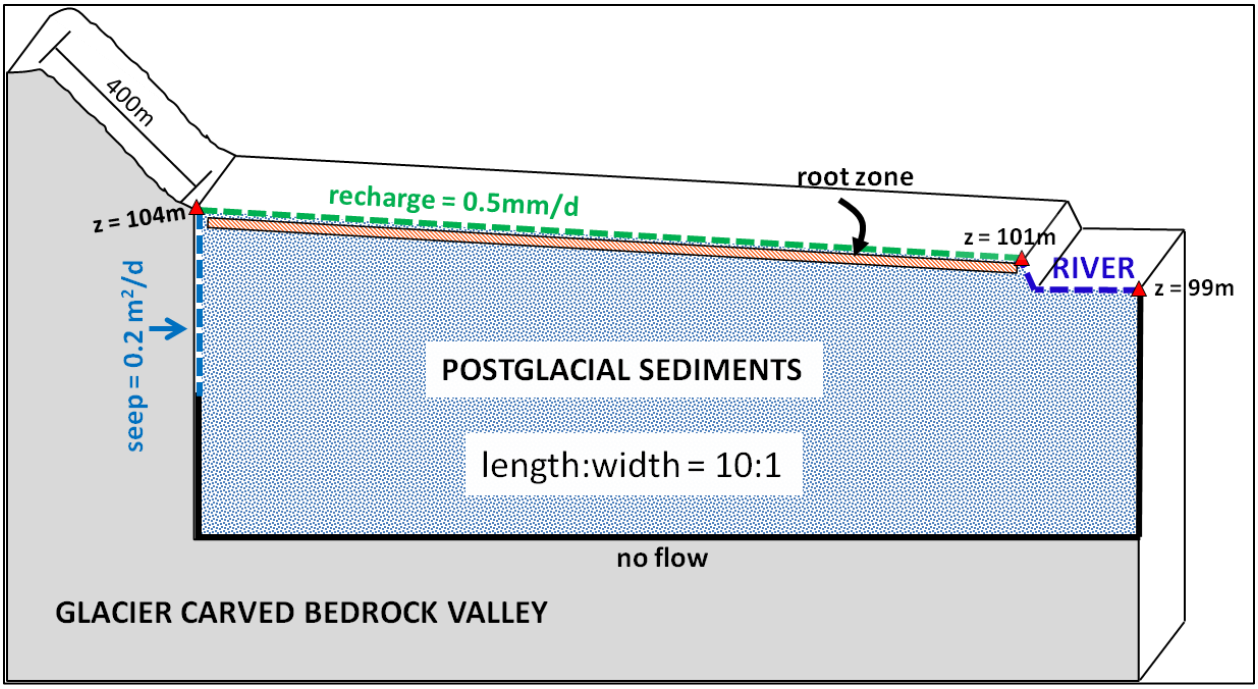

Figure 3.1 – Model diagram showing subdomain geometry and boundary conditions. Model boundaries include the earth's surface (top), bedrock walls (left, bottom) and symmetry divide below the river (right). For volumetric calculations, the domain was considered 1m thick into the page. Elevation of fixed points above an imaginary datum are shown as red triangles. Horizontal and vertical dimensions of the model domain vary between different model versions, but the length to width ratio of 10:1 remains constant.

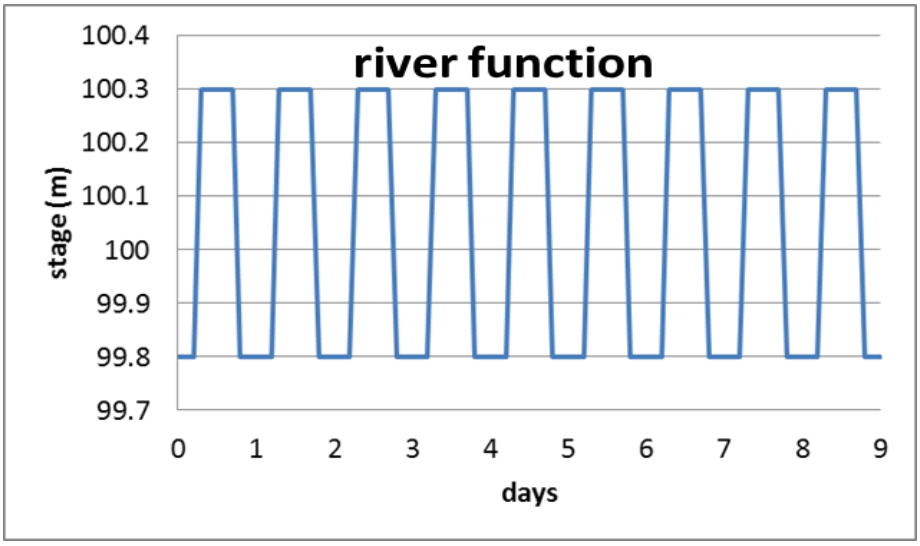

Figure 3.2 – River stage varies as a function of time about an average value of 100.05m above an arbitrary datum.

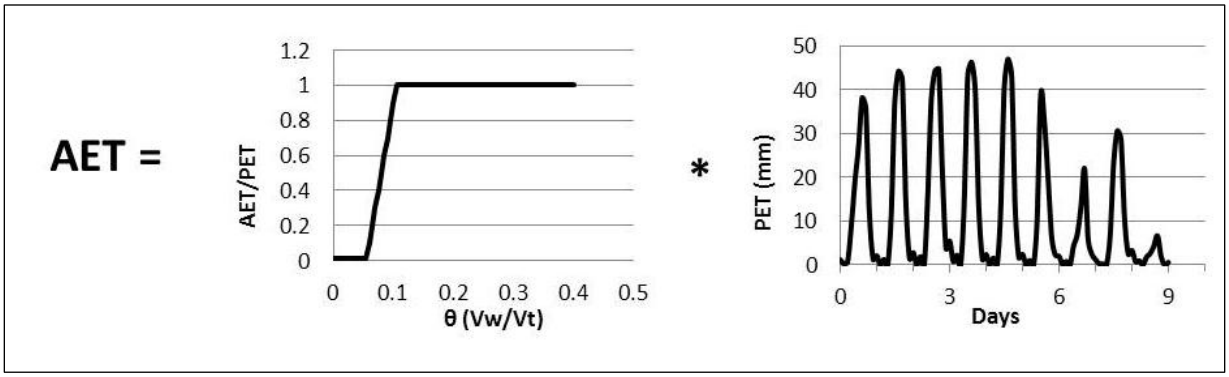

Figure 3.3 - Actual evapotranspiration (AET) is calculated as a function of the water content and evaporative forcing (PET) as determined by Penman's equation. This procedure occurs at each node for each time step within the rooting zone subdomain.

Subdomain	Van Genucten values	Porosity	Specific retention	K (m/d)
Aquifer	α = 2, n = 2, l = .5	0.4	0.05	Varied = 100, 10
Root Zone	same	same	same	Same

Table 3.1 – Subdomain properties.

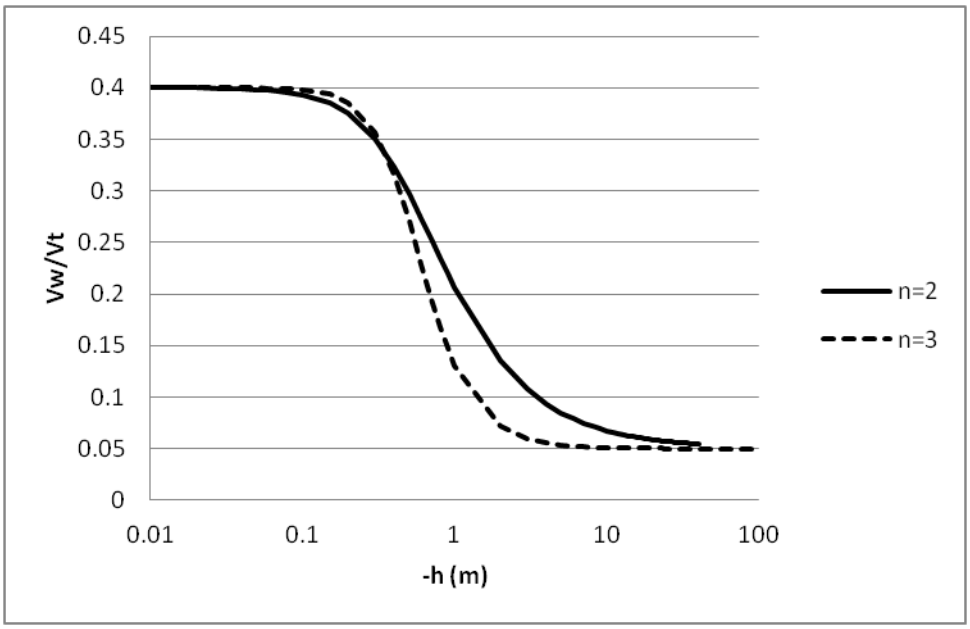

Figure 3.4 – Soil water retention curves for two values of n.

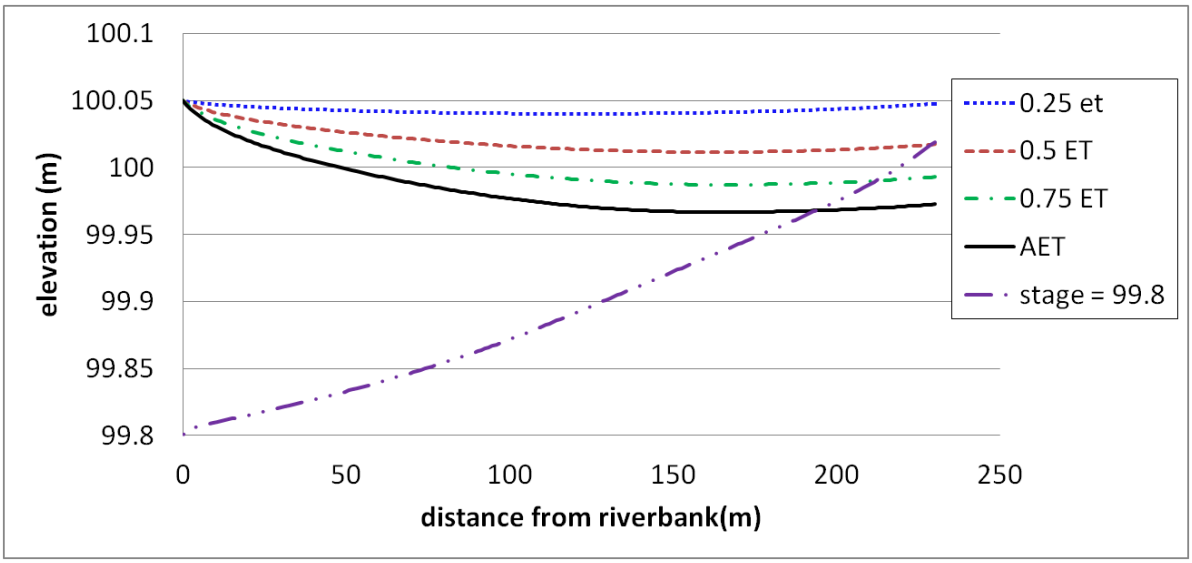

Figure 3.5 – Water table elevations away from the riverbank (at left) as simulated during steady state solutions under various ET values ranging from a maximum of [AET=average PET] (solid black line) to smaller fractions of PET. The riverbank is located at 0 in the x-dimension and stage = 100.05 for all initial conditions except the low stage test (s = 99.8). Dashed purple line (lowest) shows the shape of the water table if summer stage were lowered to 99.8m, the lower end-member of the stage function shown in figure 3.2. For the model conditions and geometry, the river only gains water if the stage is low during summer months.

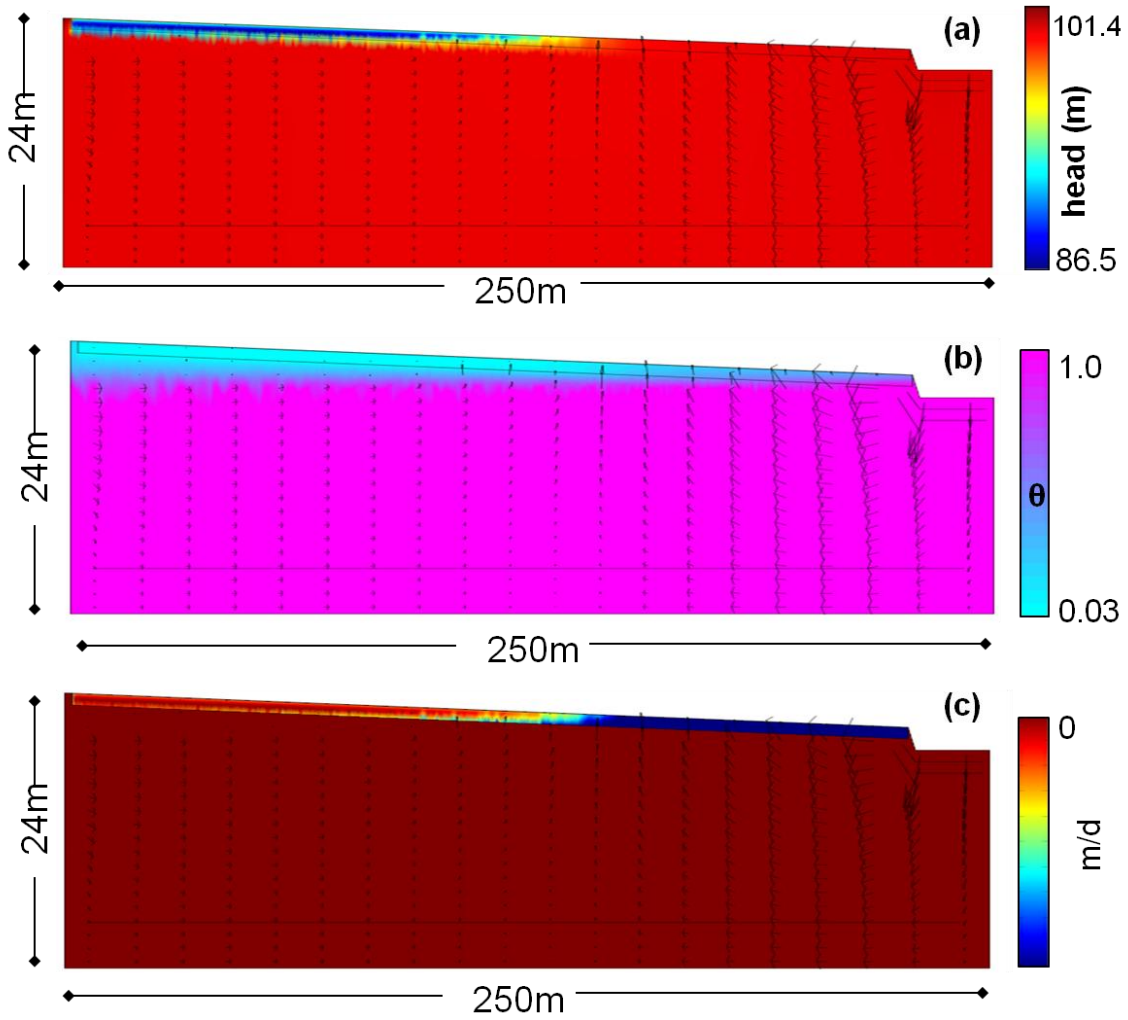

Figure 3.6 – (a) Initial head distribution and relative seepage velocity (arrows) at steady state for 500m wide model (when multiplied to account for symmetry divide). Hydraulic conductivity equal 10m/d in this output. (b) Water content in the same model run calculated V_{water}/V_{pores} showing low soil moisture in the river distal root zone. (c) Evapotranspiration distribution showing greatest removal of water in the river-proximal root zone at the top-right of the model domain indicated by cool colors.

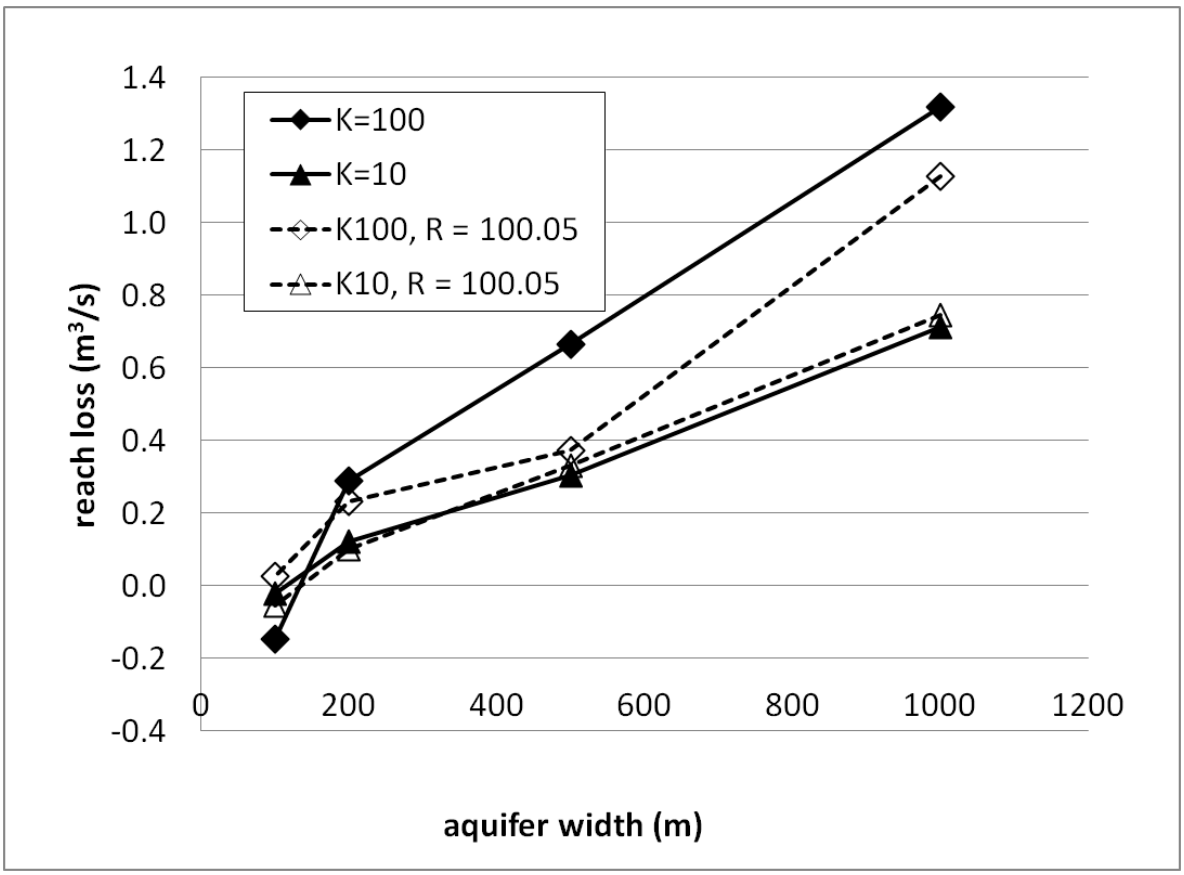

Figure 3.7 – Model results showing projected losses from a 19.5km river reach. Negative values depict conditions where the river gains water from the groundwater system. Solid lines with filled data point markers depict model runs with a hydropeaking river stage; dashed lines with hollow symbols show results from fixed river stage of 100.05m above an arbitrary datum.

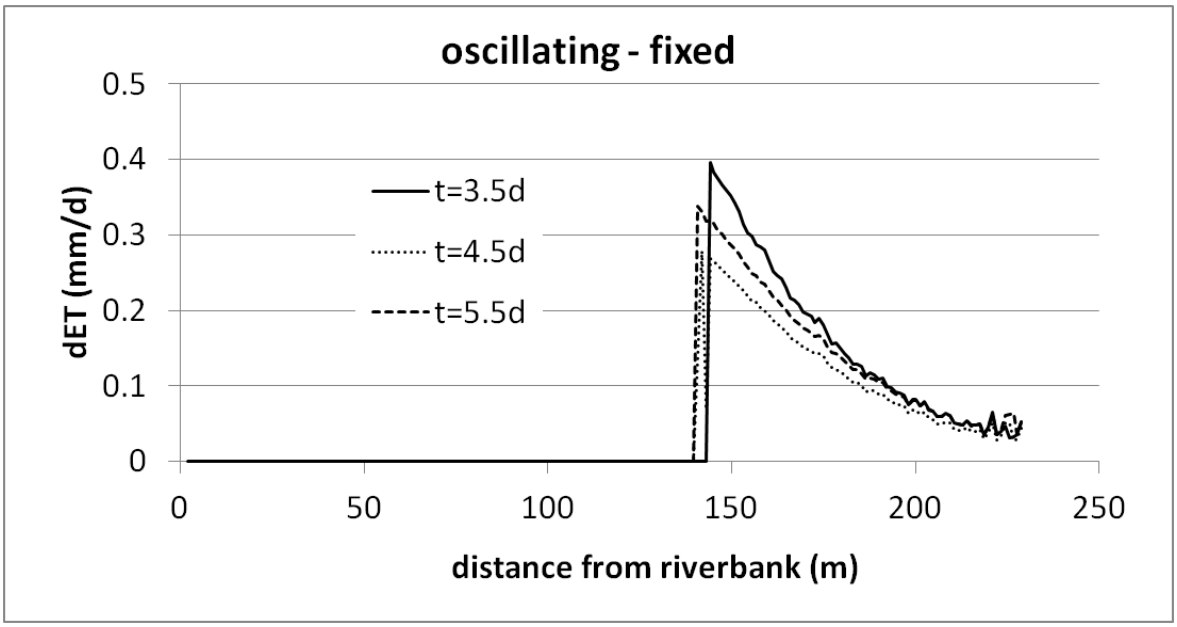

Figure 3.8 - Snapshots of the difference in ET flux [dET = oscillating – fixed] for the oscillating river stage and fixed river stage in 500m wide models. Each snapshot is taken at the bottom of the rooting zone at midday. Towards the valley margins, ET in the oscillating river model exceeds the fixed high stage model on all three days shown. Daily average ET rates are much lower than those in the figure since these shown were extracted at the maximum midday ET.

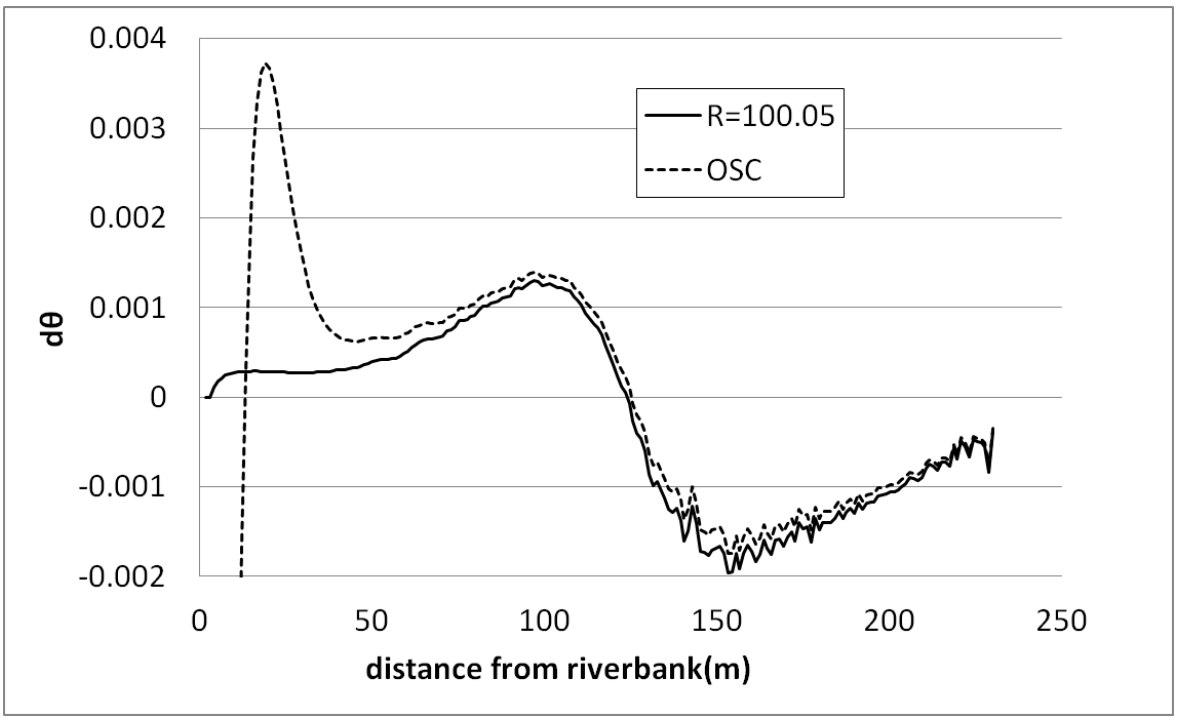

Figure 3.9 - Change in root zone water content from the initial condition to final condition for an oscillating river function (OSC) and constant high stage function (R=100.05). The final value (99.8m) of the oscillating river stage function at low stage causes θ next to the river (x=230m) to drop. Note that the oscillating model results in more storage of water within the unsaturated zone at all model distances except adjacent to the river, which is a function of the time within the river oscillation cycle.

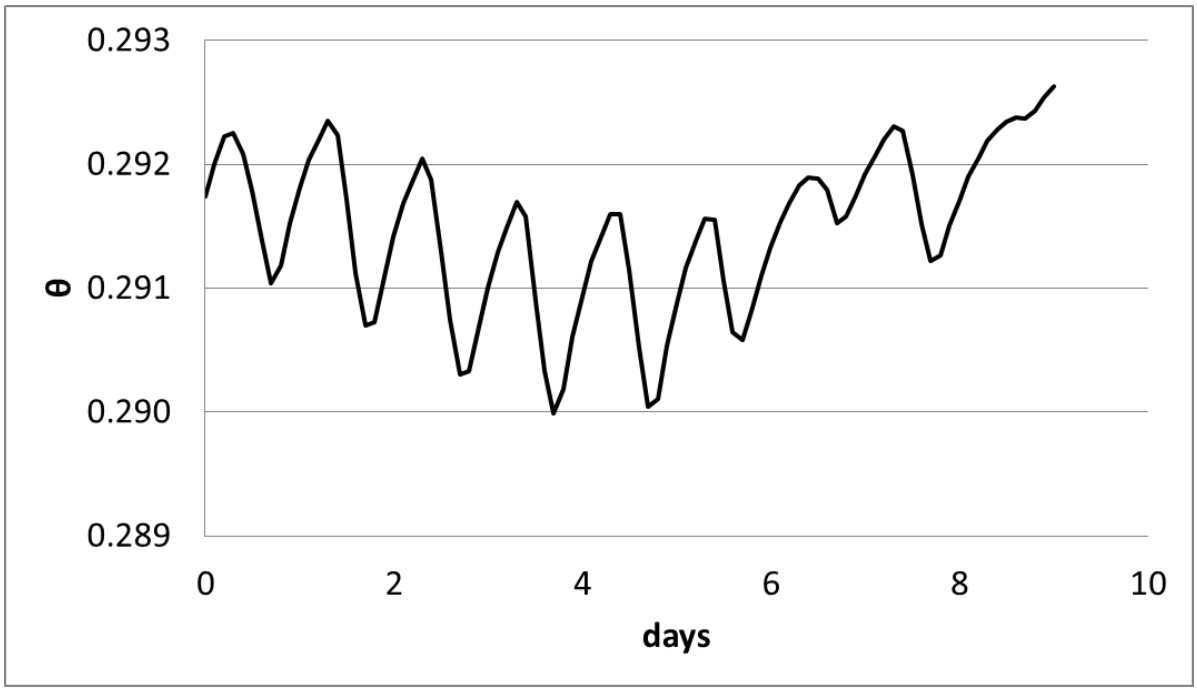

Figure 3.10 - Time series of water content over the course of nine day fixed river stage model run at the base of the root zone 50m from the river in the 500m width model. Daily ET forcing drives changes in θ potentially causing water to be stored in the vadose zone even in the absence of hydropeaking.

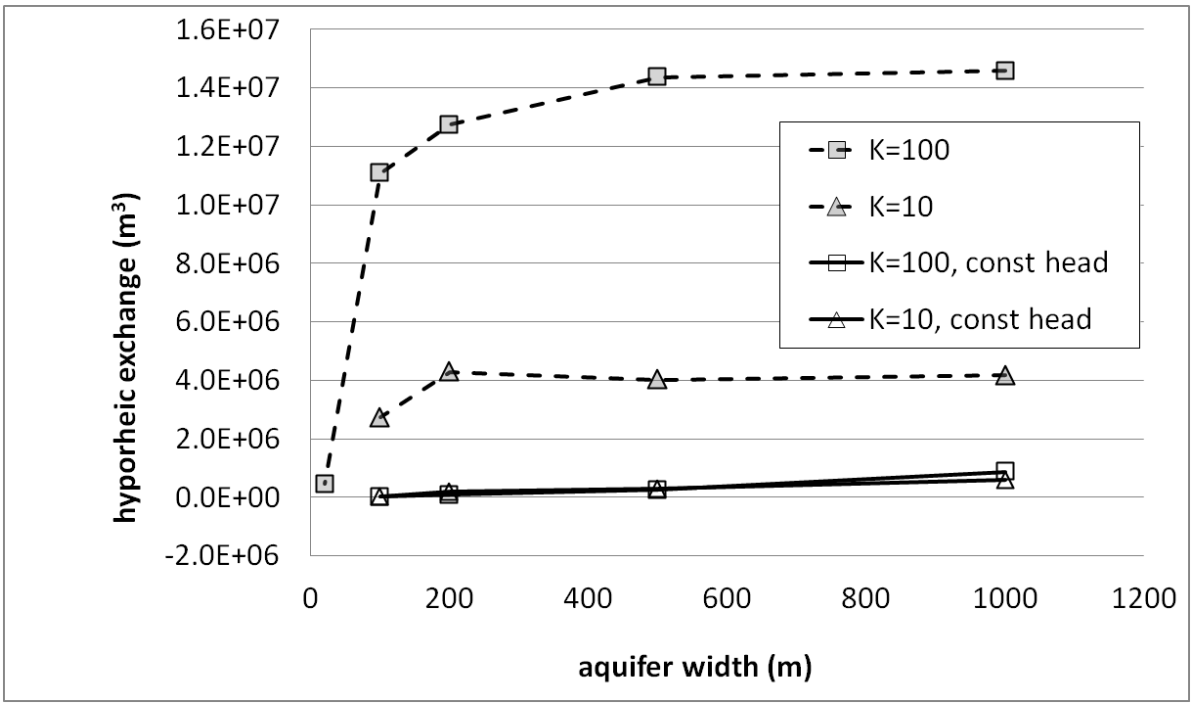

Figure 3.11 – Total hyporheic volumetric exchange over 9 rain-free days for a 19.5 km river reach for oscillating (dashed lines) and fixed stage (solid lines) river conditions. Predictably, oscillatory stage fluctuations (K=100, K=10) produce much greater hyporheic exchange due tohead gradient reversals. Small increases in aquifer width in narrow valley systems (w<100m) result in large increases in hyporheic exchange under oscillatory stage regimes, but increases level off in wider valleys (w>500m).

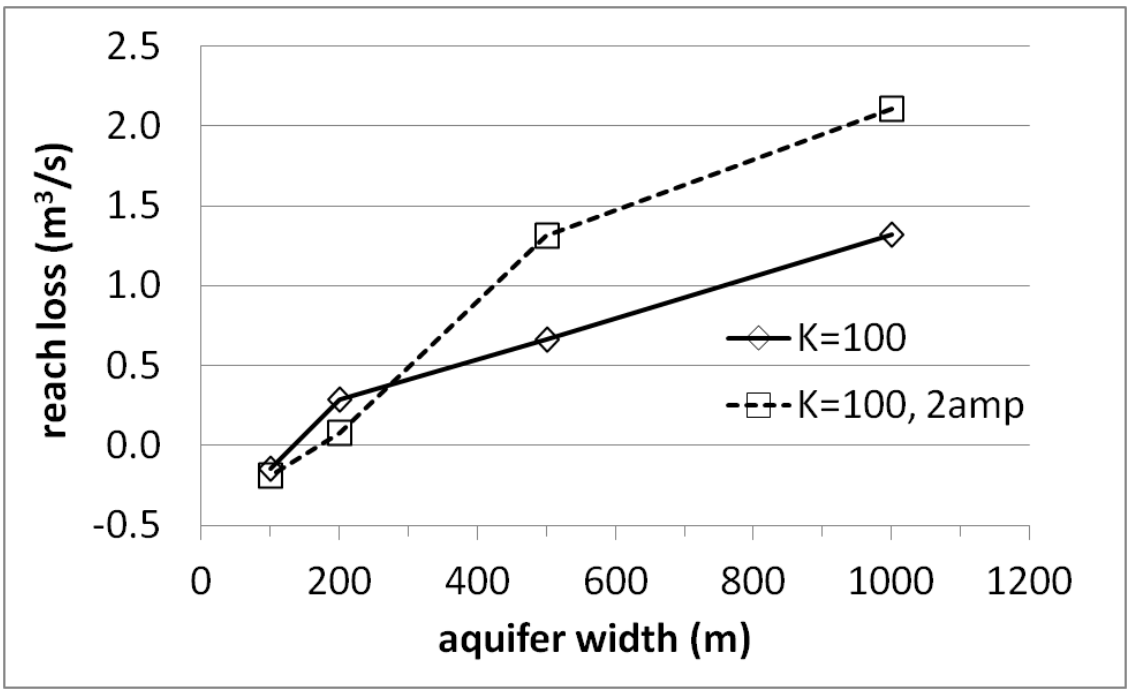

Figure 3.12 – Projected reach-scale losses from a 19.5 km homogenous river reach given hydropeaking amplitudes of 1m (K=100) and 2m (K=100, 2amp) fluctuations. Both sets of models were run at the higher value of K. For wide riparian aquifers, losses increase dramatically when stage fluctuation magnitudes increase.

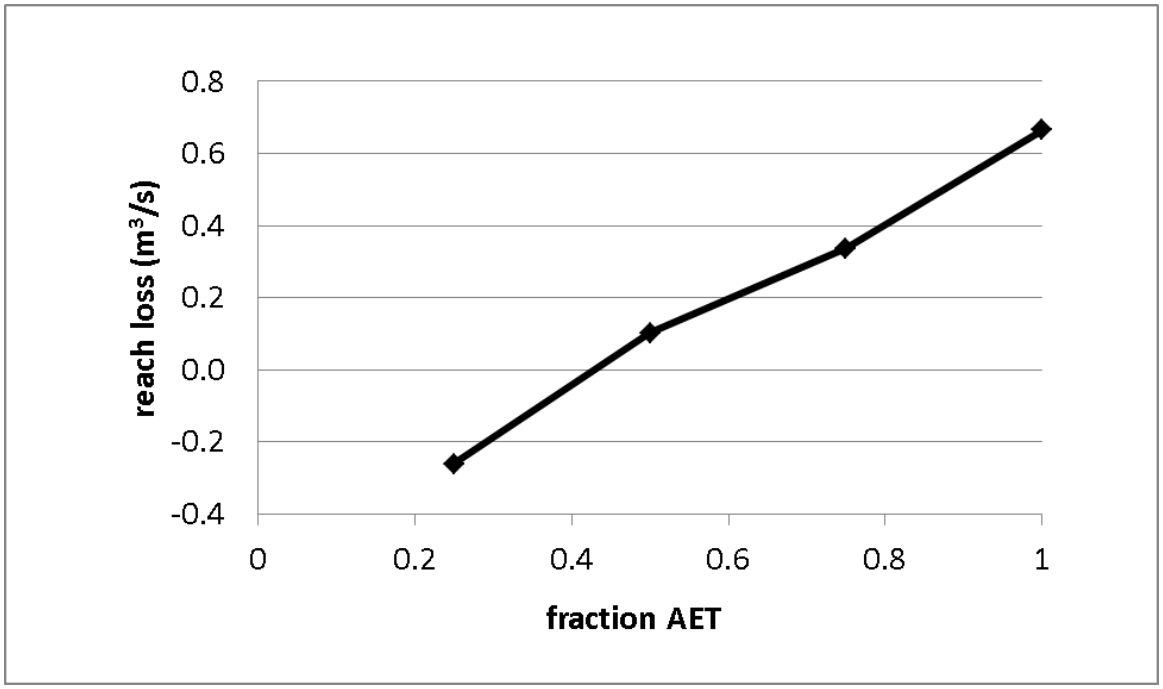

Figure 3.13 – Reach-scale losses for a 19.5 km river reach increase almost linearly with increased riparian ET under a hydropeaking river stage regime. Positive values show conditions for which the river gains water from the riparian aquifer.

Width (m)	K (m/s)	River Function	ET
100	**100**	**Oscillating (99.8-100.3)**	**Fig 3.3**
	10	**Oscillating (99.8-100.3)**	**Fig 3.3**
	100	**stage = 100.05m**	**Fig 3.3**
	10	**stage = 100.05m**	**Fig 3.3**
	100	**Oscillating (99.55-100.55)**	**Fig 3.3**
200	**100**	**Oscillating (99.8-100.3)**	**Fig 3.3**
	10	**Oscillating (99.8-100.3)**	**Fig 3.3**
	100	**stage = 100.05m**	**Fig 3.3**
	10	**stage = 100.05m**	**Fig 3.3**
	100	**Oscillating (99.55-100.55)**	**Fig 3.3**
500	**100**	**Oscillating (99.8-100.3)**	**Fig 3.3**
	10	**Oscillating (99.8-100.3)**	**Fig 3.3**
	100	**stage = 100.05m**	**Fig 3.3**
	10	**stage = 100.05m**	**Fig 3.3**
	100	**Oscillating (99.55-100.55)**	**Fig 3.3**
	100	**Oscillating (99.8-100.3)**	**0.75PET**
	100	**Oscillating (99.8-100.3)**	**0.5PET**
	100	**Oscillating (99.8-100.3)**	**0.25PET**
1000	**100**	**Oscillating (99.8-100.3)**	**Fig 3.3**
	10	**Oscillating (99.8-100.3)**	**Fig 3.3**
	100	**stage = 100.05m**	**Fig 3.3**
	10	**stage = 100.05m**	**Fig 3.3**
	100	**Oscillating (99.55-100.55)**	**Fig 3.3**

Table 3.2 – Summary of all model runs showing various permutations of varying aquifer width, hydraulic conductivity (K), the time dependent function of river stage and the time dependent evapotranspiration function (ET).

CHAPTER 4

FIELD OBSERVATIONS

Introduction

Water budget analysis indicated that the DFR study reach loses water, likely as a result of a combination of hydropeaking and riparian vegetation ET demand. Modeling efforts using parameters taken from the field have shown that it is possible to remove water from the river reach in volumes similar to those calculated via water budget means. Field monitoring at key locations within the study reach was undertaken to evaluate whether we could directly observe phenomena occurring at specific sites in accordance with a broader-scale understanding of the system.

After the field campaign, it was determined that the spatially heterogeneous nature of field conditions with respect to the collected data rendered that information useful mostly to corroborate findings rather than to draw new conclusions. Generally, patterns gleaned from the field data support the main findings from the water budget and modeling analyses that: 1) the river reach does lose water to the groundwater system; 2) the magnitude of loss correlates positively with the cross-sectional area of the riparian aquifer; 3) total hyporheic exchange varies considerably depending on hydrogeologic conditions. In addition, field monitoring of hyporheic zone (HZ) dissolved oxygen and microbial metabolic rates was undertaken to evaluate one potential impact of hydropeaking on HZ biota.

Methods

Five locations within the study reach were selected as representative of the range of hydrogeologic conditions within the valley-fill aquifer (figure 1.4). Site selection strategy was driven by a hypothesis that in hydropeaking rivers, aquifer transmissivity (T), more than site geomorphology, would play a dominant role in governing the magnitude of stage change-

induced hyporheic exchange. Transmissivity, the product of hydraulic conductivity and thickness of conducting unit, is an aquifer characteristic that describes the ability of an aquifer to transmit water.

Site 1, 0.1 km downstream of Fife Brook Dam, is characterized by the most limited transmissivity, with parts of the river flowing directly over bedrock and cobble sections directly underlain by till. Four kilometers downstream, site 2 is a 200m wide valley bottom where seismic refraction indicated a depth to bedrock of 7-10m. Further downstream, sites 3 and 4 overlie 40-50m of glacially derived sediments. However, whereas the riverbed lies on top of fine sand at site 3, at site 4 it overlies a thin, silty glaciolacustrine layer. This silty layer grades thicker downstream (figure 1.3) as the depth of the bedrock basin pinches out at site 5. Site 5, located at the USGS gauge site, marks the end of the contiguous basin spanning sites 3 and 4.

Hydraulic conductivity (K), one of two factors used to determine T, proved too spatially heterogeneous to confidently attach a value at each site. Connant (2004) found K varying over four orders of magnitude within the stream bed in a single 50m reach of river. Aquifer K therefore could not be factored into our site characterization.

At each site, vertical hydraulic gradient (VHG) as well as vertical temperature distribution were monitored. Limited equipment precluded simultaneous monitoring at all sites. Between two and five days of observations were taken at each site. Each monitoring deployment captured at least two dam-induced floods, ensuring that we captured changes in the direction of the hydraulic gradient.

VHG describes the potential that drives water up or down across the SWGW interface. It is defined as the ratio of the difference in head between the river and the underlying

groundwater over the distance between the river bottom and the top of the piezometer screen (Arntzen et al., 2006):

$$VHG = \frac{h_R - h_{HZ}}{z_R - z_S} \quad [4.1]$$

where h_R and h_{HZ} are head in the river and hyporheic zone respectively. Symbols z_R and z_S are elevation above an arbitrary datum of the river bottom and the top of the well screen respectively. To collect these data, a 4 cm outside diameter, 1.5m long galvanized steel pipe was threaded to a 0.15m long drive point and driven 0.6m into the river bed using a 9 kg slide sledge. The maximum outside diameter of drive point was 4.5 cm, thus creating a 2.5 mm lip at the coupling with the steel pipe (figure 4.1). Six 1 cm diameter holes were drilled into the pipe 10 cm above the drive point. The 10 cm spacing above the drive point allowed debris to fall to the bottom of the piezometer and avoid clogging the holes.

At 5 min intervals, two absolute pressure transducers (Solinst LevelLogger 3001, 1.4mm resolution) monitored the height of the overlying water column – one inside the piezometer and one in the river. Following piezometer deployment, once the water level inside had reached a constant height, a dry wooden dowel was inserted and removed from the pipe. The length of the dry interval was measured. This distance was compared that outside the piezometer. The difference between the two distances at the time of pressure transducer deployment was used as a datum to reference the two records to one another and extract a continuous series of difference in head (dh). The same difference was checked again when the equipment was removed to validate the initial reading. While the dh invariably was different at the end of the test, after adjusting the two pressure transducer time series to the initial dh, the final dh in the record had to match the field observation or the records were discarded due to measurement error.

Falling head slug tests were completed at each piezometer deployment. A slug of water added to the top of the piezometer induced a head gradient. As the head in the piezometer subsequently fell and equilibrated with that in the surrounding HZ media, a pressure tranducer (described above) monitored change in head over time. These records were analyzed using the AQTESOLV software package and the Bouwer-Rice (1976) method for partially penetrating wells in an unconfined setting.

In addition to VHG, vertical temperature distribution (VTD) was collected to make use of differences in river and groundwater temperature and use heat as a natural tracer. A threaded rod fitted with circular rubber baffles spaced 10 cm apart was inserted into a piezometer identical to that described above. Temperature loggers (Ibutton model DS1921Z, 0.125 ˚C resolution) were placed midway between rubber baffles and logged temperature at 5 min intervals. Modeling results (Cardeñas, 2010) have shown that a solid steel pipe of minimal diameter is ideal for minimizing dampening of the temperature signal as it conducts through the piezometer wall.

Past studies (Arntzen et al., 2006; Howard, 2006) have shown an increase in the dissolved oxygen (DO) levels of HZ pore water in hydropeaking rivers. Elevated stage associated with dam releases drives well-oxygenated river water into the streambed. It was hypothesized that this added DO would boost microbial metabolic rates in the subsurface, manifested as a more rapid breakdown of organic material in the HZ. To test this hypothesis, a cotton strip assay was used. Past studies have shown that the reduction in strength of an organic textile correlates well with the rate of microbial metabolism in a soil or porous medium environment (Tiegs et al., 2007; Clapcott and Barmuta, 2010).

Strips of unbleached 100% cotton canvas (Fredrix brand 12-ounce duck, style number 548) measuring 35 mm by 60 mm were placed in the HZ at study sites 1-5. Three additional sites in unregulated tributaries were selected as a control group to compare to DFR sites. At each site, two locations in 20-30 cm water depth at low stage were excavated by hand to a depth of 20 cm below streambed grade. A collection of loose gravel and smaller sized material was collected with a trowel and analyzed for grain size distribution (appendix figure A.3). A steel spackle knife was then wedged into the loose material below the hole to allow for insertion of up to three cotton strips. Care was taken to minimize disturbance and preserve fine-grained material that was likely to wash away.

Cotton strips were deployed for a total of 28 or 30 days, after which they were recovered and air dried. The material deployed at site 4 was not recovered. A 4411 Instron Corp model tensiometer was used to measure the tensile strength of each cotton strip deployed as well as a group of control strips that were soaked in distilled water for 1 day. Tensiometer clamps held 10mm of fabric at either end of a cotton strip, leaving a 40mm portion susceptible to tension. The machine then moved one clamp away from the other at a constant rate of 24.5 mm/min and monitored the applied load. Tensile strength was determined as the maximum load that each strip could withstand before failure. Failure was defined by the point at which the loading value decreased, which occurred due to brittle failure of the textile to accommodate the increasing tensile stress.

Analysis

VHG records were inspected visually for large, unexpected changes in dh that would indicate tampered field equipment or a clogged well screen. Very large dh values for the first flood cycle of observation at sites 2 and 4 provided cause to discard these data and use only the latter flood cycles. It is likely that these large dh values were due to clogged well screens at

early time. After sufficient flushing, often provided by a stage change and accompanying gradient reversal, water was able to pass through the small well screen and more accurately reflect actual field conditions.

After cleaning, the total sum of each VHG record was summed and the absolute values of the record were averaged. The sum gives a gross approximation of how strongly gaining or losing the river is at each field study location. Average of the magnitude (absolute values) of each VHG series, indicates the duration or intensity of the hydraulic gradient maintained between the river and the hyporheic zone (HZ).

VHG at each site was plotted against stage to show the hysteretic nature of SWGW interactions – namely that the sign (positive or negative) of the VHG value depended not only on the stage, but also on the time within the stage change cycle (figure 4.2b, 4.3b). The location of the stage-VHG series with respect to the x-axis gives a sense of how strongly the river gained or lost water at that particular site during the monitoring interval.

Two significant defects in piezometer design introduced significant error to VHG data. As the piezometer was driven into the riverbed, the small lip present where the drive point was threaded to the steel pipe of the piezometer (figure 4.1) created a boring slightly larger than the diameter of the pipe. Thus, the piezometer pipe was not in direct contact with sediment allowing for a narrow sleeve of water to connect the well screen to the river and short circuit the flow path through the porous medium that we intended to monitor. This proved more problematic in slug tests, which were performed immediately after piezometer deployment.

Over the course of a few hours, the sediment could settle in around the piezometer and nullify this shortcoming in longer term monitoring deployments. However, well screen deficiencies made data from longer term monitoring unreliable as well. Due to the extremely

small screened interval, only a very limited portion of the subsurface was effectively sampled. It is well-known that grain size, and closely coupled hydraulic characteristics can vary by orders of magnitude within a distinct porous medium (Bear and Braester, 1969; Berkowitz and Scher, 1995). Therefore, it is possible that instances of large observed head gradients (such as early time at sites 2 and 4) were due to intersecting an anomalously low conductive layer at the small well screen. A longer well screen would have provided greater chance of intersecting more conductive layers, which can account for the majority of aquifer transmissivity.

Results

Site 1

Site 1, just below the Fife Brook dam is characterized by a bedrock bound channel with very limited tranmissivity in the limited to non-existent riparian aquifer (figure 1.4). As a consequence of the limited volume of porous media and accompanying storage, it was predicted that any change in river stage would quickly permeate the entirety of the narrow strip of bank alluvium and minimal gradient could be maintained between river head and that in the HZ. Figure 4.2A indicates that indeed the head in the HZ nearly equaled river head regardless of stage changes4. Figure 4.2B shows that the VHG-stage relationship is nearly flat. Thus, regardless of changes in stage, VHG remained nearly constant.

Vertical temperature distribution at site 1 generally tells the same story of limited stage-change-induced hyporheic pumping. Fife Brook Dam, Lower Bear Swamp Reservoir's bottom release dam, discharges cold water resulting in a near constant river temperature and minimal diurnal temperature swings. HZ temperature 10 cm below the riverbed weakly echoes surface temperature signals. However, 30 cm into the HZ, temperature variation is barely above the

resolution of the logging instrument. The continuous low temperature of the HZ here makes it unlikely that significant volumes of river water are advected below the riverbed.

Site 2

At this site, where the river runs over a moderately wide (~200m) bedrock valley bottom filled with glacial sediments, it was expected that moderate SWGW exchange would be permitted. With neither historical borehole logs nor personal subsurface investigation, we cannot be sure what comprises the roughly 10m of sediments here. The VHG record suggests that the bank and HZ media impede porous flow to a greater degree than sites subsequently described herein. The low K here is evidenced by significant dh values following abrupt stage changes (figure 4.3A). The wide circle of the stage-VHG relationship suggests that gaining or losing conditions are highly hysteretic. The near symmetry of the record about the x-axis indicates that the river here is neither strongly gaining or losing over longer time periods.

The diurnal temperature record here begins to look more like a natural river, with values starting to rise during the morning hours. However, the daily arrival of cold dam releases from upstream terminates the increase in surface water temperature. Ten centimeters below the river bottom temperature closely mirrors that at the surface, though never exceeds it. As observed in other VTD records (Hatch, 2006), the diurnal temperature signal at depth lags behind that at the surface due to the time it takes for heat to reach depth. At the deepest level, 30 cm, the diurnal signal is barely visible. The very low temperature at this level suggests that river water rarely advects this deep and the diurnal signal can be attributed mostly to conduction through riverbed media.

Immediately following abrupt stage increases, evidence for a unique and interesting phenomenon manifests itself. The 10 cm temperature logger records a short-lived drop in

temperature just as the river head increases and we would otherwise expect surface water to be driven down and raise the HZ temperature. Boutt (2009) noted that loading of the riparian aquifer by the sudden arrival of the dam release flood wave caused a jump in head in layers below a semi-confining layer. If the same process occurred at site 2, one would expect a brief upward hydraulic gradient, pushing lower, colder water towards the surface. Poroelastic loading driving colder water up may explain this brief drop in temperature when we would otherwise expect an increasing trend.

Sites 3 and 4

Sites 3 and 4 have similar valley geometries, similar hydrogeologic settings and appear to respond similarly to abrupt stage increases (figure 4.4). At both sites, wide and deep glaciofluvial deposits fill upwards of 40m of over-deepened bedrock depression. Postglacial deposition of silty-fine to very fine sand underlies the streambed and likely grades finer downstream towards site 4 (figure 1.3). At both sites, referenced stage elevation exceeds HZ head at almost all times resulting in a negative dh. Immediately following flood-wave arrival, the difference in head becomes especially pronounced, when a higher stage likely strongly drives water out of the river and into the riparian aquifer.

Both sites 3 and 4 display hysteretic VHG-stage curves (figures 4.4B and F) that remain almost entirely below the x-axis. Daily dam releases together with the influence of antecedent HZ head conditions on the direction of the VHG bring about this cyclic pattern in the VHG-stage relationship. For example, just before an abrupt stage increase, the hydraulic gradient between surface and HZ water is at its minimum. When the flood wave arrives, river head (h_R) jumps dramatically above HZ head (h_{HZ}), making the VHG strongly negative. As h_{HZ} slowly rises in response to downward seepage from the river, data points approach the x-axis, signaling a reduction in the VHG. When stage falls abruptly, h_{HZ} remains briefly elevated, causing the line to

go slightly above the x-axis and the river to gain back some of the lost water before the next flood wave arrives and drives more water into the subsurface.

At sites 3 and 4, most data points on the VHG-stage relationship (figures 4.4 B, F) fall below the x-axis, indicating that the river likely loses water at both locations. In general, the magnitude of VHG at site 4 is greater than that at site 3, perhaps reflecting the downstream decrease in grainsize which would cause a similar decrease in hydraulic conductivity and serve to better maintain a downward gradient during high stage events.

Streambed temperature records at sites 3 and 4 (figures 4.4 D, H) both show closely coupled stream and HZ temperatures. The VTD probe at site 3 malfunctioned, so data are shown from the VHG pressure transducer pair, which record temperature in addition to absolute pressure. The HZ pressure transducer was at a depth of 50 cm, 20 cm below the lowest thermistors at other sites. All other variables constant, the added depth of the site 3 piezometer would cause expected additional dampening and lagging of the diurnal temperature signature.

Site 5

Site 5, located at the USGS gauge that marked the downstream end of the study reach, marks the end of the filled bedrock basin shown in figure 1.3. Here, the full extent of flood wave dispersion across the 19.5km reach results in a less abrupt stage increase. Due to well screen clogging at this site, only a short (2 flood cycles) record of VHG was retrieved (figure 4.5 A, B). Clogging of the well screen here, as well as the large dh maintained during floodwave recession curves point to low K at this site. The presence of glaciolacustrine fines here (figure 1.3) further supports this evidence for low K media.

Time series of dh (figure 4.5 a) and VHG (figure 4.5 B) both indicate that the river at site 5 is likely strongly gaining. Head in the HZ exceeds stage at nearly all times except immediately following stage increases. Although the VHG-stage series is nearly centered about the x-axis, the vast majority of data points fall in the positive y-value range due to the upward VHG at most times. Local geomorphology provides a clue as to what makes this site different from all of the others. Located at the downstream end of an extensive bedrock basin, river-parallel hyporheic flowpaths on the order of kilometers are forced to the surface here by the subsurface bedrock ridge. Water forced upward by this bedrock lip explains the predominantly upward vertical hydraulic gradient here and appearance that the river is gaining.

Despite an apparent upwards VHG, arrival of the daily floodwave shortly after the daily thermal maximum explains the significant temperature response 10 cm below the streambed (figure 4.5 D). At 30 cm below the streambed, however, temperature is nearly constant. It is worth noting that similar constant temperature observed in the deepest thermistor at site 2 was 3-4 degrees below that at site 5. This warmer temperature of HZ water at site 5 likely reflects its origin from within the mainstem DFR rather than regional groundwater observed at site 2.

Slug Tests

Given the extreme spatial variability of streambed hydraulic conductivity (Conant, 2004) and limited area of influence around an in-stream piezometer (Hatch, 2006), little credence can be given to results from piezometer slug tests. The flawed design of the piezometer used added to uncertainty in the results. Specifically, the small annulus created around the piezometer by the wide drive point allowed surface water to communicate directly with the well screen. The initial head displacement during each slug test was therefore sometimes able to equilibrate

partially via flow through this annulus and not the desired porous media. Slug test results are shown in table 4.1. It is worth noting that sites 3 and 4 had the highest observed K and sites 1 and 2 had the lowest. If slug test attempts at site 5 had been successful , well screen clogging by fines indicates that K there is lower still than sites 1 and 2.

Microbial Metabolism

Results from the CSA proved true the null hypothesis. Little difference between the DFR and the unregulated tributaries was observed (figure 4.5). All sites showed a significant reduction in tensile strength from the control strips. However, no generalizable trend is evident within the DFR sites or between DFR and unregulated tributary sites. The profound difference between site 8 (North River) and other sites may be explained by the 3˚C higher average temperature there (Cole, 2007).

Discussion

These field observations, despite their limited spatial coverage, generally agree with previous model-based and water budget-based approaches to understanding SWGW interactions on the dam controlled DFR. At sites with broad unconsolidated riparian aquifers (sites 3, 4), streambed head and temperature observations indicated that the river strongly loses water at nearly all stage conditions. The magnitude and direction of SWGW exchange, however, is highly hysteretic. Losses from the river are observed at all sites immediately following stage increases. At sites 2 and 5, where the river is not strongly losing, these ephemeral losses are likely due to a locally elevated head at the river boundary which takes some time to equilibrate with the far field head regime. A model snapshot following a stage increase (figure 4.7) shows locally reversed head gradient close to the river.

Initially, it was hypothesized that aquifer width or area would correlate well with VHG. The greater the dewatered pore volume adjacent to the river available to fill during high stage, the greater the SWGW exchange induced by abrupt stage changes. In figure 4.8, average VHG magnitude is plotted against the estimated cross-sectional area of the riparian aquifer at sites 1-5. Clearly, there is no relationship between the two variables. However, the volume of water that must pass through the HZ is not the only factor that influences VHG magnitude. Lower hydraulic conductivity would also increase the magnitude of observed VHG. Therefore, the average VHG was plotted against a ratio of area, which should scale positively with VHG, over K, which should scale negatively with VHG. Figure 4.9 shows an improved explanation of determinants of SWGW exchange volumes.

Given this positive relationship between VHG and riparian aquifer extent and negative relationship between VHG and K, a broad riparian aquifer made up of highly conductive media would be expected to maximize SWGW exchange. These conditions are most closely approximated in the field at site 3 and in model space in the 1000m wide, high K model run. Site 3 showed significant deep diurnal temperature response, supporting high exchange volumes. The corresponding model run showed the highest exchange volumes.

Without the support of corroborating water budget and modeling approached, these field data are of only limited use. Budgetary limitations contributed to non-ideal field data collection. Limited equipment meant that VHG data had to be observed asynchronously. As shown in the time series of river losses (figure 2.9), there is a cumulative effect of ET on groundwater levels which may influence SWGW exchange. Therefore, VHG data collected later in the season may reflect not only local geologic conditions, but also a seasonal overprint, which was not the desired goal. Similar studies in the future should make every effort to collect simultaneous spatially distributed SWGW interaction observations.

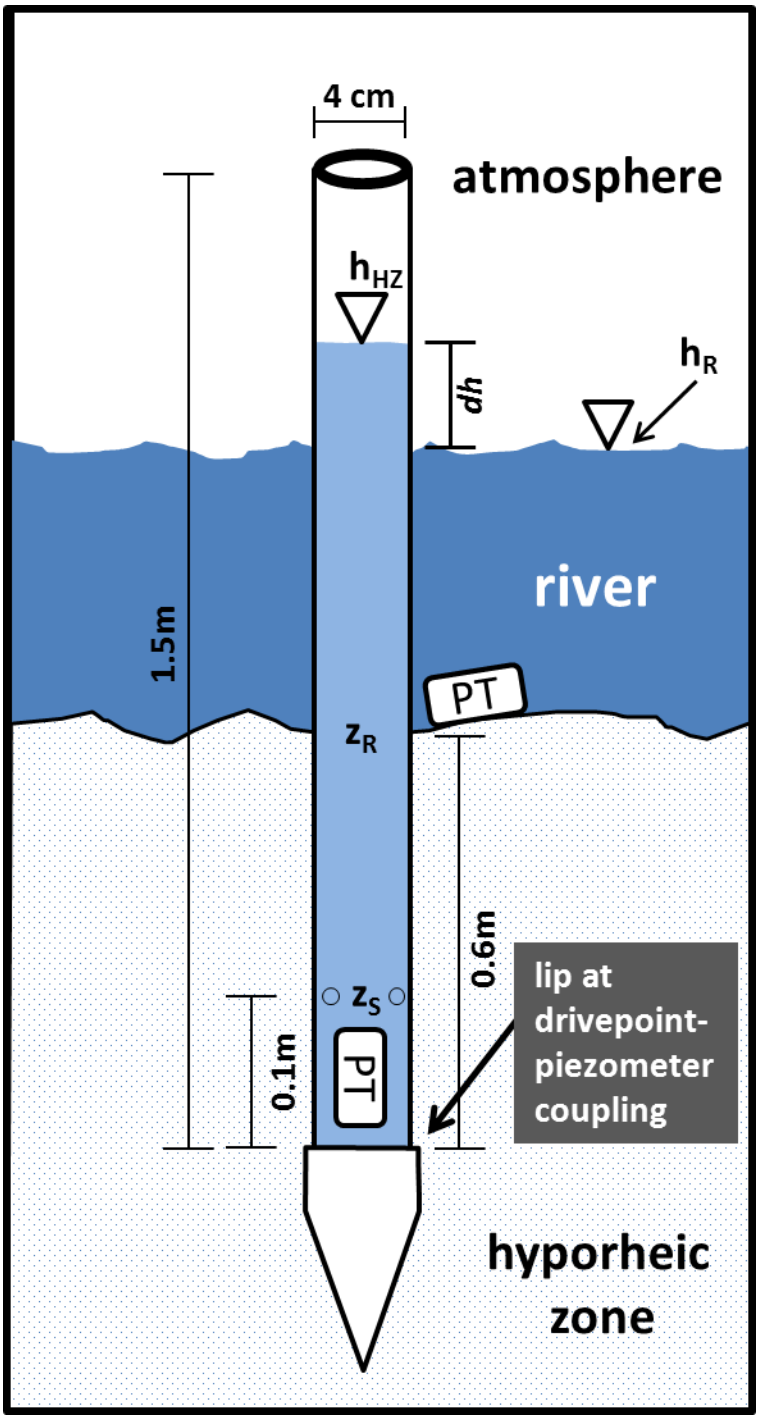

Figure 4.1 – Diagram of VHG piezometer as used during field deployment. Triangles indicate the head level in the river and hyporheic zone piezometer, each of which is measured by a pressure transducer (PT). In the diagram above, hyporheic zone head (h_{HZ}) exceeds river stage (h_R), indicating that the river is gaining at this time. Water enters the piezometer at z_S, the well screen. The elevation of the streambed is denoted z_R.

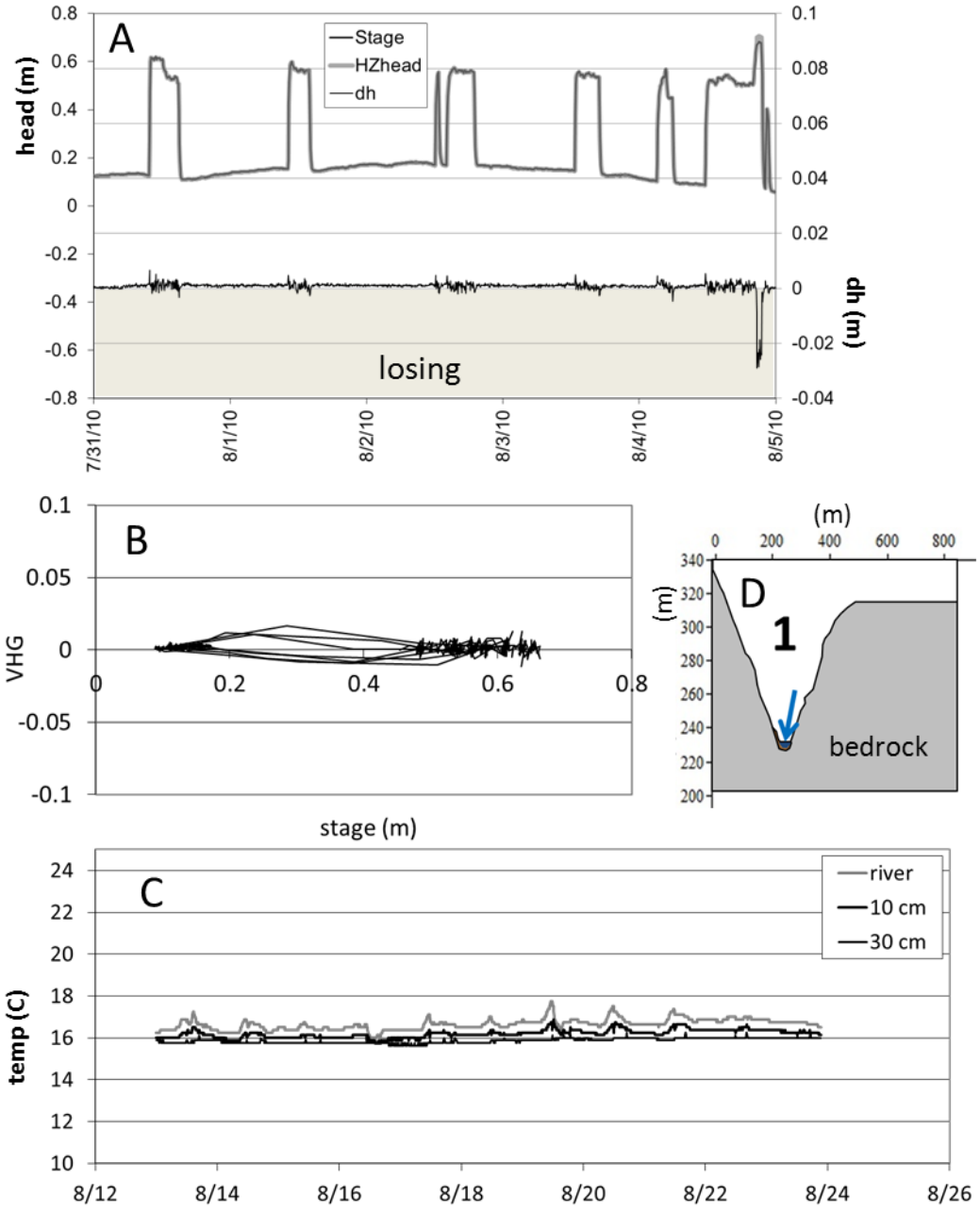

Figure 4.2: Site 1, located just downstream of Fife Brook Dam. (A) Time series of river stage and HZ head as measured 50 cm below the stream bed. (B) Stage versus VHG shows the limited hysteresis and minimal observed VHG throughout observation times. (C) River and subsurface temperatures 10 cm and 30 cm below the stream bed. The highest line is the river temperature, below which is that 10 cm down and 30 cm down. (D) Interpreted geologic cross section.

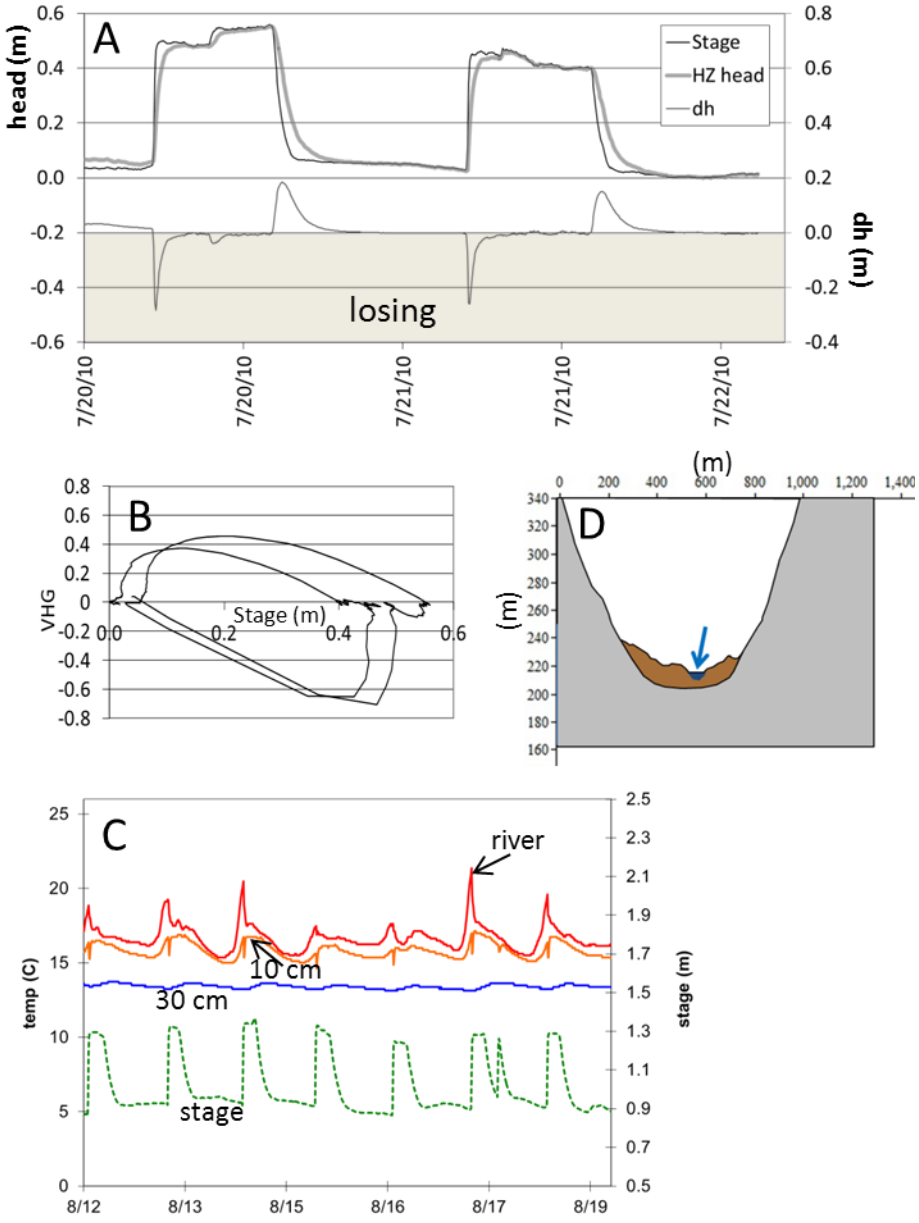

Figure 4.3: Site 2, located 4 km downstream of Fife Brook Dam. (A) Time series of river stage and HZ head as measured 50 cm below the stream bed. (B) Stage versus VHG shows a large gradient observed between the river and HZ. (C) River and subsurface temperatures 10 cm and 30 cm below the stream bed. The highest line is the river temperature, below which is that 10 cm down and 30 cm down. Stage changes observed at site 3 are shown; they have been advanced 1.25 hr to reflect floodwave propagation time from site 2 to 3. (D) Interpreted geologic cross section.

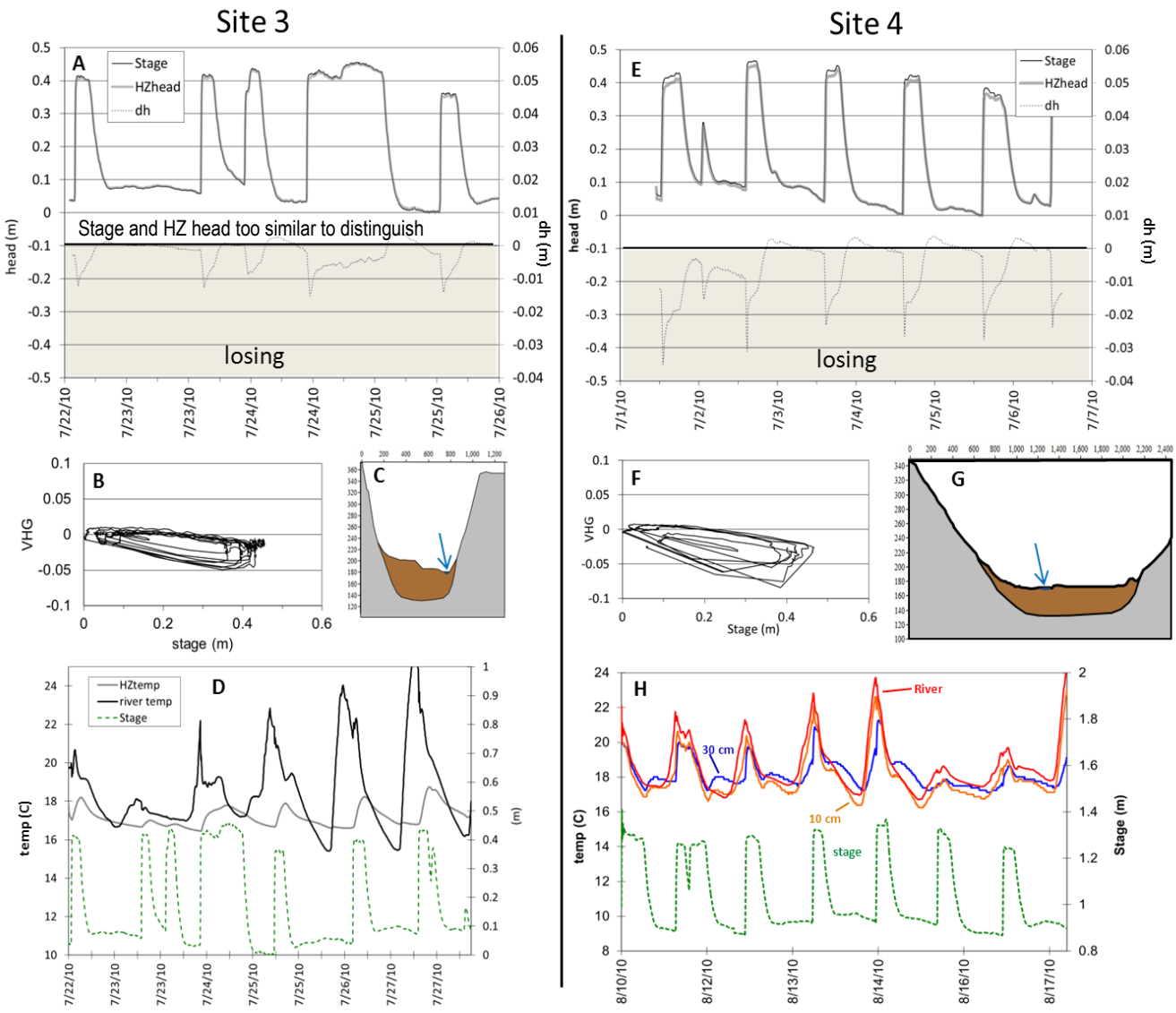

Figure 4.4: Sites 3 (left) and 4 (right), located 12 and 15 km downstream respectively of Fife Brook Dam. (A, E) Time series of river stage and HZ head as measured 50 cm below the stream bed. (B,F) Stage versus VHG shows similar losing streams and highly hysteretic patterns. (D) River and subsurface temperatures 50 cm below the stream bed at site 3. Stage is shown as well. (H) River and subsurface temperatures 10 cm and 30 cm below the stream bed at site 4. Stage changes observed at site 3 are shown; they have been lagged 0.75 hr to reflect floodwave propagation time from site 3 to 4. (D, H) Interpreted geologic cross sections showing the widest, most expansive filled basin of all the sites.

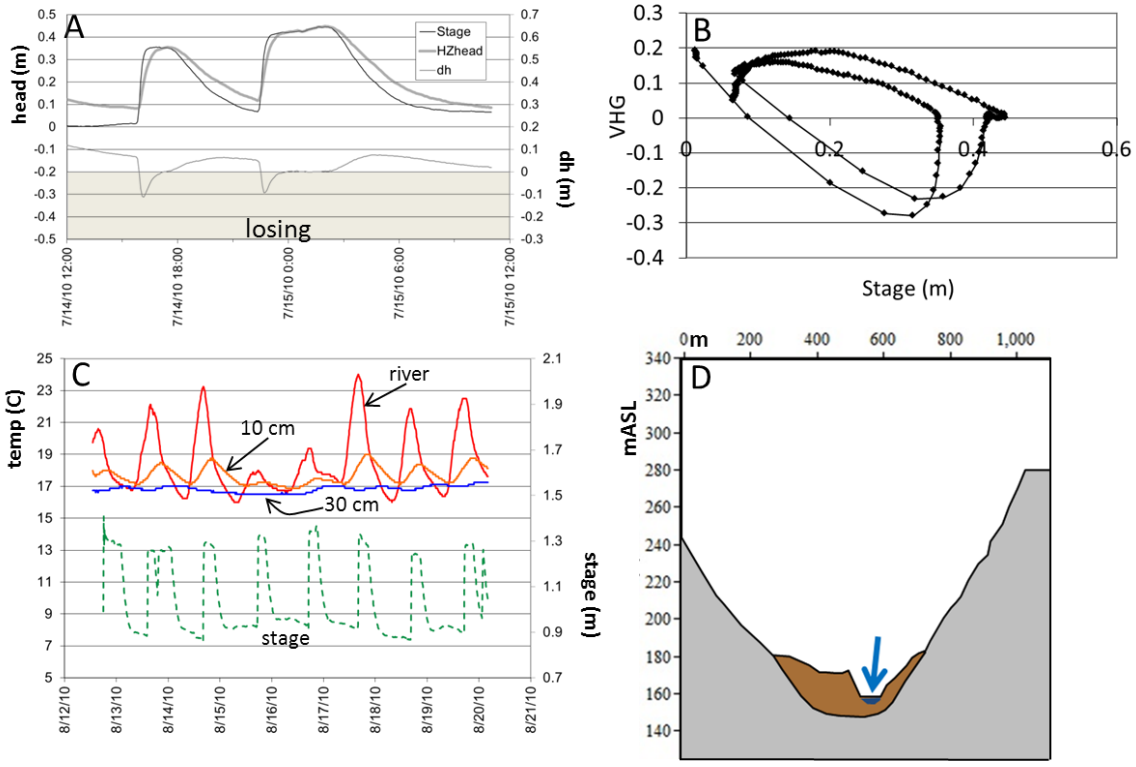

Figure 4.5: Site 5, located 19.5 km downstream of Fife Brook Dam. (A) Time series of river stage and HZ head as measured 50 cm below the stream bed. (B) Stage versus VHG shows a large gradient observed between the river and HZ. A hi9gh density of data points above the x-axis indicates longer periods of gain than loss. (C) River and subsurface temperatures 10 cm and 30 cm below the stream bed. The highest line is the river temperature, below which is that 10 cm down and 30 cm down. Stage changes observed at site 3 are shown; they have been lagged 1.5 hr to reflect floodwave propagation time from site 3 to 5. (D) Interpreted geologic cross section.

Site	1	2	3	4	5
Trial 1	1.6E-04	4.1E-04	4.1E-03	1.7E-03	No data
Trial 2	2.7E-04	4.2E-04		1.6E-03	
Trial 3	2.7E-04	3.9E-04		1.3E-03	
Average	2.4E-04 m/s	4.1E-04 m/s	4.1E-03 m/s	1.5E-03 m/s	No data

Table 4.1: Slug test results from DFR sites 1-5 reported in m/s. Results from site 3 are limited due to a poor connection between the piezometer and streambed media, allowing for a rapid attenuation of the initial head disturbance. Site 5 data are absent for the opposite problem; there the well screen was clogged and head disturbances did not equilibrate on observable time scales.

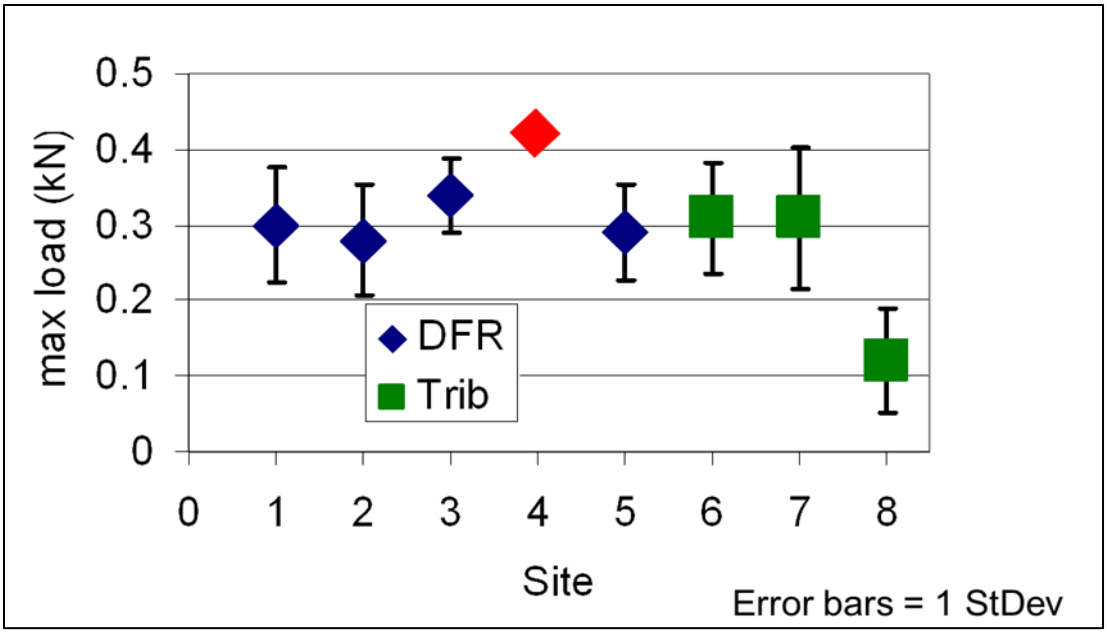

Figure 4.6: Data from cotton strip assay showing maximum sustained load before failure of cotton strips at DFR sites (1-5) and unregulated tributary sites (6-8). Red data point shows the control, for which standard deviation error bars are smaller than the diamond symbol.

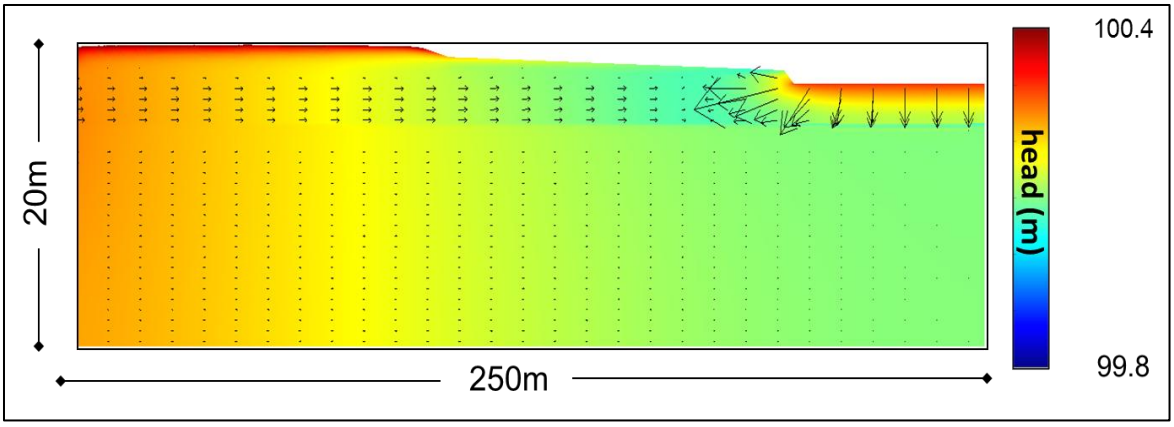

Figure 4.7: Head distribution within the riparian aquifer from a model run with generally gaining river conditions. This snap shot was taken immediately after a stage increase showing the locally reversed head gradient out of the river. Head is shown by the color bar at left; black arrows indicate the direction and relative velocity of groundwater flow. This model was not used in chapter 3.

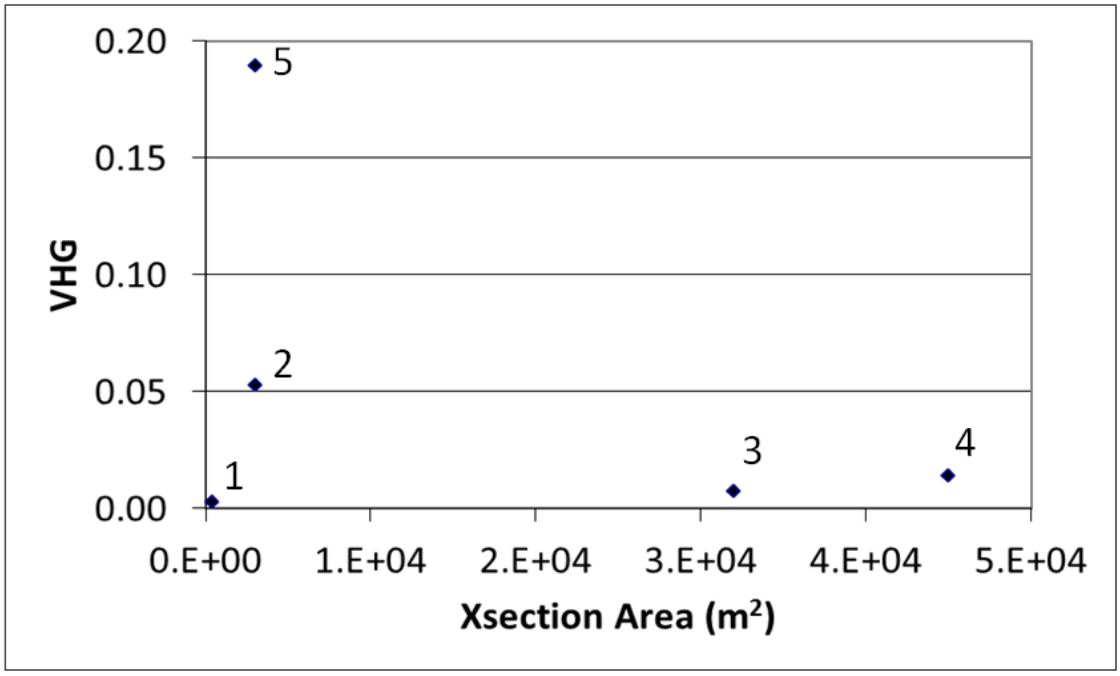

Figure 4.8: Cross sectional area of sites 1-5 versus average VHG during data collection time period. Data point labels correspond to site numbers.

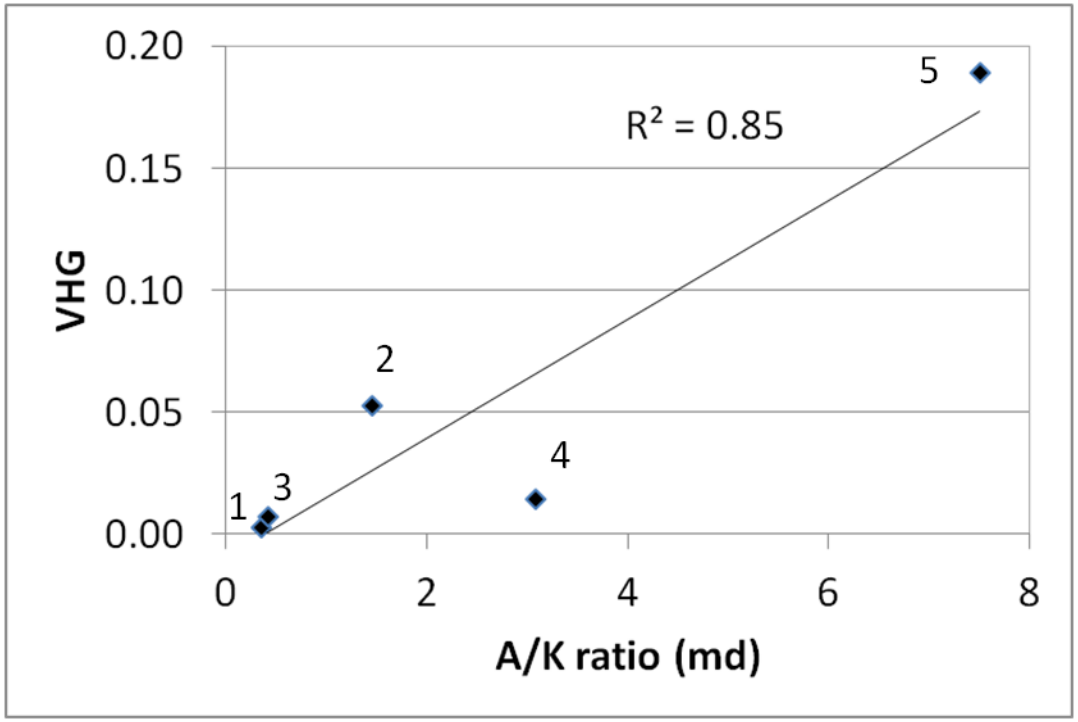

Figure 4.9: The ratio of aquifer cross sectional area to hydraulic conductivity (A/K) from slug tests versus average observed VHG for sites 1-5. Data point labels correspond to site numbers.

APPENDIX 1

SUPPLEMENTARY FIELD DATA

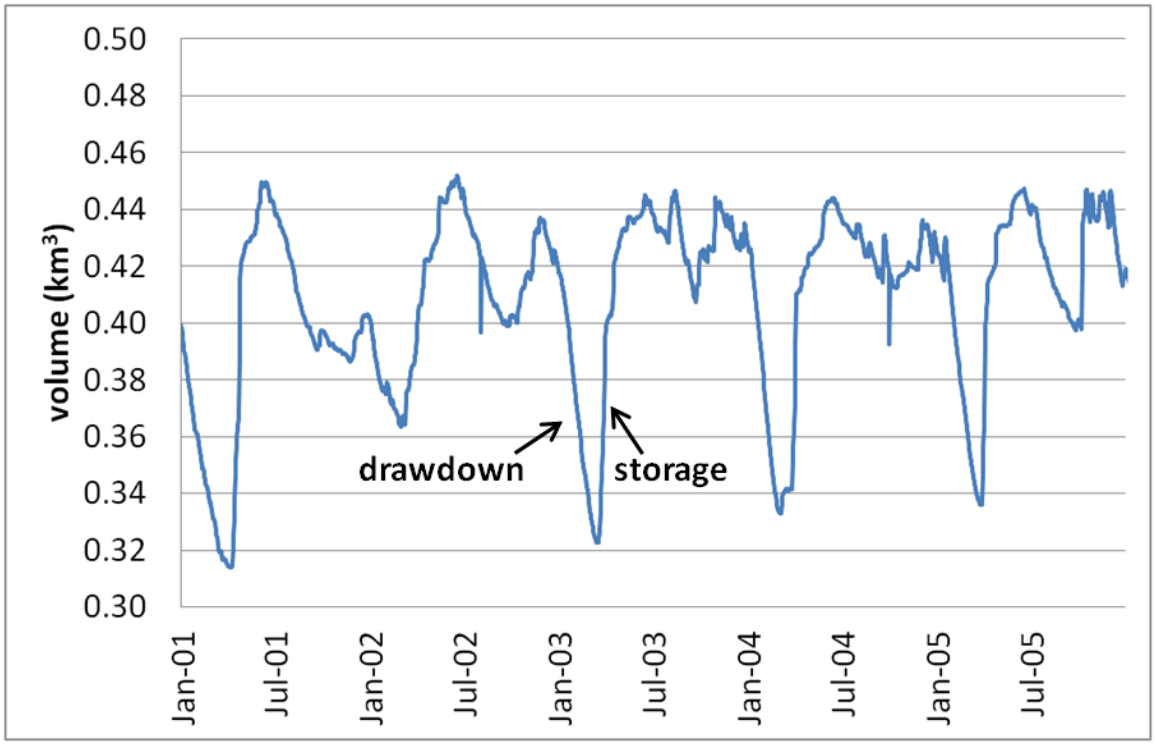

Figure A.1 – Combined volume of Harriman and Somerset reservoirs showing typical drawdown in late winter and subsequent storage of spring hydrograph. Spring storage increase equates to an average April discharge reduction by 12.2 m^3/s and summer discharge increase of 4.7 m^3/s.

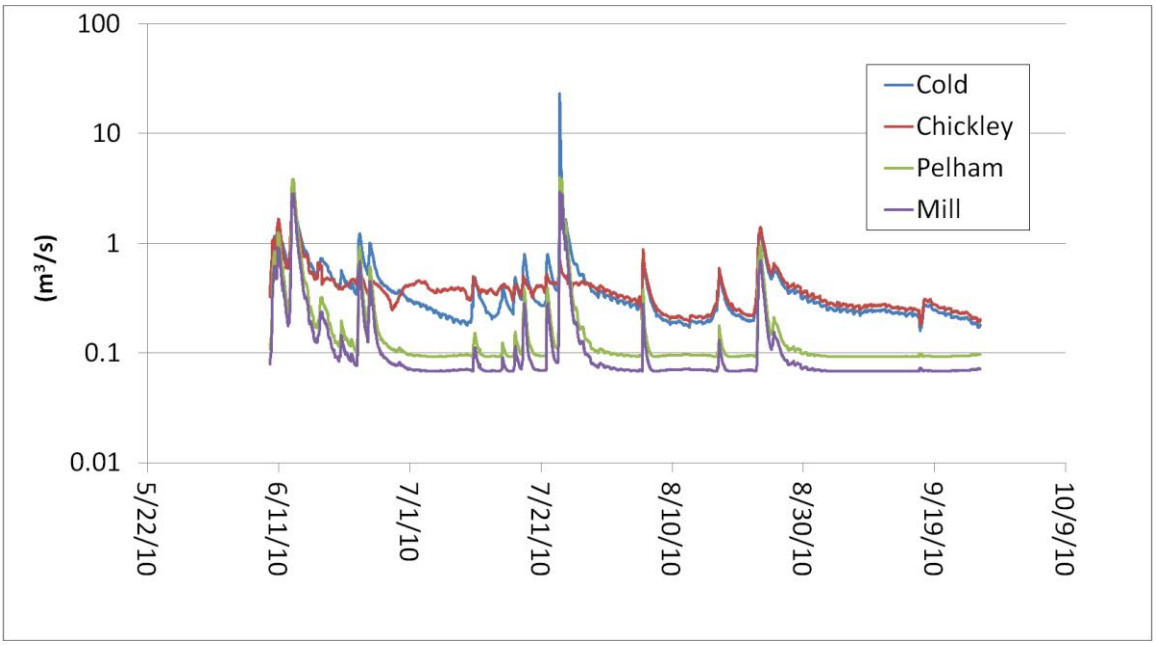

Figure A.2 – Tributary hydrographs of four largest sub-watersheds within study reach. After 25 July, all records are reconstructed using the Cold River discharge record. This was done due to limited monitoring equipment.

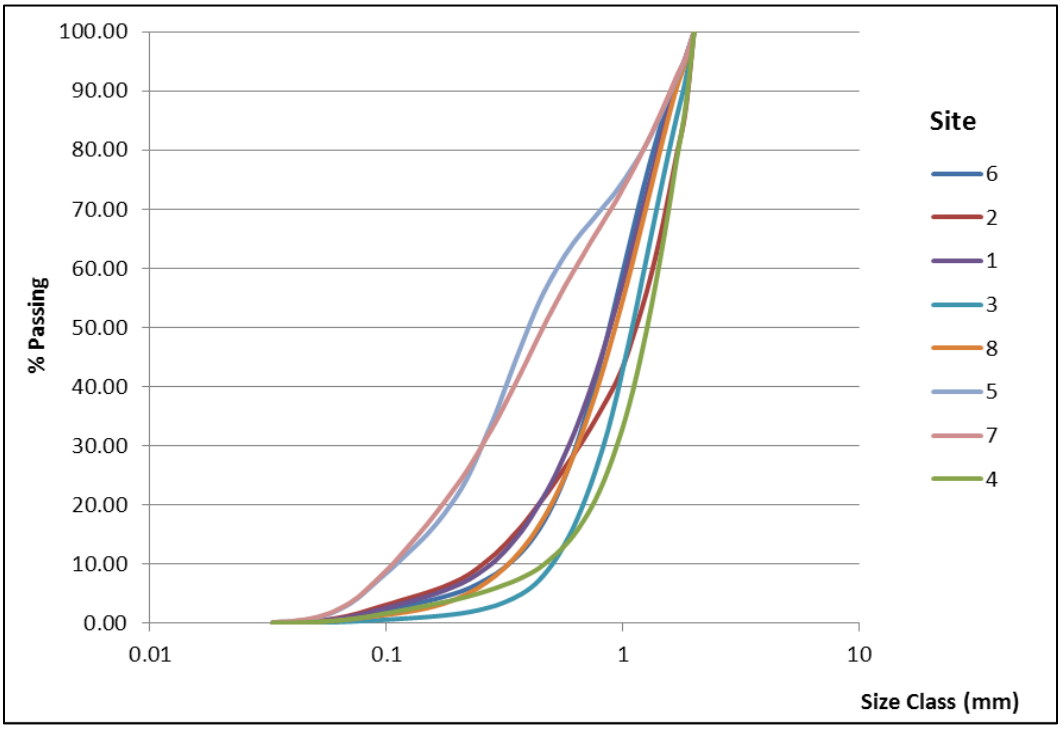

Figure A.3 – Sub 2mm camsizer data from mainstem DFR sites (1-5) and tributaries (6-8). Sites 3 and 4 were the coarsest, sites 5 and 7 (Chickley River) were the finest.

APPENDIX 2

RICHARD'S EQUATION

The following syntax of Richard's equation is used to define fluid flow at each node within the defined domain of each cross section model simulation:

$$(C/\rho g + SeS/\rho g)\, dp/dt + \nabla \cdot (-K_s/(p_f g) k_r \nabla(p + \rho_f g D)) = Q_s \quad \text{[A. 3.1]}$$

where:
ρ is the density of water
g is acceleration due to gravity
p_f is fluid pressure
S is storage
K_s is the saturated hydraulic conductivity
t is time
D is elevation above some datum in meters
Q_S is the change in storage
k_r is the permeability of unsaturated nodes
Se is a term that relates head to permeability when head < 0
C is a term that determines the pressure head of the node as a function of its water content

$$Se = \frac{1}{\left(1+|\alpha H_p|^n\right)^m}, H_p < 0 \quad \text{[A. 3.2]}$$

where:
H_p is pressure head
α is a Van Genuchten term that describes soil capillarity
n is a constant that controls the steepness of the soil-water retention curve and

$$m = 1 - 1/n \quad \text{[A. 3.3]}$$

Thus, when pressure head (H_p) falls below zero due to soil capillarity, COMSOL uses pressure head to define Se, which determines the permeability at that value of pressure head as follows:

$$k_r = Se^l[1 - (1 - Se^{1/m})^m]^2 \quad \text{[A. 3.4]}$$

where:
l is a user-defined constant, generally set equal to 0.5

CITATIONS

Anderson, M. P. (2005). Heat as a ground water tracer. *Ground Water, 43*(6), 951.

Allen, R., Pereira, L., Raes, D., Smith, M. (1998). Crop evapotranspiration - Guidelines for computing crop water requirements - FAO Irrigation and drainage paper 56.

Arntzen, E., Geist, D., Dresel, P. (2006). Effects of fluctuating river flow on ground water/surface water mixing in the hyporheic zone of a regulated, large cobble bed river. *River Research and Applications*, v 22, pp. 937-946.

Bear, J., and Braester, C. (1969) On the flow of two immiscible fluids in fractured porous media. Proc. 1st Int. Symp. on the Fundamentals of Transport Phenomena in Porous Media, Haifa, Israel, pp. 177-202.

Berkowitz, B and Scher, H. (1995). On Characterization of Anomalous Dispersion in Porous and Fractured Media. *Water Resources Research*, vol. 31, no. 6, pp. 1461-1466.

Boulton, A. J., Findlay, S., Marmonier, P., Stanley, E. H., & Valett, H. M. (1998). The functional significance of the hyporheic zone in streams and rivers. *Annual Review of Ecology and Systematics, 29*, 59-81.

Boutt, D. and Fleming, B. (2009). Implications of anthropogenic river stage fluctuations on mass transport in a valley fill aquifer. *Water Resources Research*, v 45, W04427, doi:10.1029/2007wr006526.

Bouwer, H. and R.C. Rice. (1976). A slug test method for determining hydraulic conductivity of unconfined aquifers with completely or partially penetrating wells. *Water Resources Research*, vol. 12, no. 3, pp. 423-428.

Brunke, M., & Gonser, T. (1997). The ecological significance of exchange processes between rivers and groundwater. *Freshwater Biology, 37*(1), 1-33.

Cereghino, R., Cugny, P., & Lavandier, P. (2002). Influence of intermittent hydropeaking on the longitudinal zonation patterns of benthic invertebrates in a mountain stream. *International Review of Hydrobiology, 87*(1), 47-60.

Charbeneau, R.J., Johns, R.T., Lake, L.W., and McAdams III, M.J. (1999). Free-Product Recovery of Petroleum Hydrocarbon Liquids. API Publication Number 4682. American Petroleum Institute, Washington, D.C. p.1.1-6.6.

Clapcott, J. E., & Barmuta, L. A. (2010). Metabolic patch dynamics in small headwater streams: Exploring spatial and temporal variability in benthic processes. *Freshwater Biology, 55*(4), 806-824.

Cole, Michael. (May 2007). Assessment of Benthic Macroinvertebrate Communities in Relation to Regulated Flows in the Deerfield River, Massachusetts. ABR Final Report. Retrieved on June 20, 2010 in pdf format.

Conant, B. (2004). Delineating and quantifying ground water discharge zones using streambed temperatures. *Ground Water, 42*(2), 243-257.

Davy-Bowker, J., Sweeting, W., Wright, N., Clarke, R. T., & Arnott, S. (2006). The distribution of benthic and hyporheic macroinvertebrates from the heads and tails of riffles. *Hydrobiologia, 563*, 109-123.

Dingman, S.L. 1994. *Physical Hydrology,* Prentice Hall, Englewood Cliffs, NJ.

Fleming, Brandon J. (2009). Effects of Anthropogenic River Stage Fluctuations on Surface Water/Ground Water Interactions along the Deerfield River, Massachusetts. *(Masters Thesis).* Retrived from ScolarWorks@UMass: Paper 226.

Freeze, A., & Cherry, J. (Eds.). (1979). *Groundwater*. Englewood Cliffs, NJ: Prentice-Hall, Inc.

Fritz, B. G. and Arntzen, E.V. (2007). Effect of rapidly changing river stage on uranium flux through the hyporheic zone. *Ground Water, 45*(6), (753-760).

Geist, D. R., & Dauble, D. D. (1998). Redd site selection and spawning habitat use by fall chinook salmon: The importance of geomorphic features in large rivers. *Environmental Management, 22*(5), 655-669.

Hancock, P. J. (2002). Human impacts on the stream-groundwater exchange zone. *Environmental Management, 29*(6), 763-781.

Hanrahan, T. P. (2008). Effects of river discharge on hyporheic exchange flows in salmon spawning areas of a large gravel-bed river. *Hydrological Processes, 22*(1), 127-141.

Hatch, C. E., Fisher, A.T., Revenaugh, J. Constantz, J. (2006). Quantifying surface water-groundwater interactions using time series analysis of streambed thermal records; method development. *Water Resources Research, 42*, W10410, doi:10.1029/2005WR004787.

Hillel, Daniel. (1998). *Environmental Soil Physics.* San Diego: Academic Press, pp. 523.

Howard, K., Maier, H., & Mattson, S. (2006). Ground-surface water interactions and the role of the hyporheic zone. In A. Baba et al (Eds.), *Groundwater and Ecosystems.* pp131-143, Netherlands: Springer.

Kalbus, E., Reinstorf, F. and Schirmer, M. (2006). Measuring methods for groundwater-surface water interactions; a review. *Hydrology and Earth Systems Science, 10*, 873-887.

Jackson et al. (1996). A global analysis of root distributions for terrestrial biomes. *Oecologia*, vol 108, pp. 389-411.

Lai, C. and Katul, G. (1999). The dynamic role of root-water uptake in coupling potential to actual transpiration. *Advances in Water Resources*, vol. 23, pp. 427-439.

Mabee, S.B., B.J. Fleming and D.F. Boutt. (2007). Hydrogeologic assessment of the West Charlemont aquifer, Project Completing report. Charlemont, Massachusetts.

Moriarty, Patrick. Engineer at Bear Swamp Power Company. Personal communication, December 2010.

Penman, H.L. (1948). "Natural Evaporation from Open Water, Bare Soil and Grass", *Proceedings of the Royal Society of London Series A-Mathematical and Physical Sciences,* vol. 193, no. 1032, pp. 120-139.

Ruehl, C., Fisher, A. T., Hatch, C., Los Huertos, M., Stemler, G., & Shennan, C. (2006). Differential gauging and tracer tests resolve seepage fluxes in a strongly-losing stream. *Journal of Hydrology, 330*(1-2), 235-248.

Sawyer, A. H., Cardenas, M. B., Bomar, A., Mackey, M. (2009). Impact of dam operations on hyporheic exchange in the riparian zone of a regulated river. *Hydrological Processes, 23*, 2129-2137.

Slocum, M. G., Roberts, J., Mendelssohn, I. A. (2009). Artist canvas as a new standard for the cotton-strip assay. *Journal of Plant Nutrition and Soil Science,* vol. 172, pp. 71-74.

Tiegs S.D., Langhans S.D., Tockner K. & Gessner M.O. (2007) Cotton strips as a leaf surrogate to measure decomposition in river floodplain habitats. *Journal of the North American Benthological Society*, vol. 26, pp. 70–77.

Vaux, W. G. (1968). Intragravel flow and interchange of water in a streambed. *United States Fish and Wildlife Service Fishery Bulletin, 66*(3), 479-496.

Valiantzas, J.D. (2006) Simplified versions for the Penman evaporation equation using routine weather data. *Journal of Hydrology,* vol. 331, no. 3-4, pp. 690-702.